Direct measurement of cosmic rays above the atmosphere (balloons & space missions)

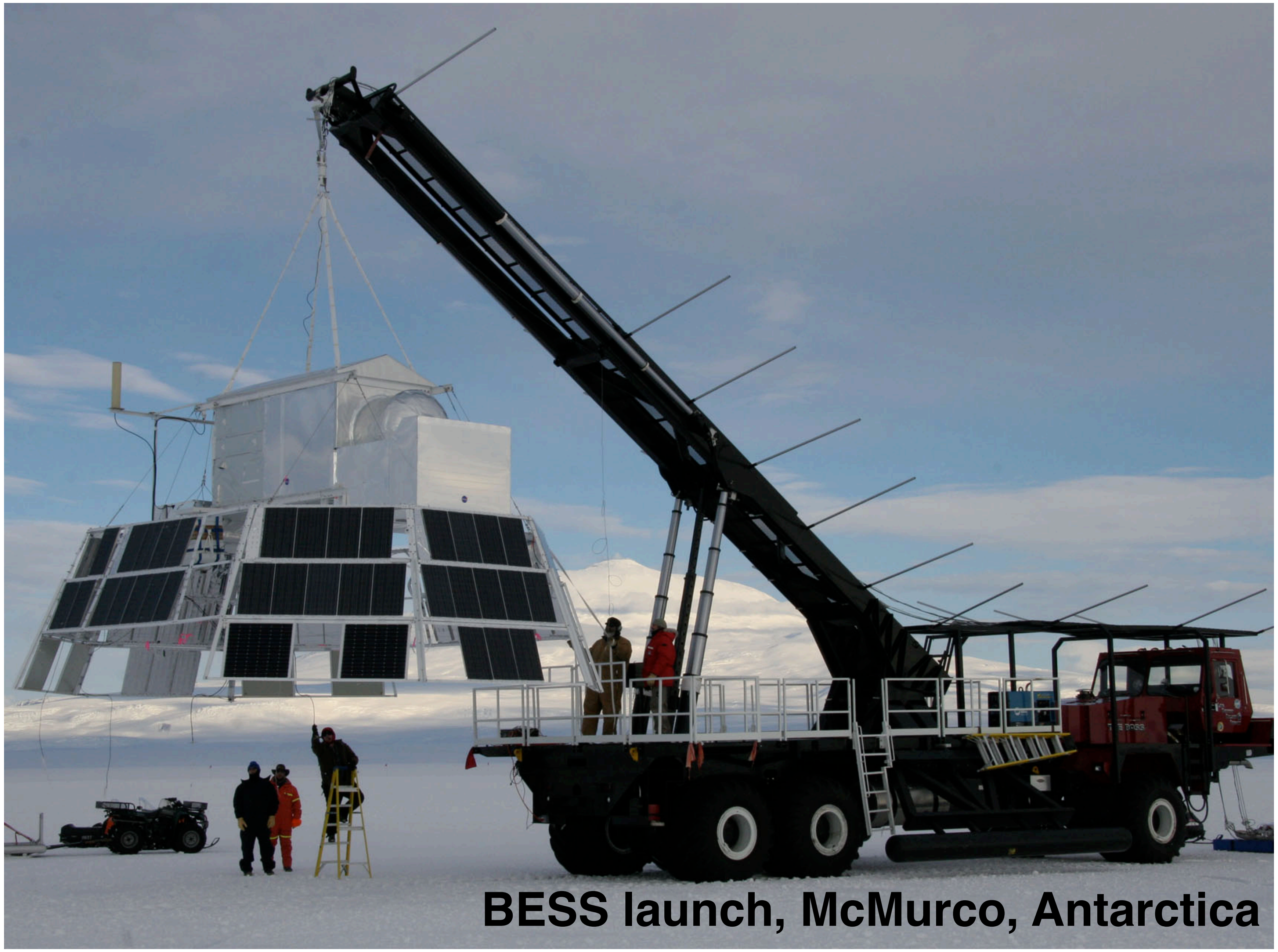

http://particle.astro.ru.nl/goto.html?astroinst2021

Magnetic spectrometer

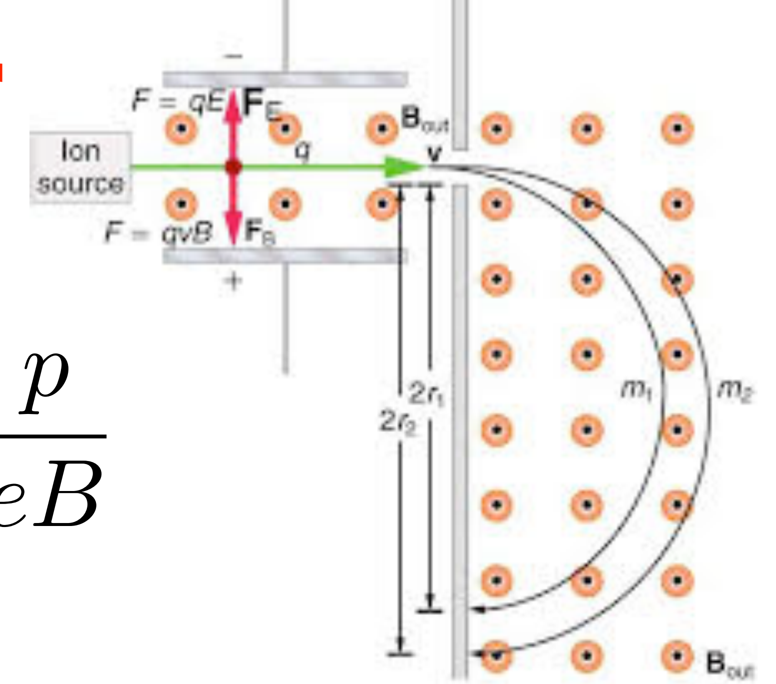

momentum measurement

particle in magnetic field $$\frac{mv^2}{\rho} = evB$$ **and** $$\rho = \frac{p}{eB}$$

deflection angle ($\rho >> L$) $$\theta = \frac{L}{\rho} = \frac{L}{p} eB$$

measured momentum $$p = eB\rho = eB\frac{L}{\theta}$$

$$\left|\frac{dp}{d\theta}\right| = eBL\frac{1}{\theta^2} = \frac{p}{\theta}$$

momentum resolution

$$\frac{\sigma(p)}{p} = \frac{2\sigma(x)/h}{eBL} p$$

$$\sigma(p) \propto p^2$$

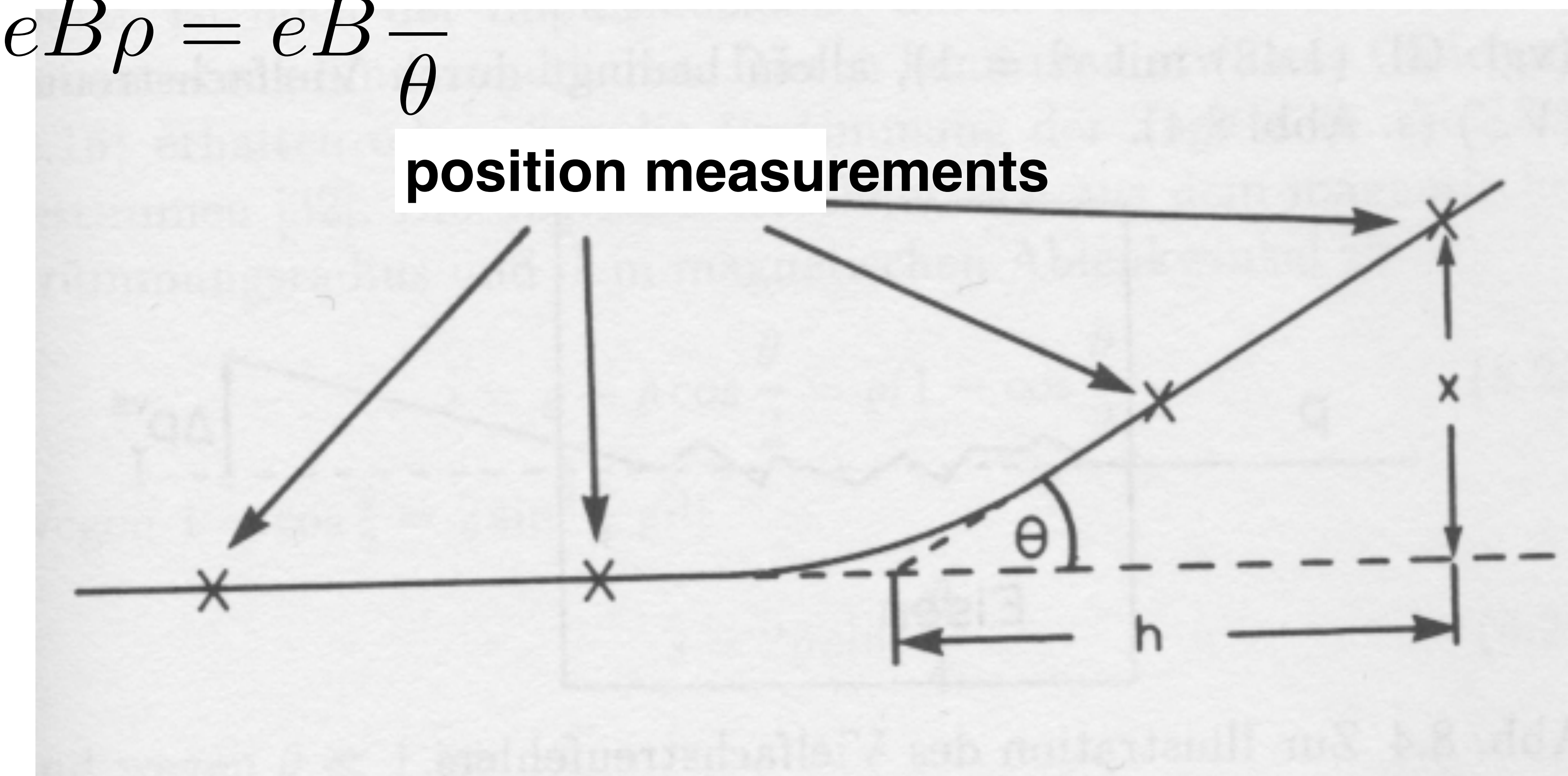

maximum momentum: $$\frac{\sigma(p_{max})}{p_{max}} = 1$$

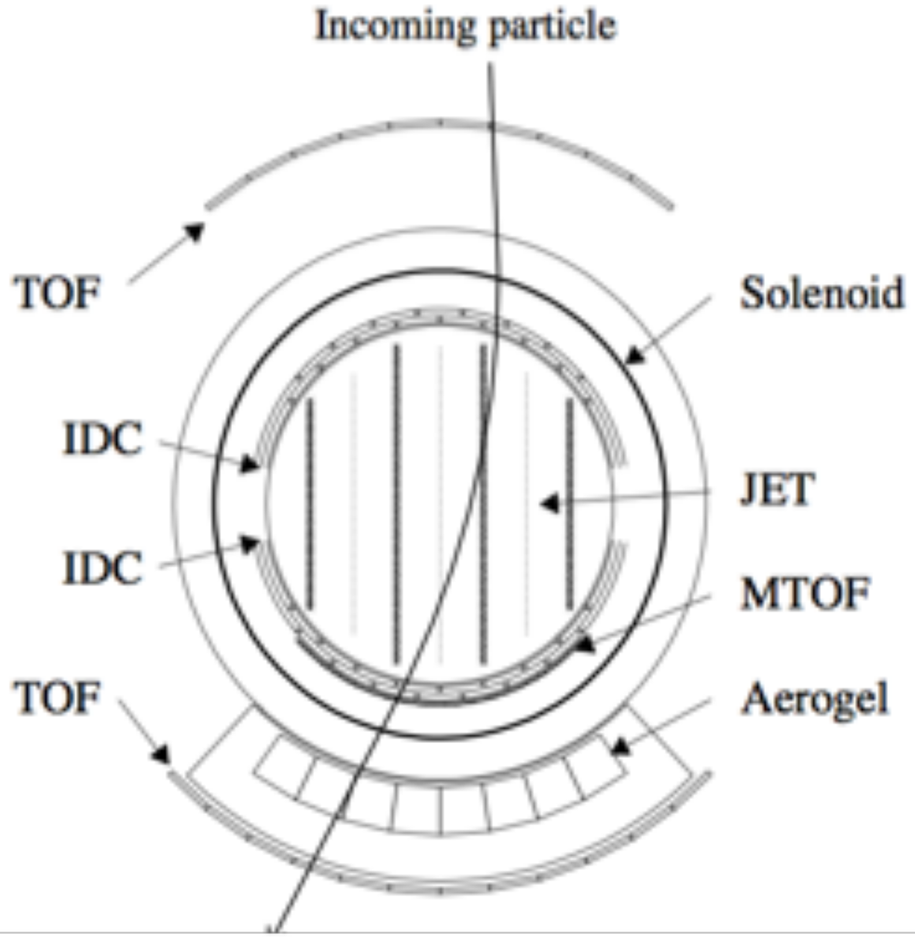

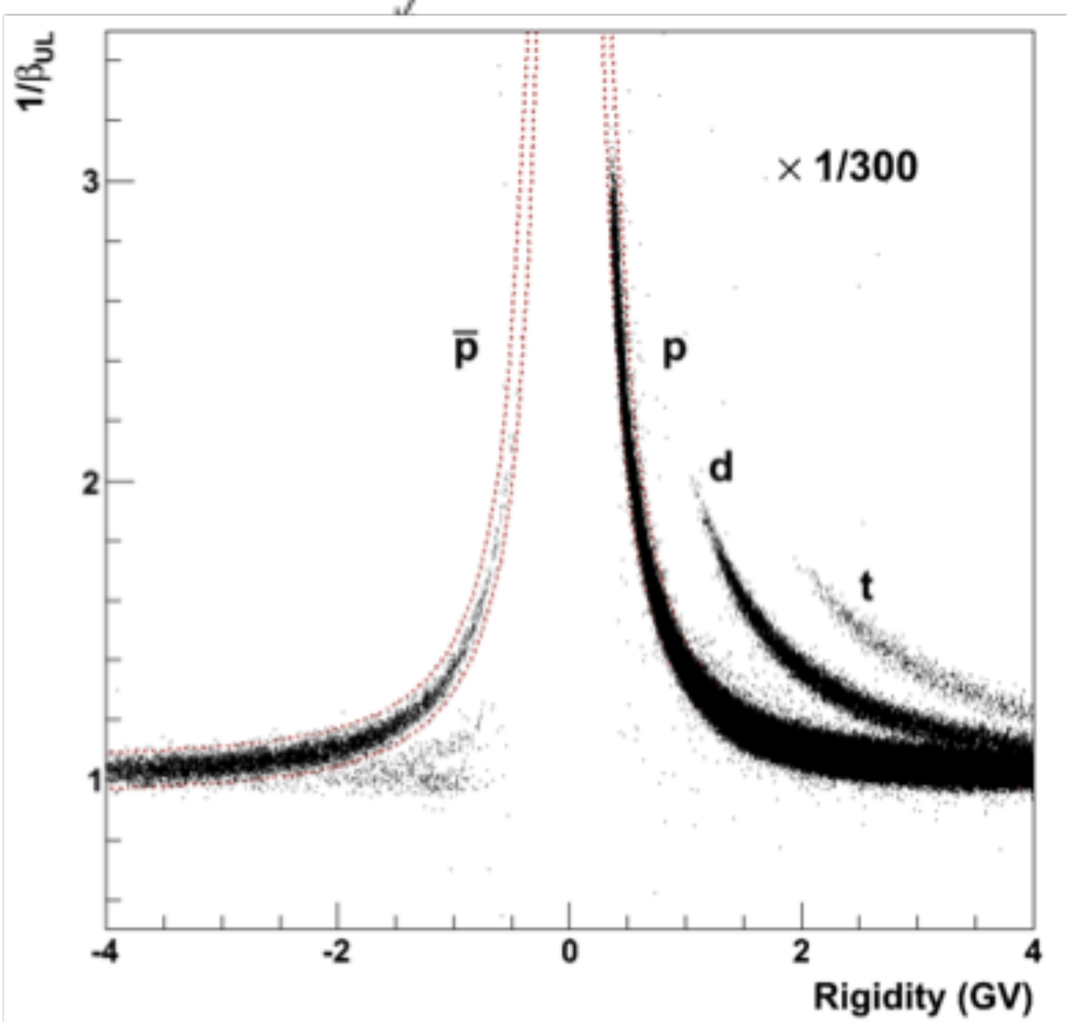

- Balloon-borne Experiment with a Superconducting Spectrometer
- Measures charge, charge-sign, mass, and energy
- Superconducting magnetic spectrometer: momentum from magnetic rigidity
  - Thin solenoidal superconducting magnet Gives very uniform field
  - Fully active “JET” and “IDC” drift chambers with 54 points on trajectory, σ <130 μm
  - MDR: 200 GV BESS; 1400 GV BESS-TeV; 240 GV BESS-Polar
- Time-of-flight system (TOF): velocity and charge
- Silica-aerogel Cherenkov detector (ACC, n=1.02/1.03): background rejection

$$m = \frac{RZe}{\gamma\beta c}$$

- Nine northern latitude flights (1+ days) 1993-2002 and two Antarctic flights in 2004 (8.5 days) and 2007 (24.5 days)
- **Including BESS-Polar I 3757 antiprotons reported 0.2 - 4.2 GeV**

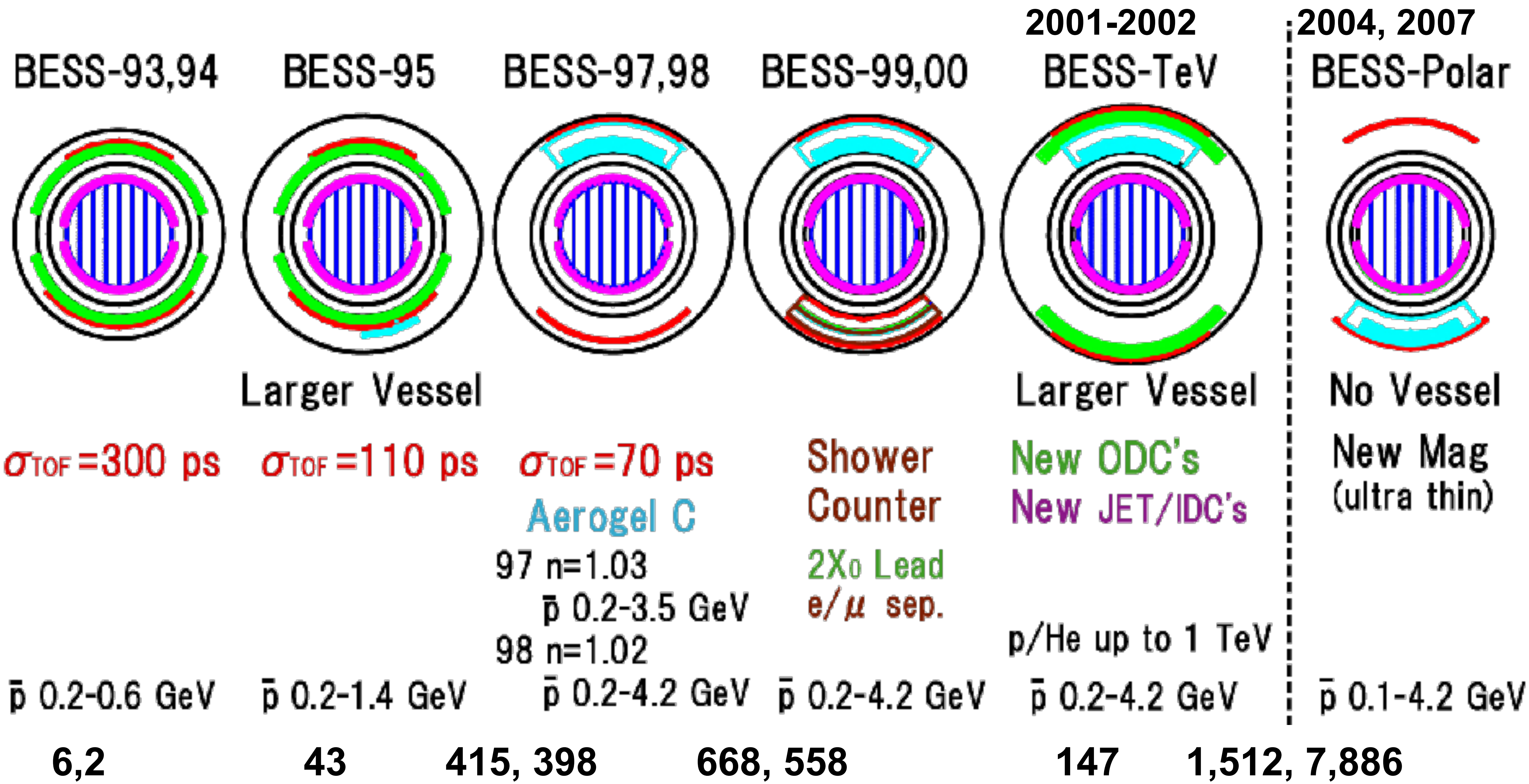

BESS Instrumentation

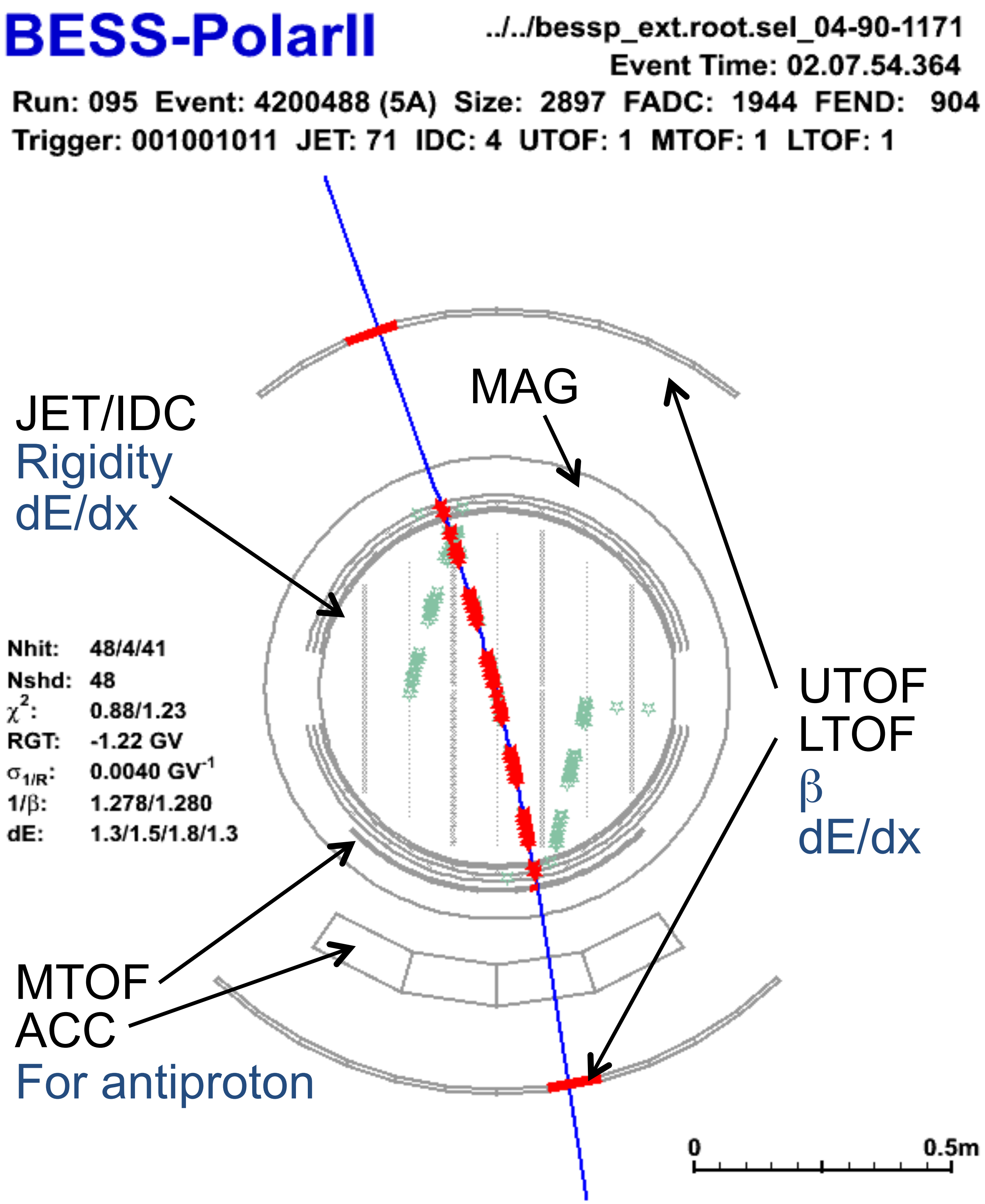

Event display with reconstructed Antiproton track is shown.

Rigidity (MDR:240GV)

Solenoid: Uniform field (ϕ=1m, B=0.8T)
Thin material (2.4 g/cm^2)

Drift chamber: Redundant hits
(σ~150μm, 32~48+4hits)

Charge, Velocity

TOF, Chamber: dE/dx measurement
(Z = 1, 2, ...)

TOF: 1/β measurement (σ~1,2%)

$$m = ZeR\sqrt{1/\beta^2 - 1}$$

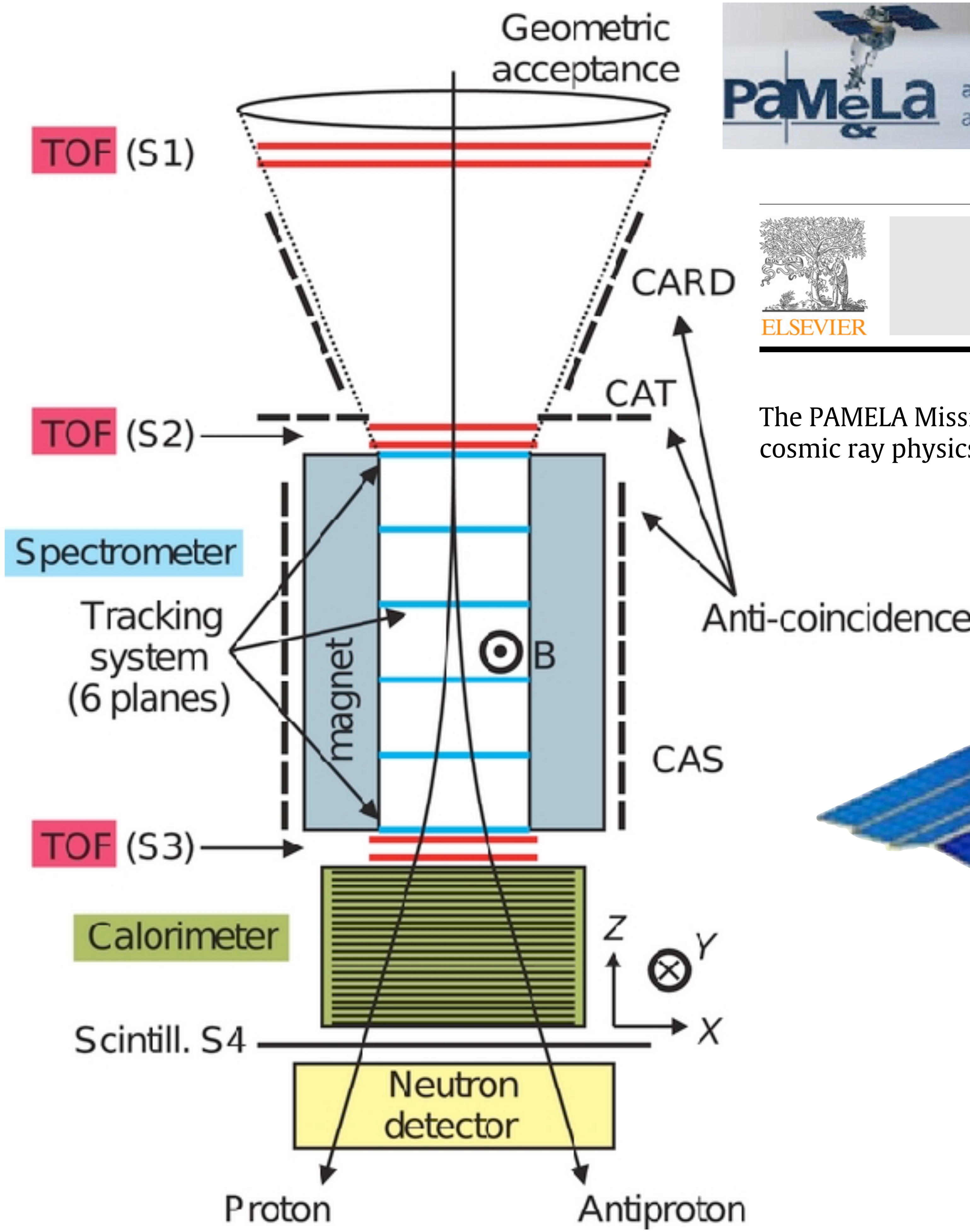

PaMeLa
a Payload for Antimatter Matter Exploration and Light-nuclei Astrophysics

Physics Reports 544 (2014) 323–370

Contents lists available at ScienceDirect

Physics Reports

journal homepage: www.elsevier.com/locate/physrep

The PAMELA Mission: Heralding a new era in precision cosmic ray physics

Energy measurement - calorimeter

electron-photon calorimeter

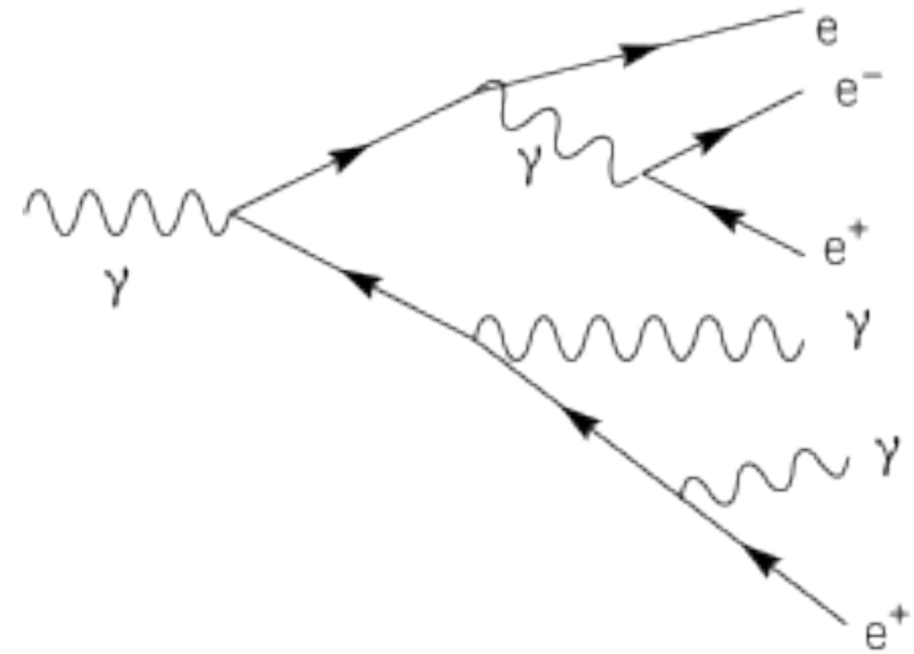

at high energies (>GeV):
electrons loose energy through Bremsstrahung
photons loose energy through pair production
--> electromagnetic cascade

longitudinal shower development/energy loss

$$\frac{dE}{dt} = const \cdot t^a e^{-bt}$$

$$t = x/X_0$$

depth in material in units of the radiation length

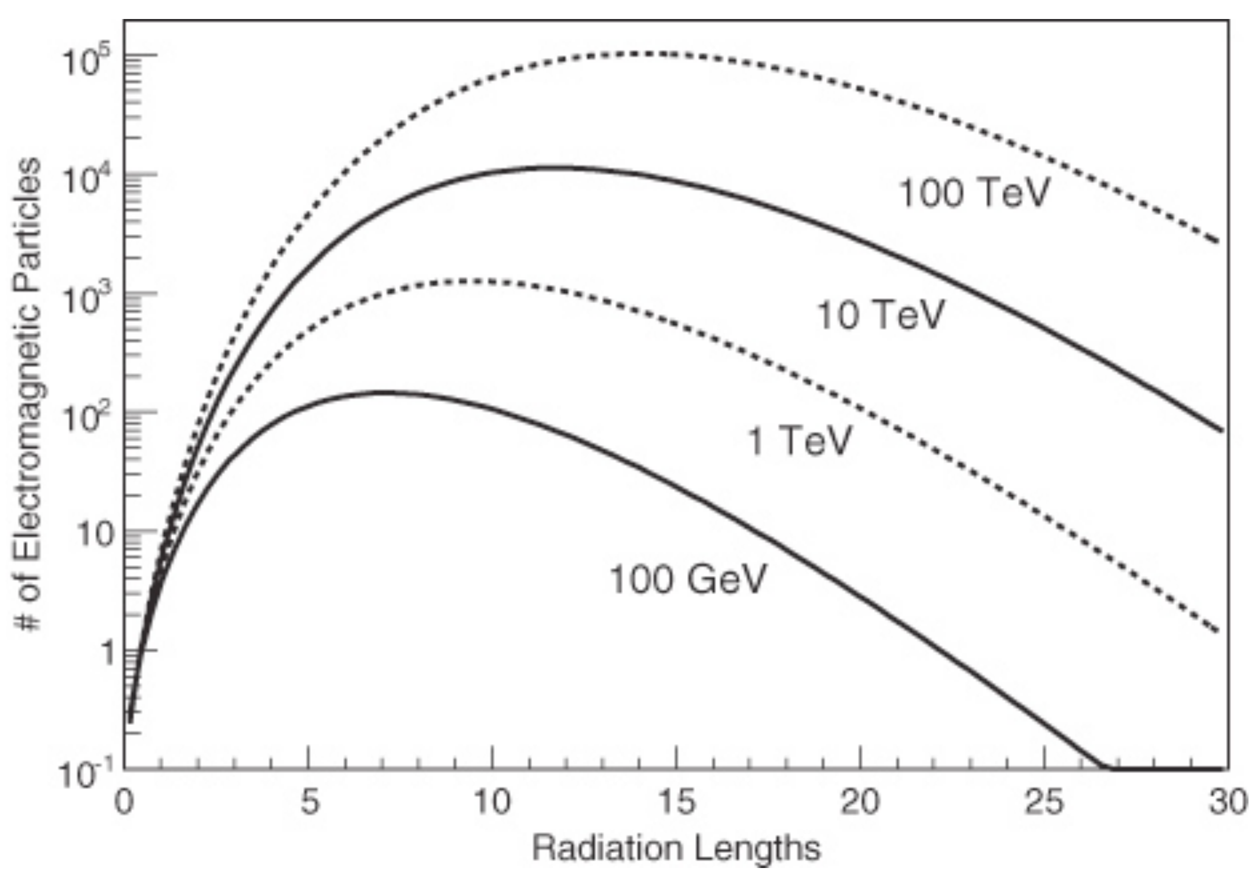

depth of maximum depends on energy as

$$t_{max} \propto \ln \frac{E}{E_c}$$

Energy measurement - calorimeter

electromagnetic cascade

lateral extension of the cascade mostly caused by multiple scattering and characterized by Molière radius

$$R_m = \frac{21\ \mathrm{MeV}}{E_c} X_0 \left[\frac{\mathrm{g}}{\mathrm{cm}^2}\right]$$

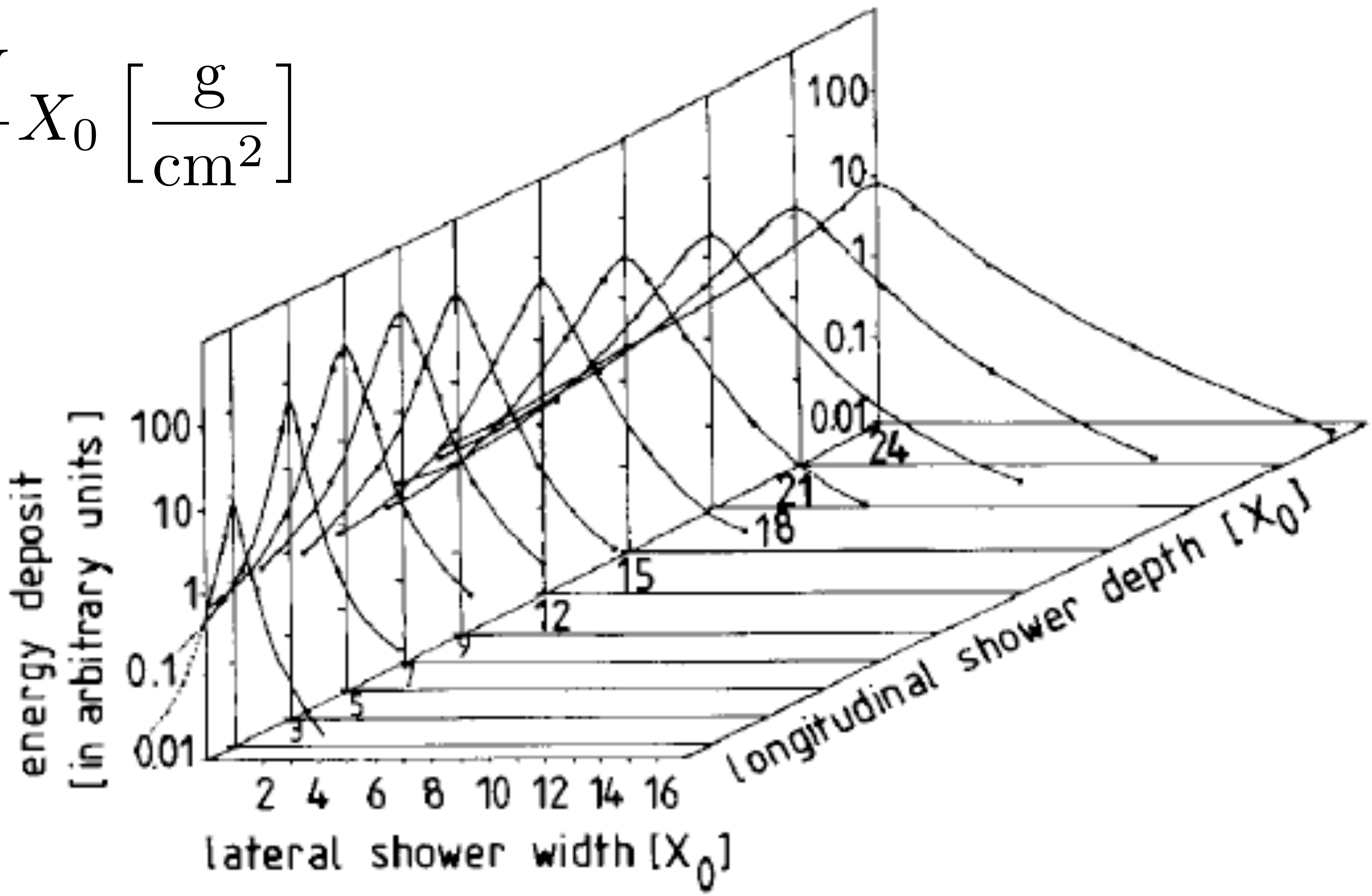

Particle identification - calorimeter

in calorimeters there are different shower responses for electrons and hadrons

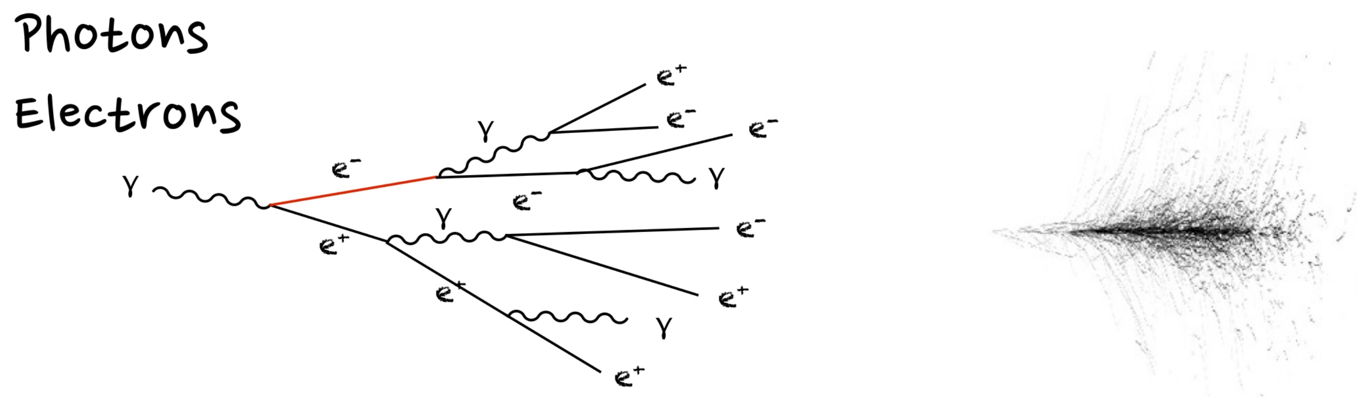

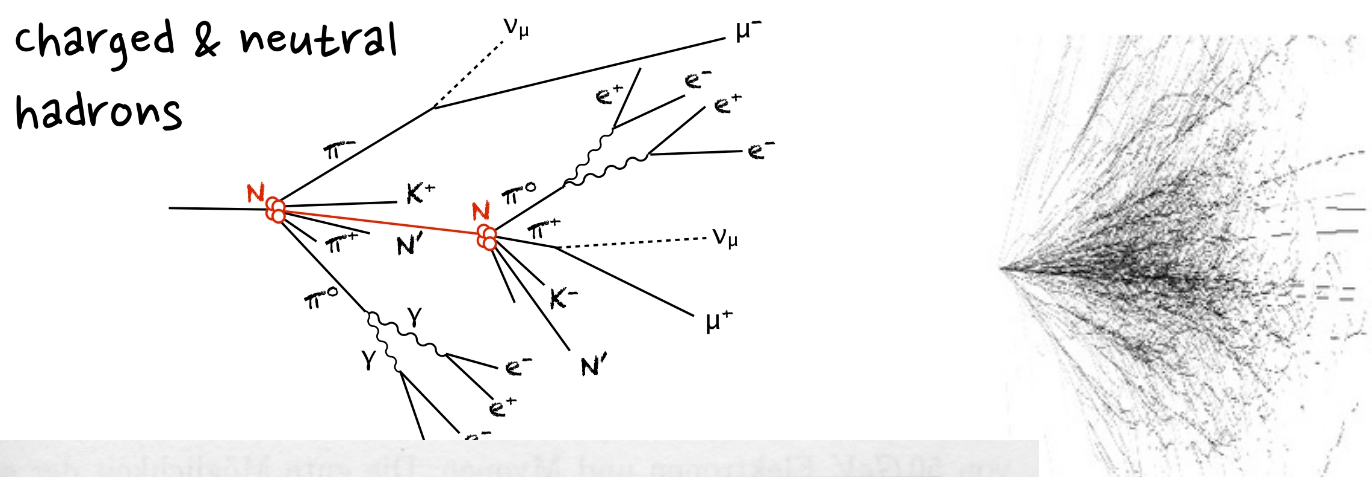

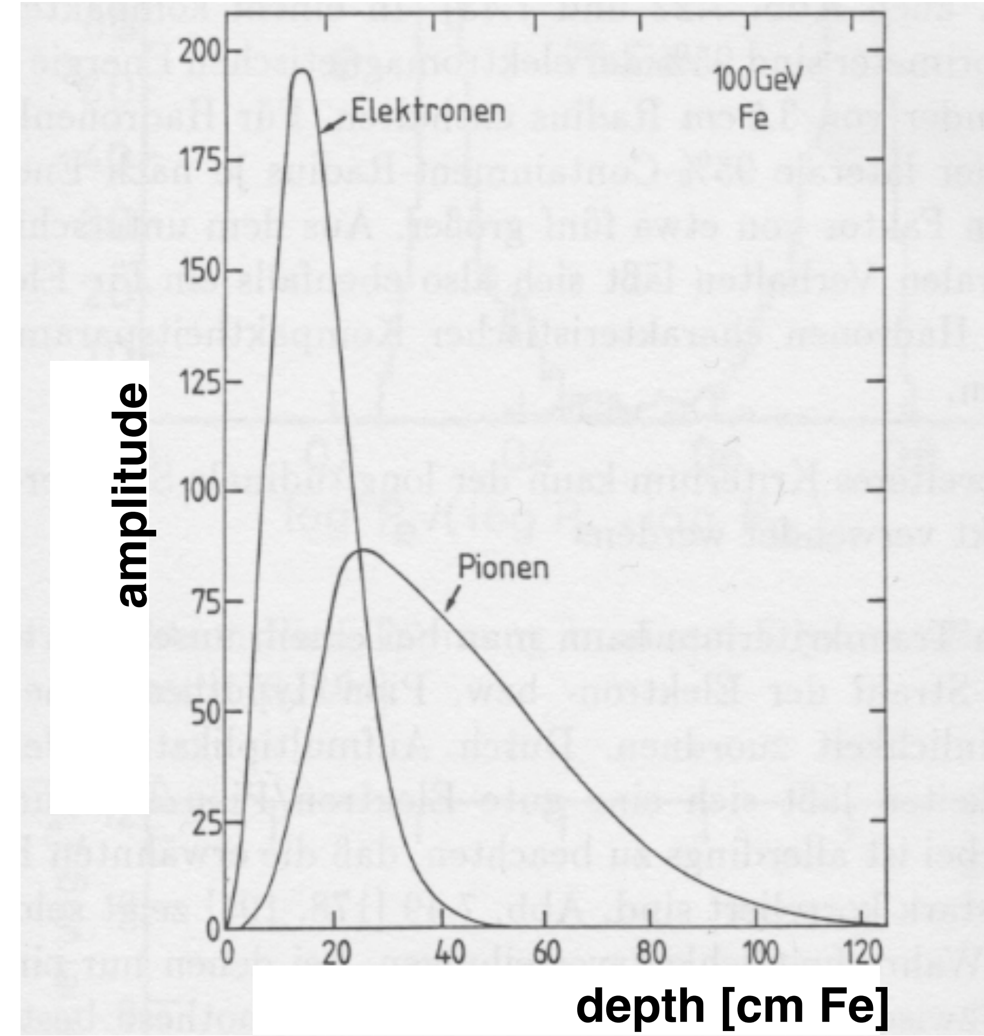

longitudinal shower development for electrons and pions

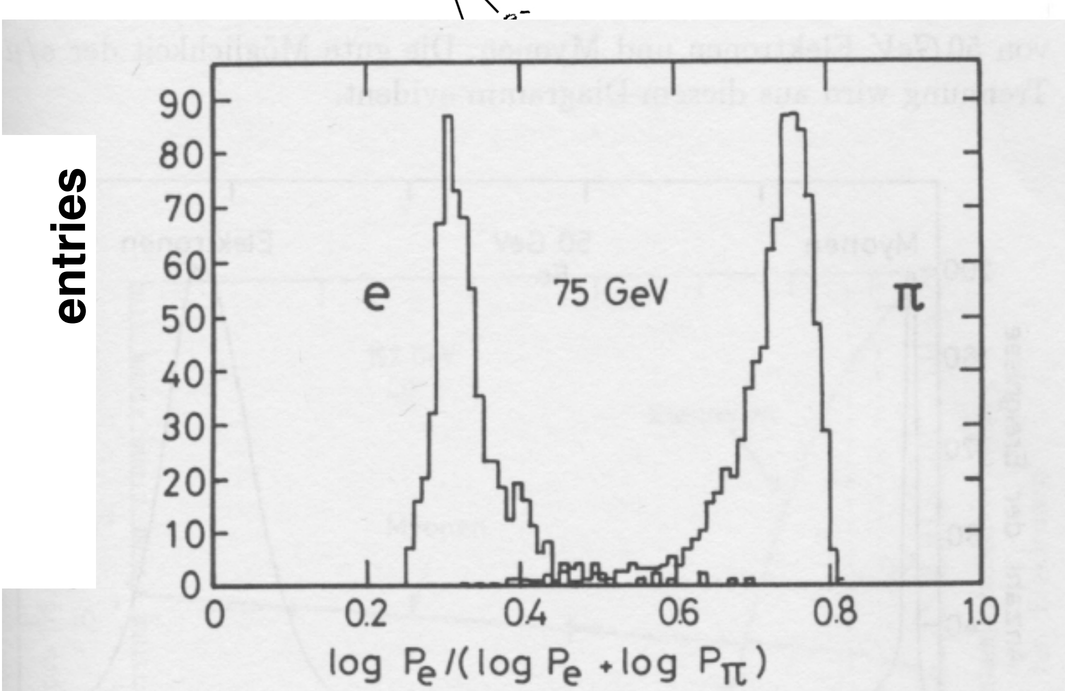

energy deposit for electrons and pions

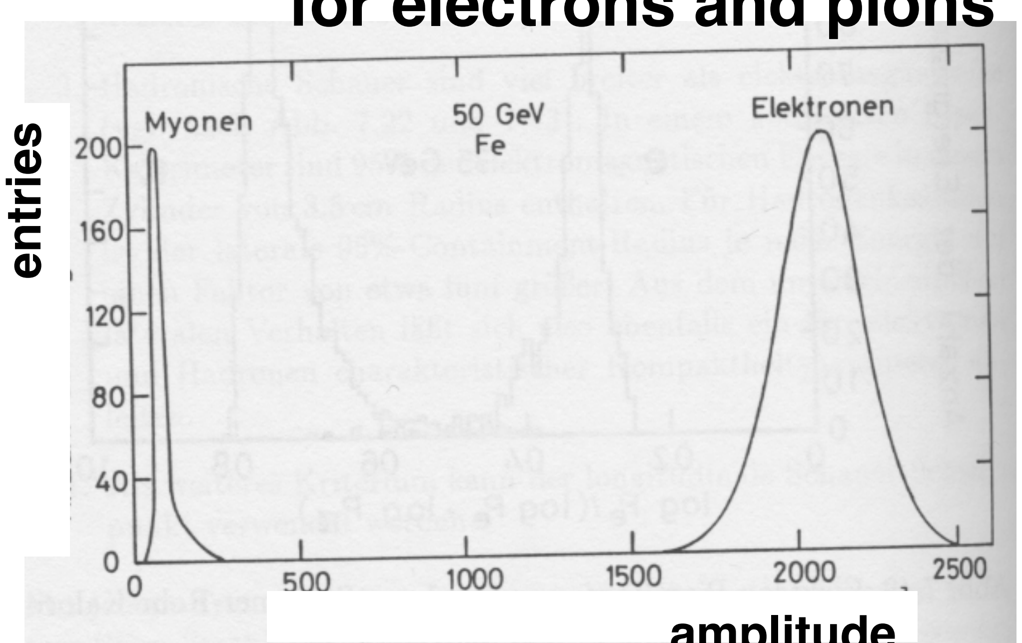

energy deposit for muons and electrons

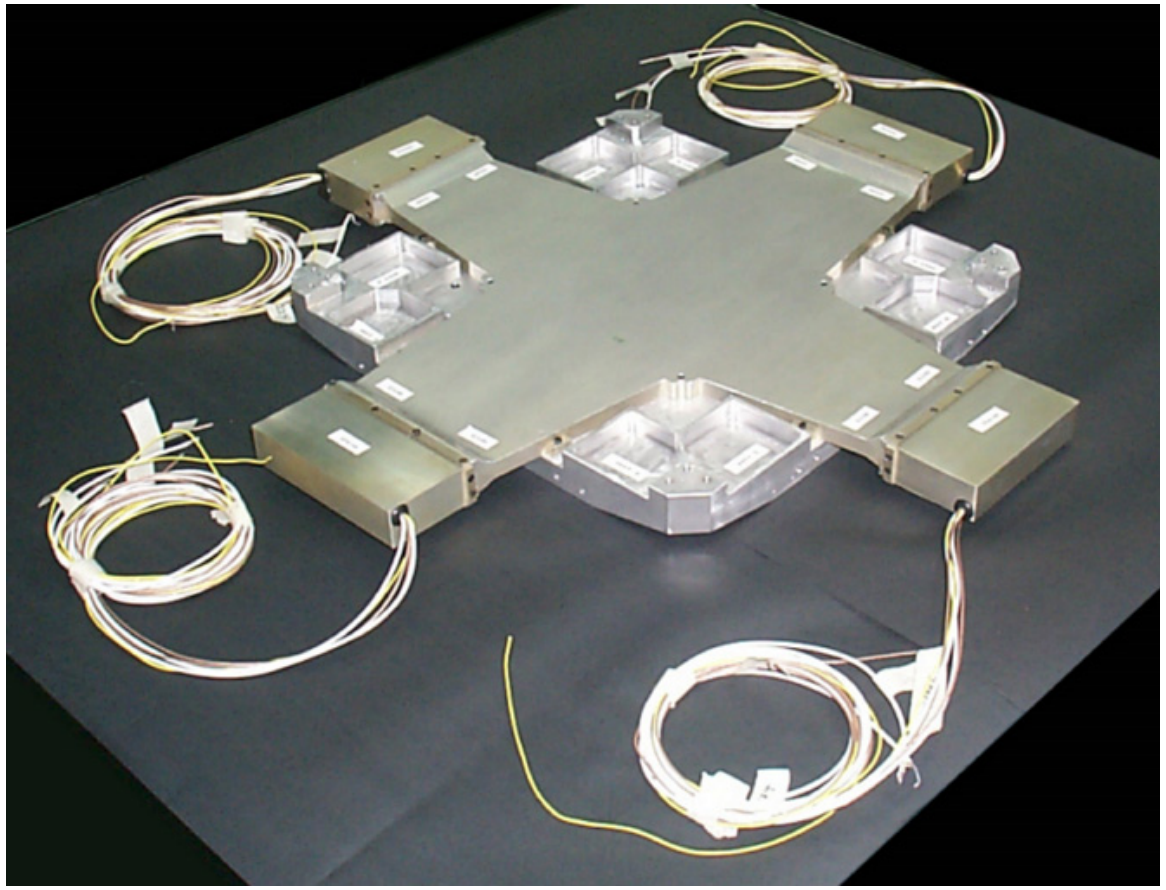

Fig. 2. A picture of the S2 plane of the time of flight system. The sensitive area is 15×18 cm^2 segmented into 2×2 orthogonal bars.

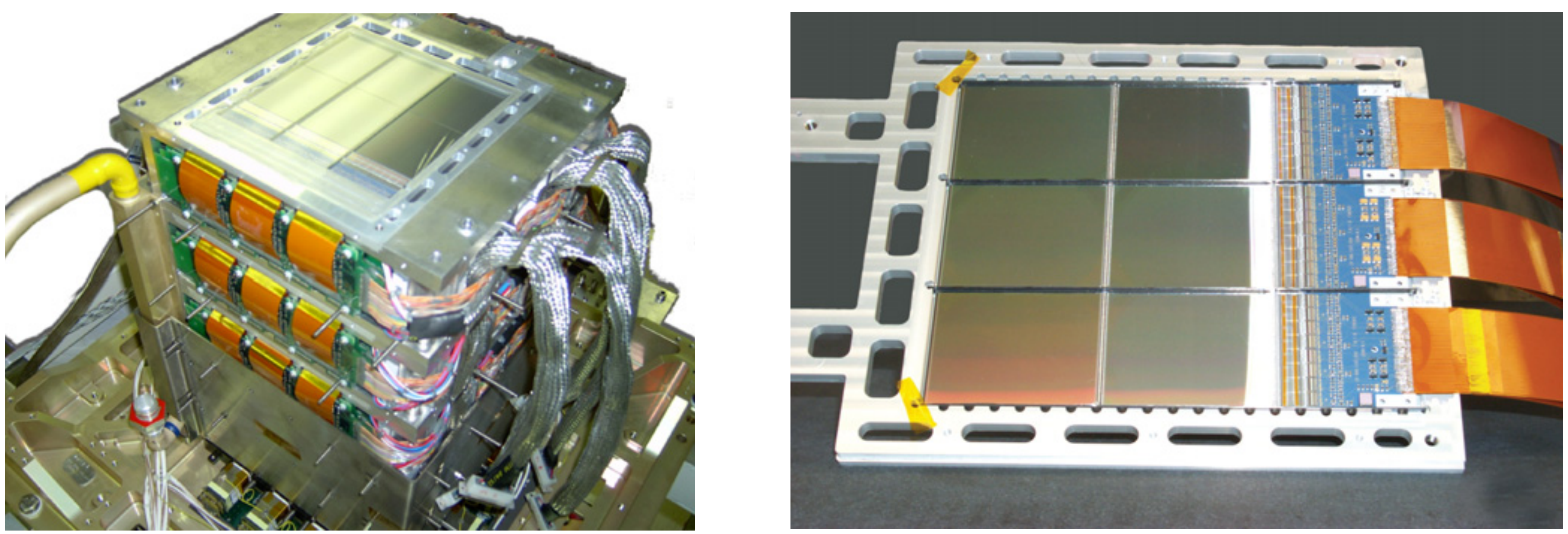

Fig. 3. Left: an overview of the magnetic spectrometer showing the top silicon plane. The magnet cavity has dimensions 13.1×16.1 cm^2. The lower part of the magnet canister is covered by a magnetic screen. Right: a silicon plane comprising six silicon strip detectors and front-end electronics.

Contents lists available at ScienceDirect

Physics Reports

journal homepage: www.elsevier.com/locate/physrep

The PAMELA Mission: Heralding a new era in precision cosmic ray physics

O. Adriani [a,b], G.C. Barbarino [c,d], G.A. Bazilevskaya [e], R. Bellotti [f,g], M. Boezio [h], E.A. Bogomolov [i], M. Bongi [a,b], V. Bonvicini [h], S. Bottai [b], A. Bruno [f,g], F. Cafagna [g], D. Campana [d], R. Carbone [d,h], P. Carlson [j,k], M. Casolino [l], G. Castellini [m], M.P. De Pascale [l,n,1], C. De Santis [l,n], N. De Simone [l], V. Di Felice [l], V. Formato [h,o], A.M. Galper [p], U. Giaccari [d], A.V. Karelin [p], M.D. Kheymits [p], S.V. Koldashov [p], S. Koldobskiy [p], S.Yu. Krut'kov [i], A.N. Kvashnin [e], A. Leonov [p], V. Malakhov [p], L. Marcelli [n], M. Martucci [n,q], A.G. Mayorov [p], W. Menn [r], V.V. Mikhailov [p], E. Mocchiutti [h], A. Monaco [f,g], N. Mori [a,b], R. Munini [h,j,k,o], N. Nikonov [i,l,n], G. Osteria [d], P. Papini [b], M. Pearce [j,k], P. Picozza [l,n,*], C. Pizzolotto [h,s,t], M. Ricci [q], S.B. Ricciarini [b,m], L. Rossetto [j,k], R. Sarkar [h], M. Simon [r], R. Sparvoli [l,n], P. Spillantini [a,b], Y.I. Stozhkov [e], A. Vacchi [h], E. Vannuccini [b], G.I. Vasilyev [i], S.A. Voronov [p], J. Wu [j,k,u], Y.T. Yurkin [p], G. Zampa [h], N. Zampa [h], V.G. Zverev [p]

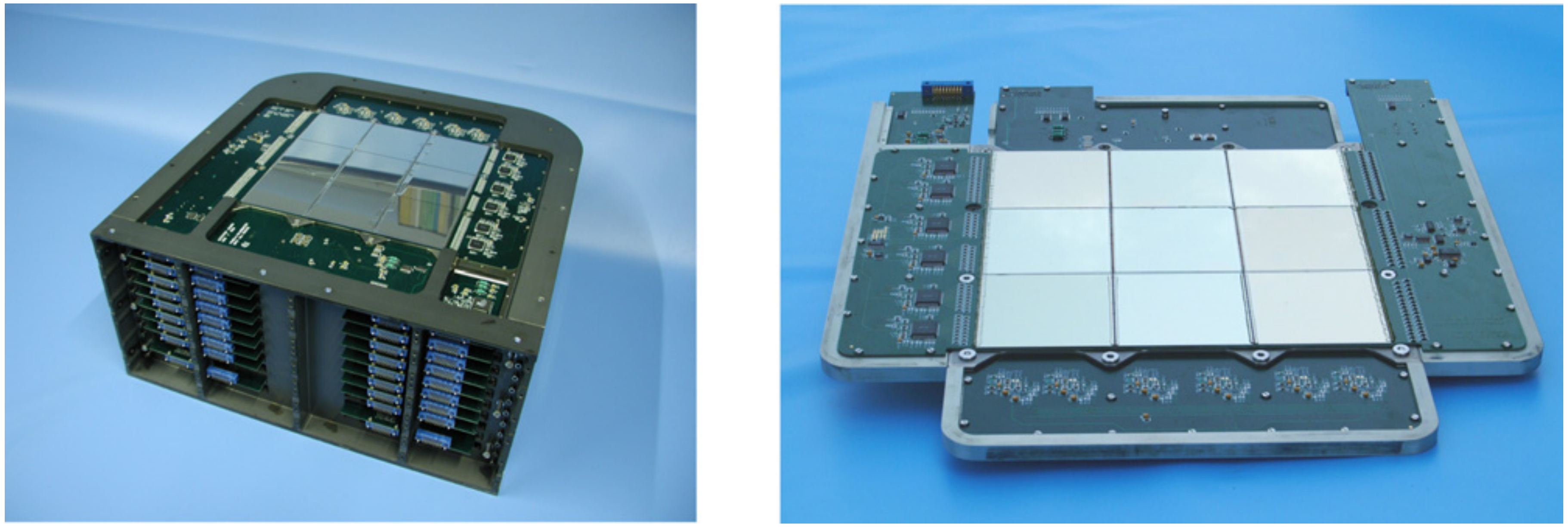

Fig. 4. Left: The PAMELA electromagnetic calorimeter with the topmost silicon plane visible. The device is ∼20 cm tall and the active silicon layer is ∼24×24 cm^2 in cross-section. Right: Details of a single calorimeter module comprising two tungsten layers each sandwiched between two silicon detector planes.

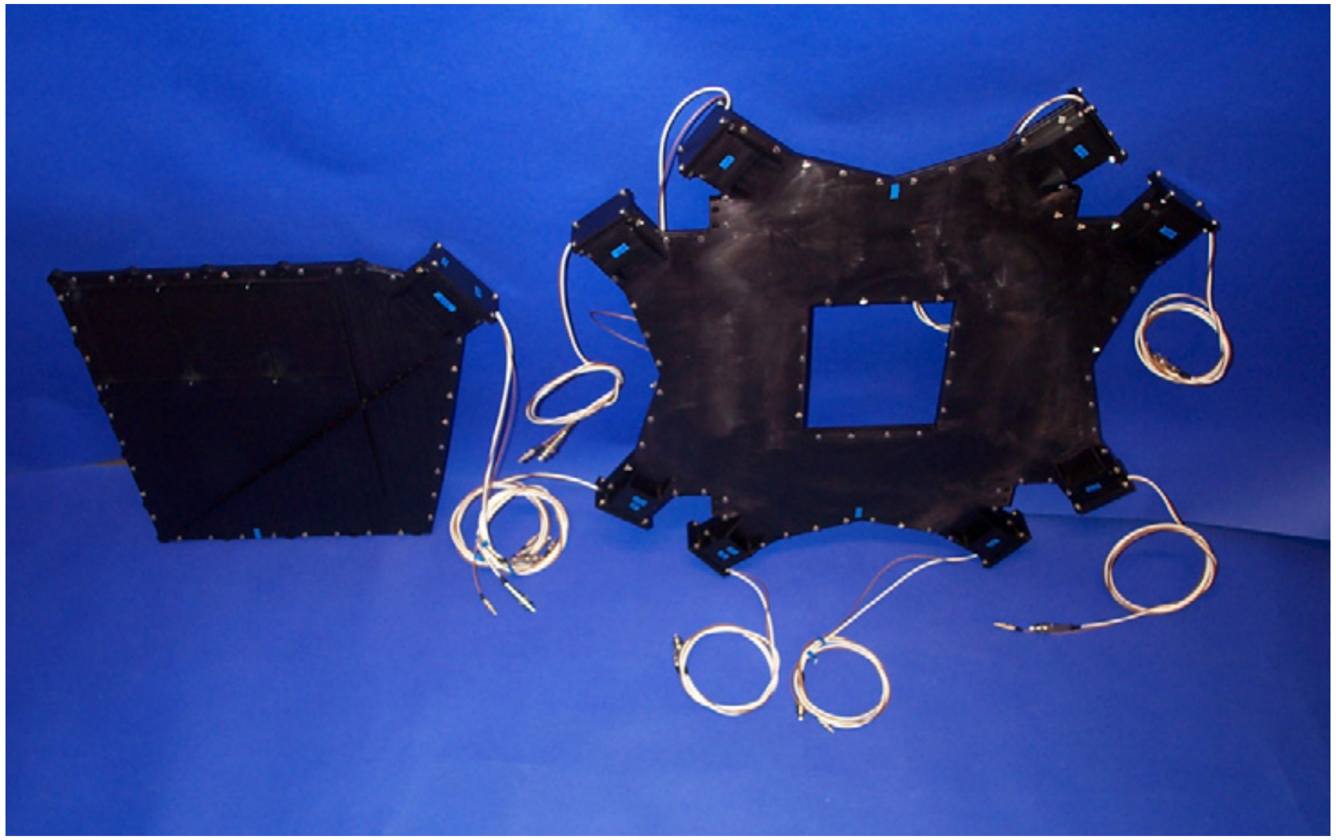

Fig. 5. An overview of the anticoincidence system. The CARD system is not shown but the design closely follows that of CAS. The CAS scintillator (on the left) is approximately 40 cm tall and 33 cm wide. The hole in the CAT scintillator (on the right) measures approximately 22 cm by 18 cm.

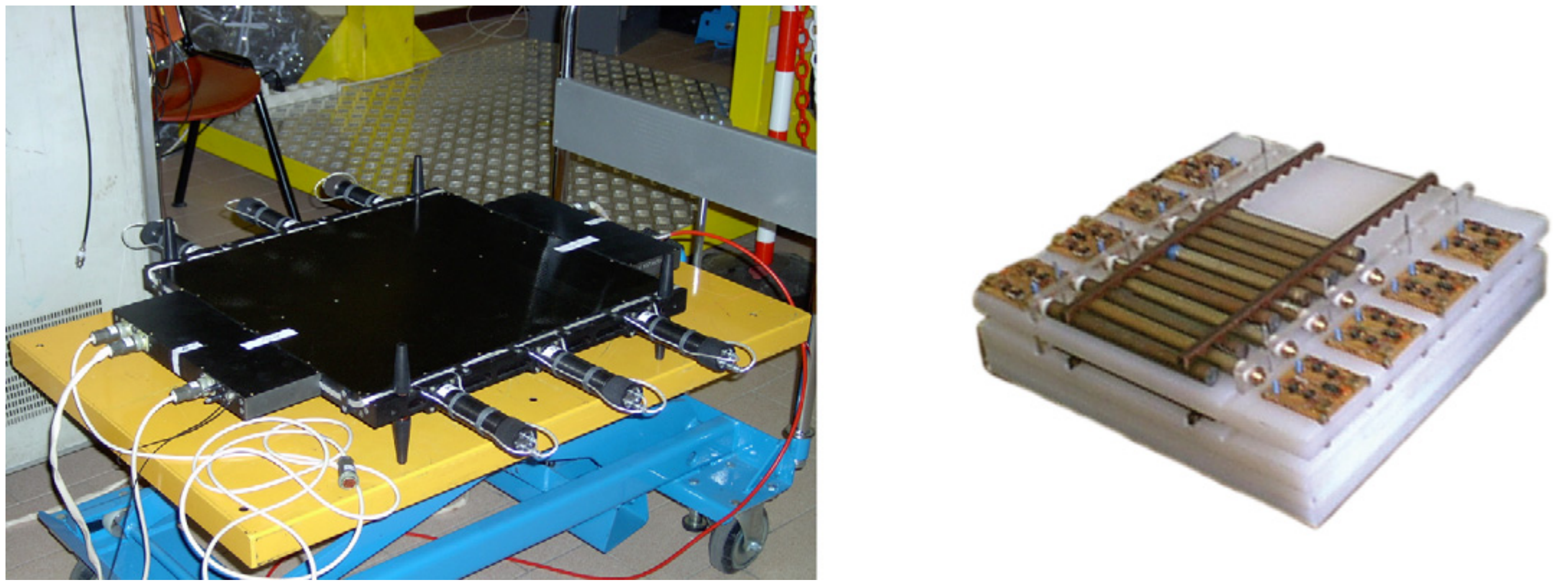

Fig. 6. Left: the shower tail catcher scintillator S4. The scintillator has dimensions 48 × 48 cm^2. Right: The neutron detector equipped (partially in the figure) with ^{3}He proportional counters. The neutron detector covers an area of 60 × 55 cm^2.

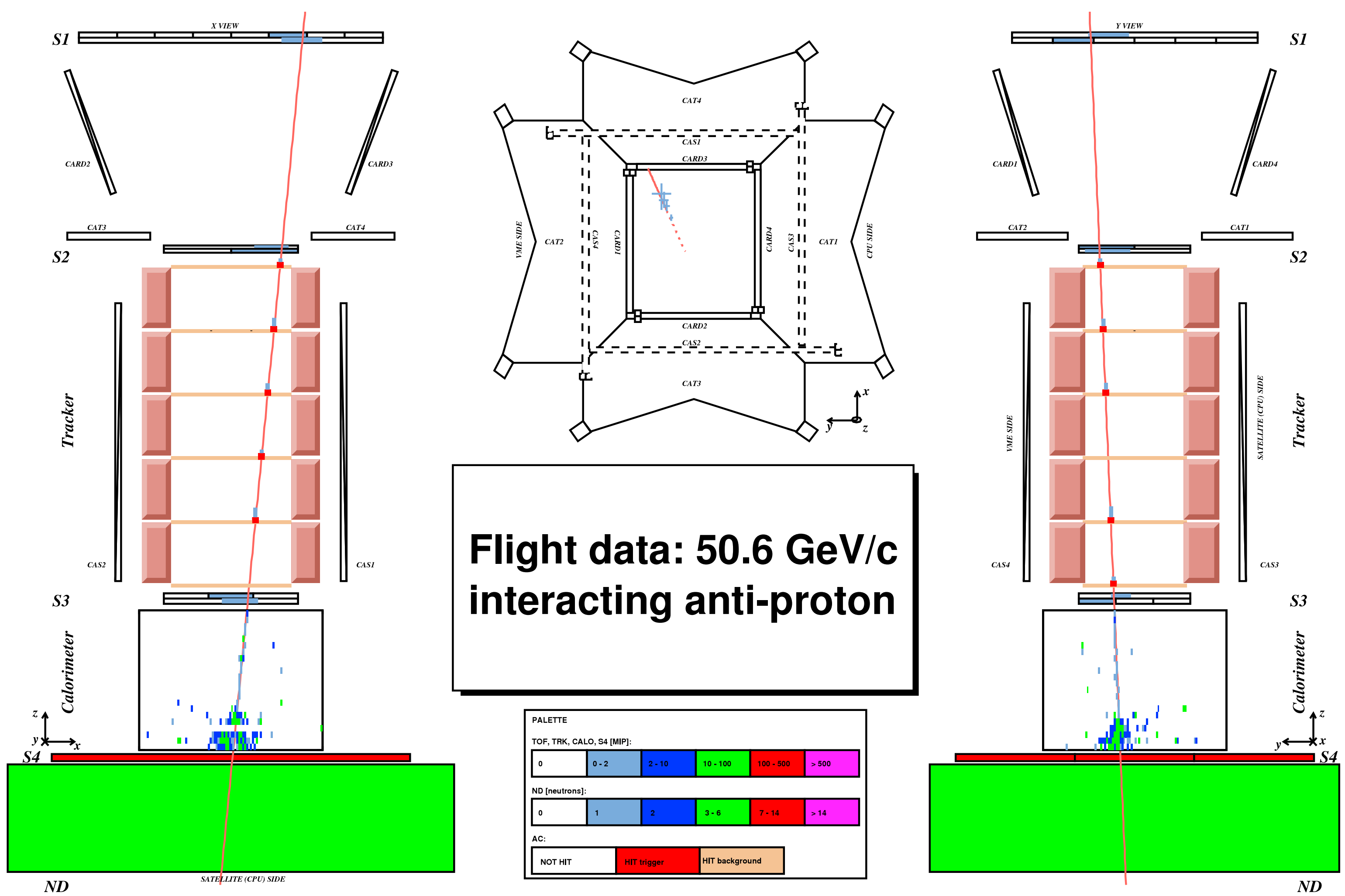

Fig. 7. A particle identified as an antiproton in the PAMELA detector. The charge sign and the rigidity are obtained from the information of the magnetic spectrometer. A hadronic shower is visible in the calorimeter; the neutron detector records neutrons from the hadronic cascade.

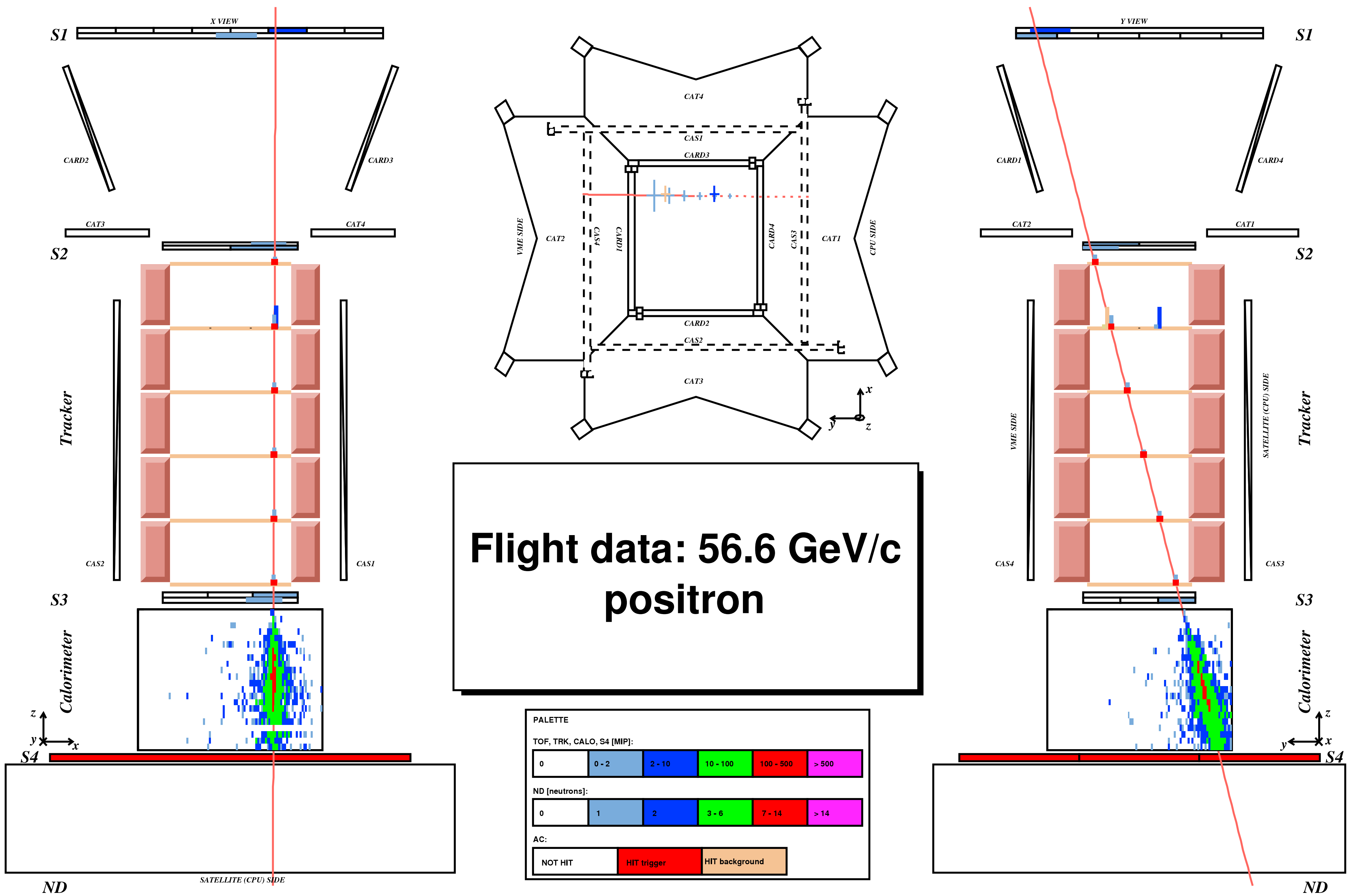

Fig. 8. A particle identified as a positron in the PAMELA detector. The charge sign and the rigidity are obtained from the information of the magnetic spectrometer. An electromagnetic shower is produced in the calorimeter, no neutrons are detected by the neutron detector.

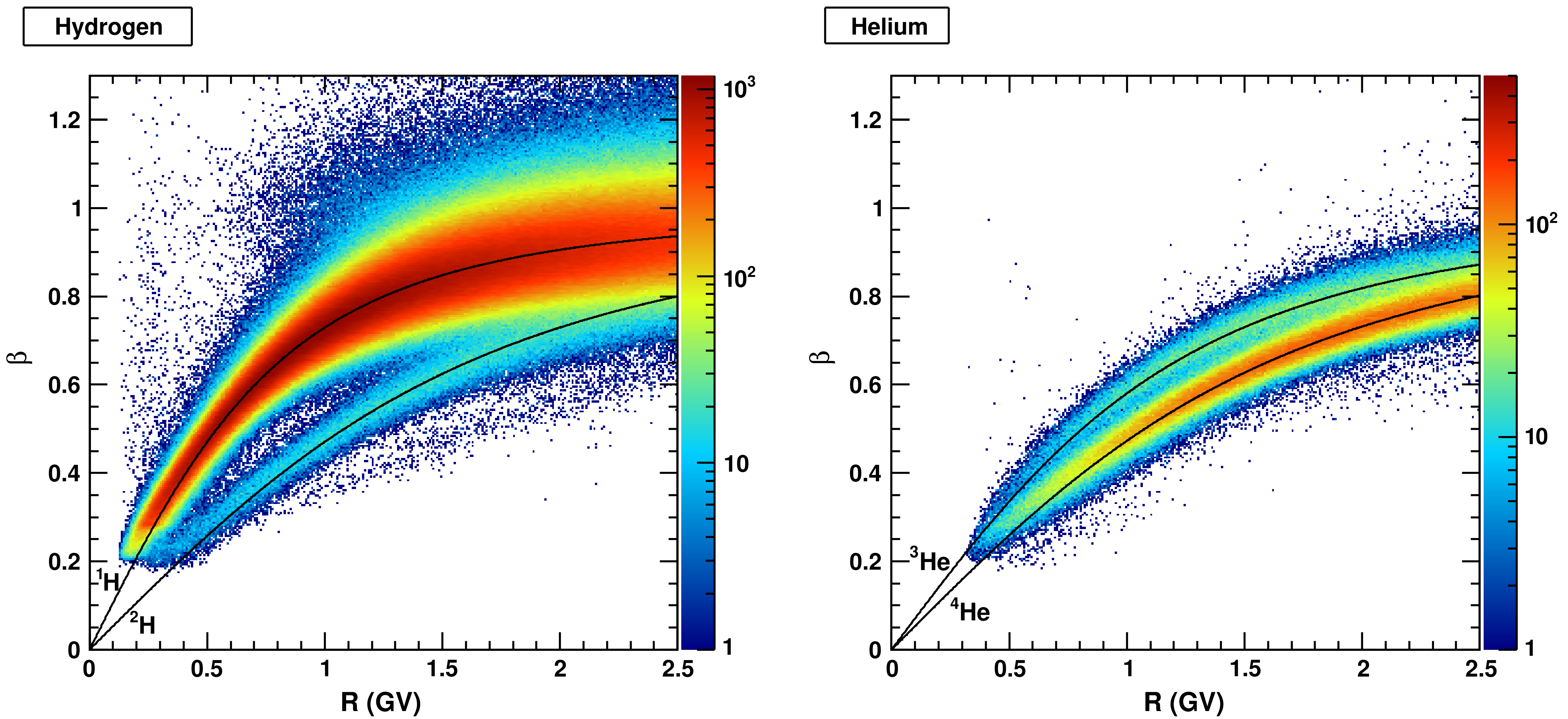

Fig. 29. Velocity versus rigidity showing the mass separation for $Z = 1$ (left) and $Z = 2$ (right) particles. The black lines represent the theoretical isotope curves.

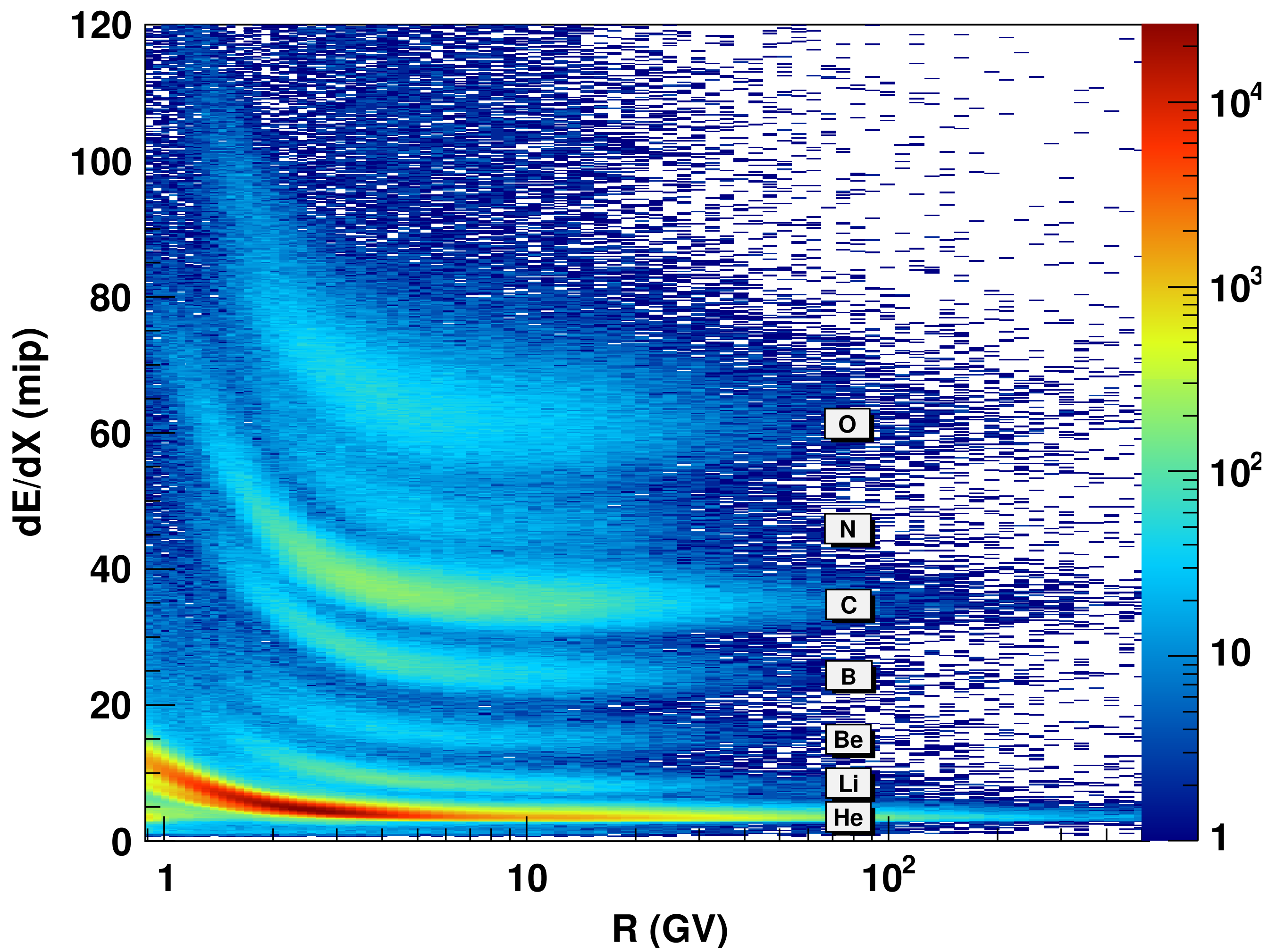

Fig. 32. The averaged dE/dx information on the middle ToF layer (S2) versus the rigidity obtained by the tracking system. Protons have been previously removed from the sample of events used to produce this figure.

Available online at www.sciencedirect.com
ScienceDirect
Nuclear Physics B (Proc. Suppl.) 243–244 (2013) 12–24
NUCLEAR PHYSICS B PROCEEDINGS SUPPLEMENTS
www.elsevier.com/locate/npbps

The Alpha Magnetic Spectrometer on the International Space Station

Samuel Ting[a]

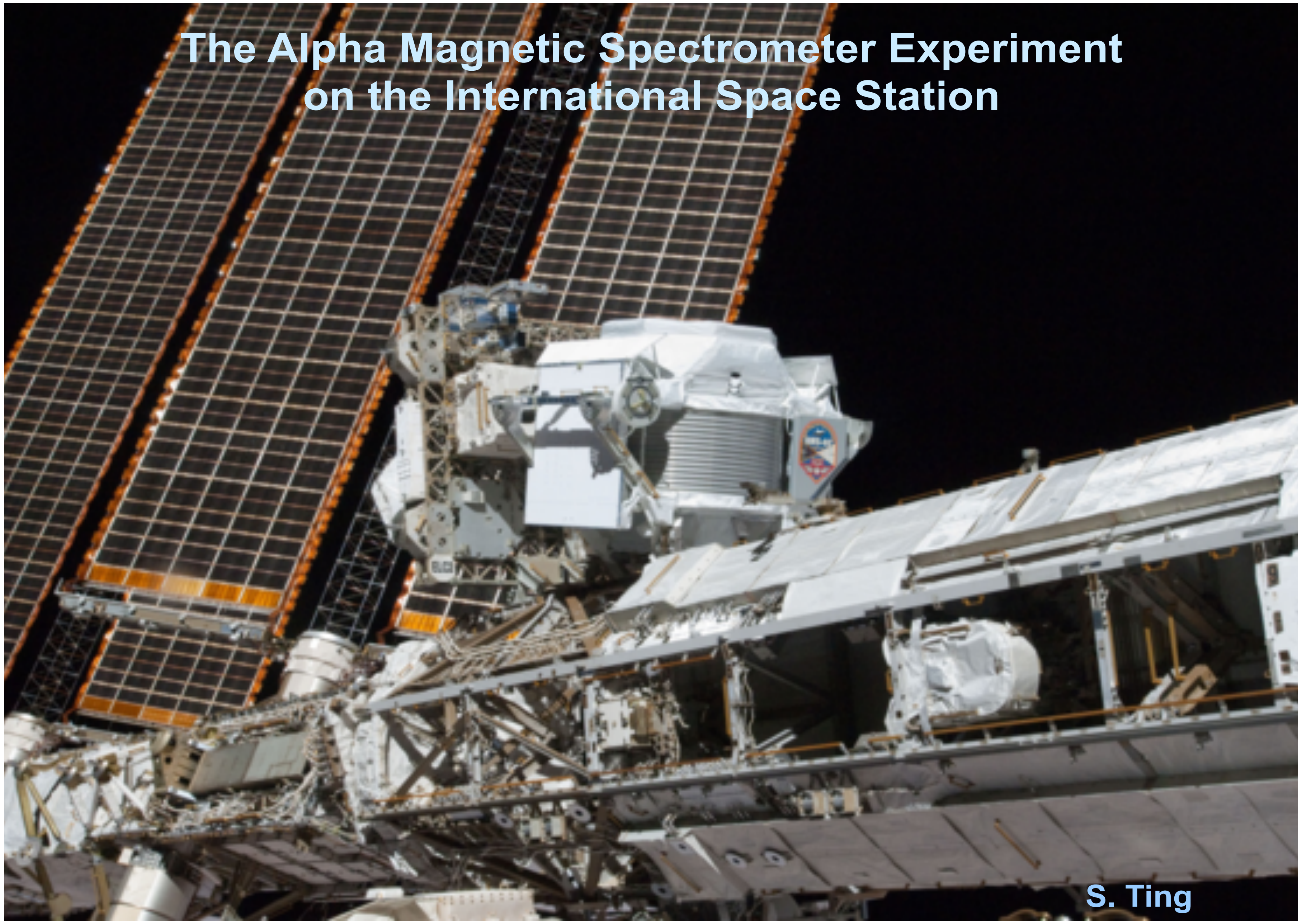

Fig. 1. AMS was delivered and installed on the ISS in May 2011.

AMS: A TeV precision, multipurpose spectrometer

Particles and nuclei are defined by their charge (**Z**) and energy (**E ~ P**)

TRD
Identify e^+, e^-

TOF
Z, E

Silicon Tracker
Z, P

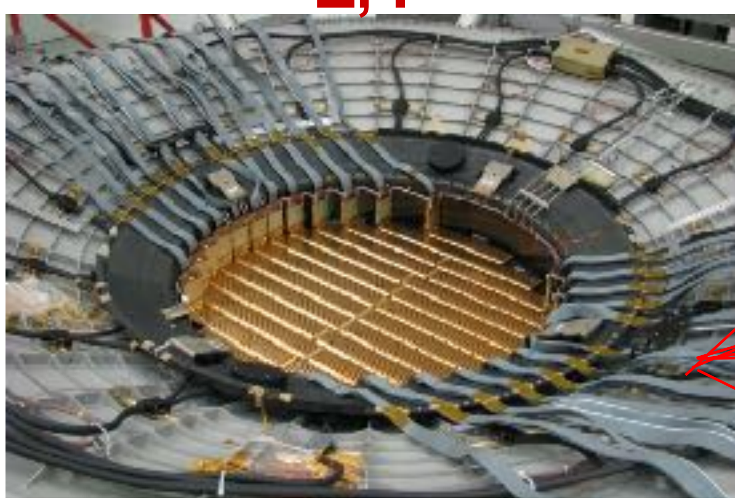

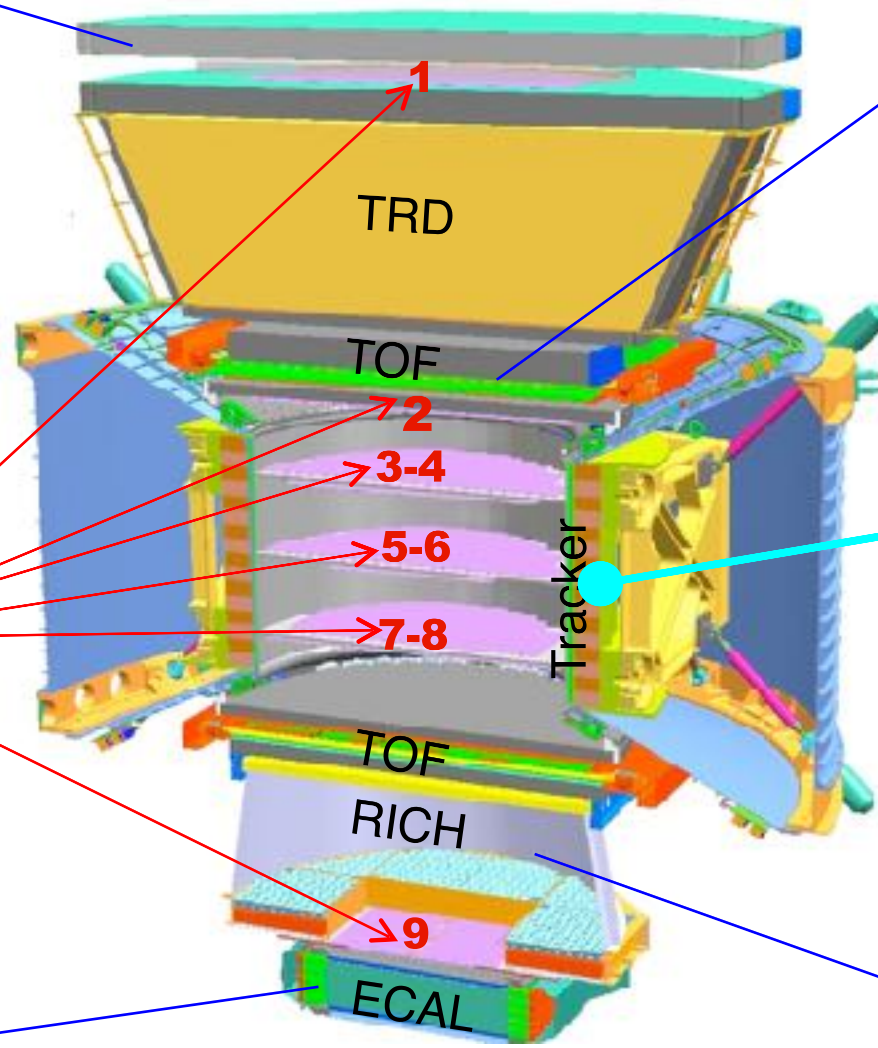

Magnet
±Z

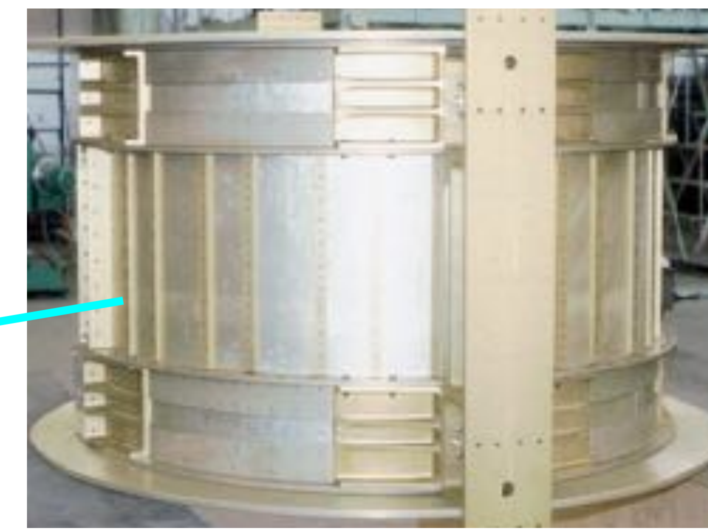

ECAL
E of e^+, e^-, γ

RICH
Z, E

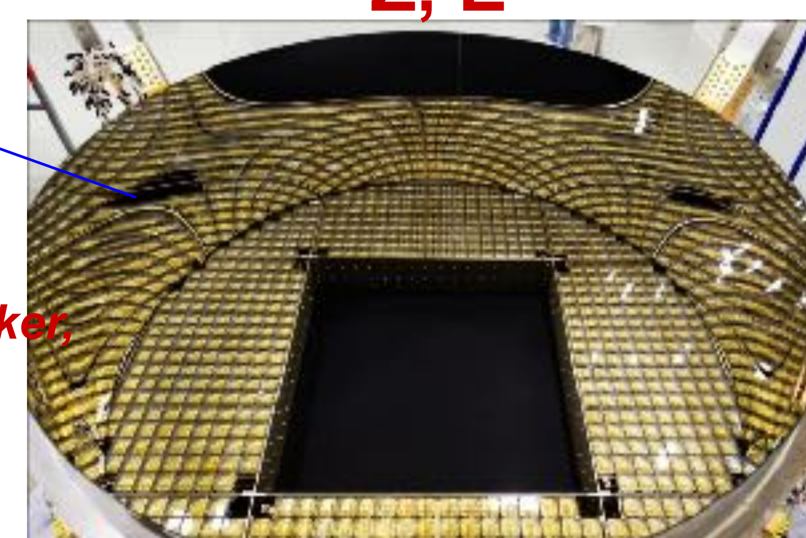

***Z, P** are measured independently by the Tracker, RICH, TOF and ECAL*

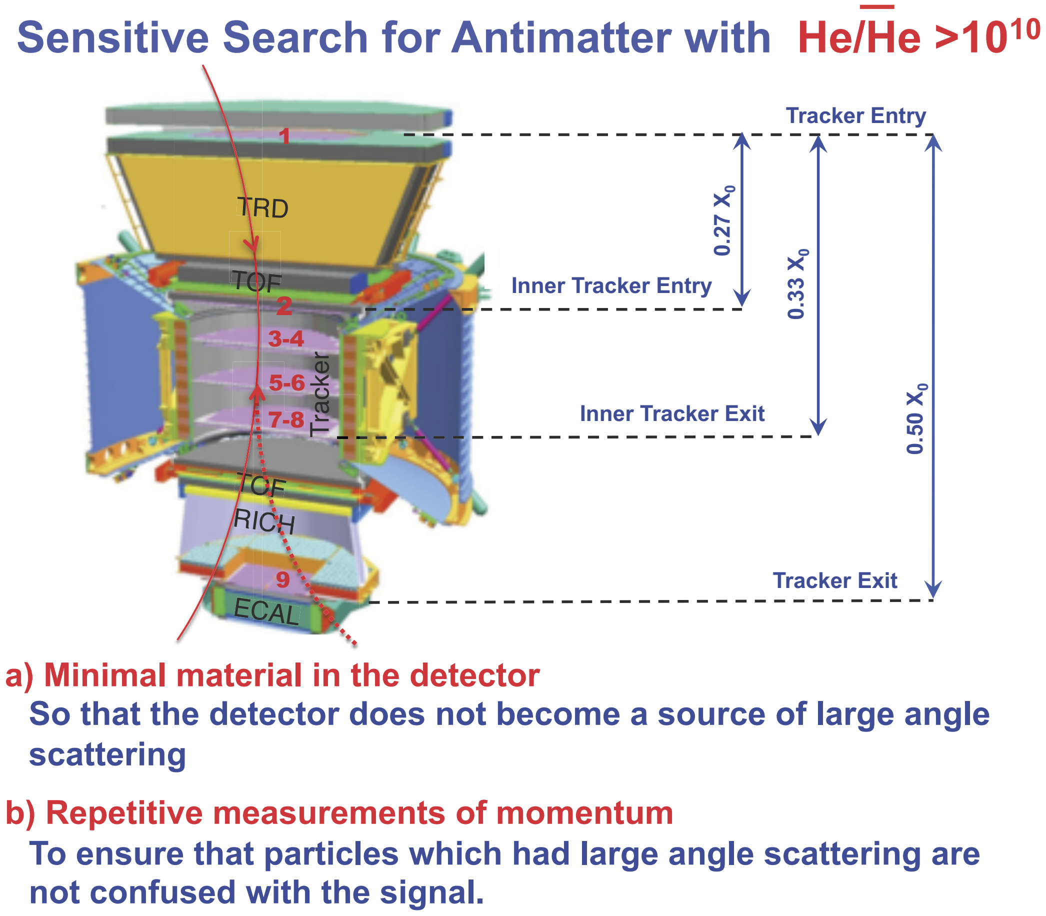

Fig. 4. High sensitivity search for antimatter is a goal of AMS.

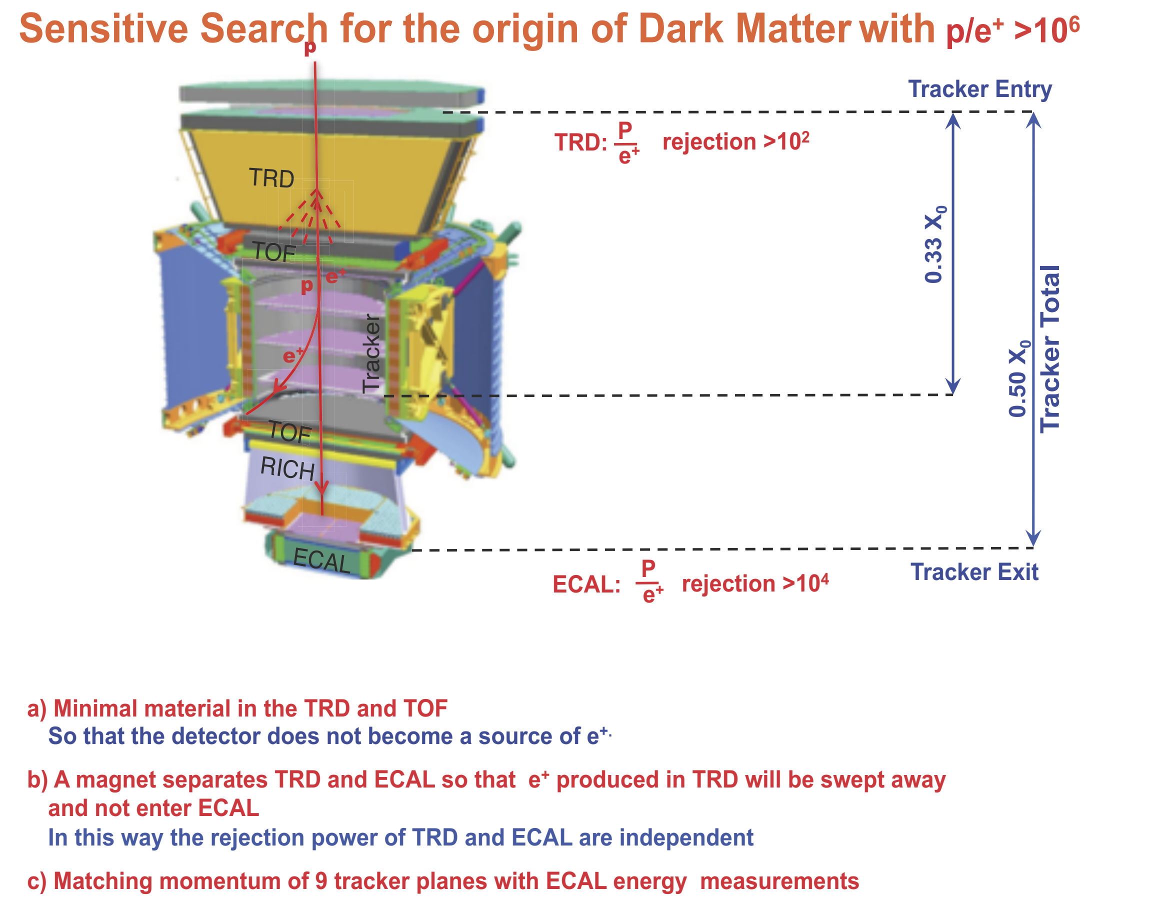

Fig. 6. High sensitivity search for Dark Matter is a goal of AMS.

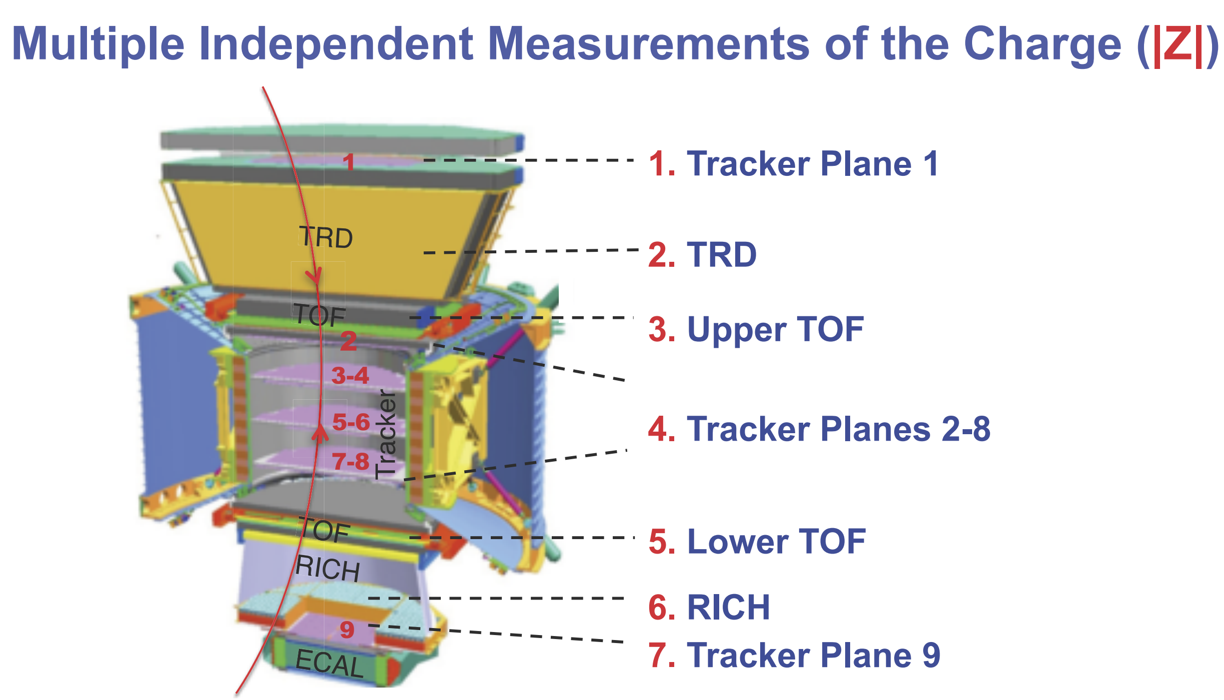

Fig. 5. Multiple independent measurements of the charge of passing particles.

Alpha Magnetic Spectrometer - AMS

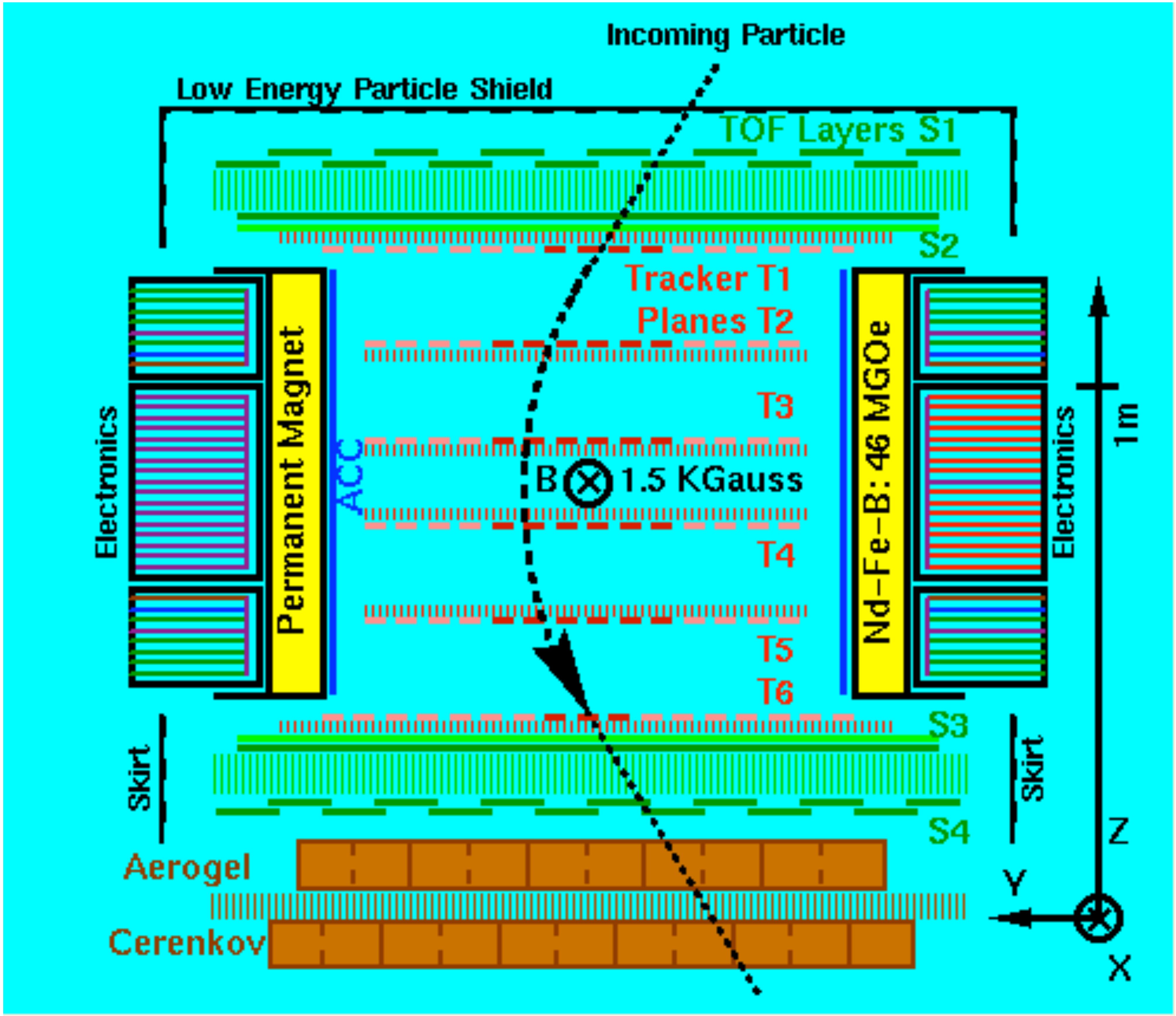

Test Beam Results at CERN 2010

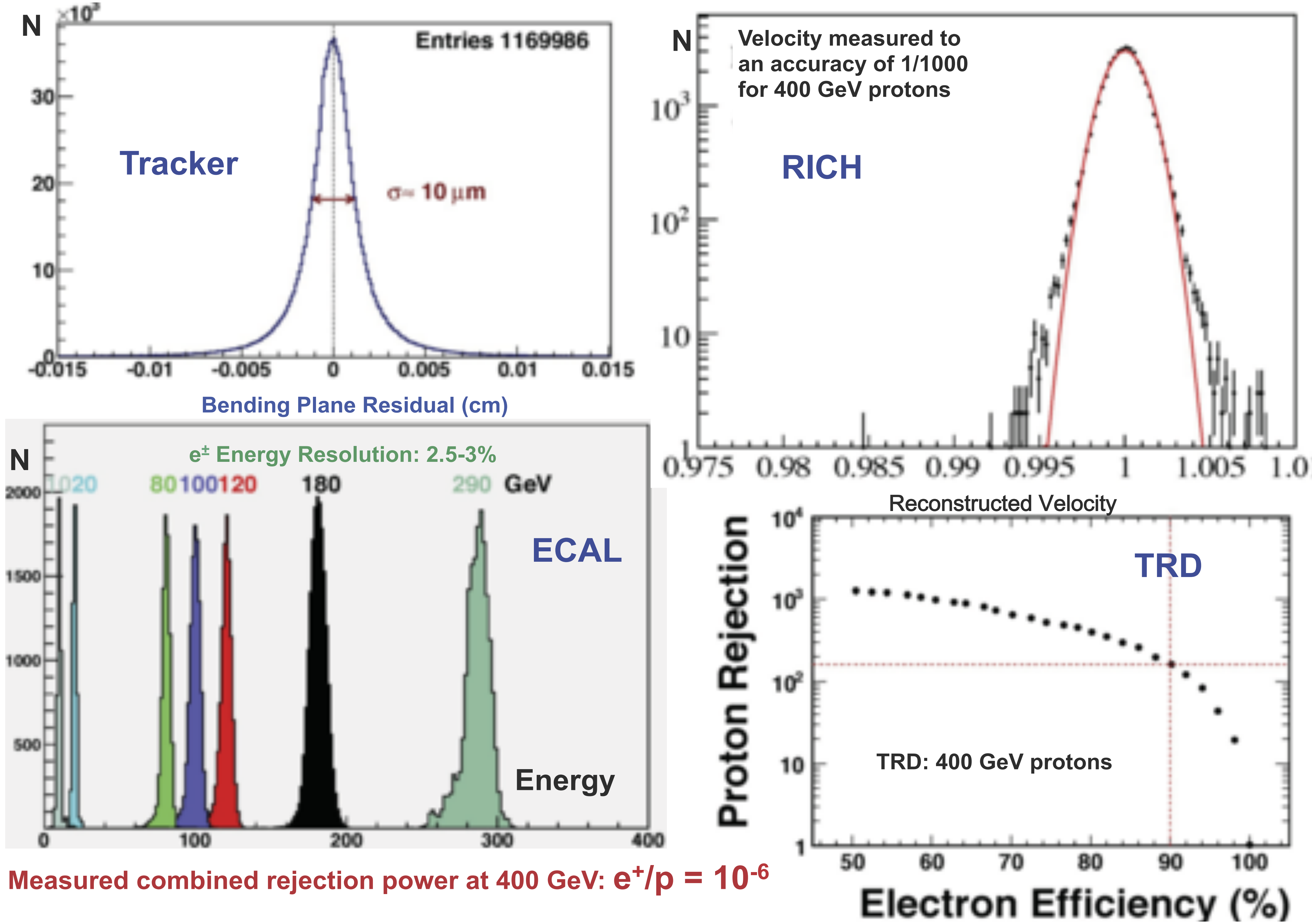

Measured combined rejection power at 400 GeV: $e^+/p = 10^{-6}$

Fig. 7. Major results from the AMS test beam calibration at CERN (2010)

Transition Radiation Detector

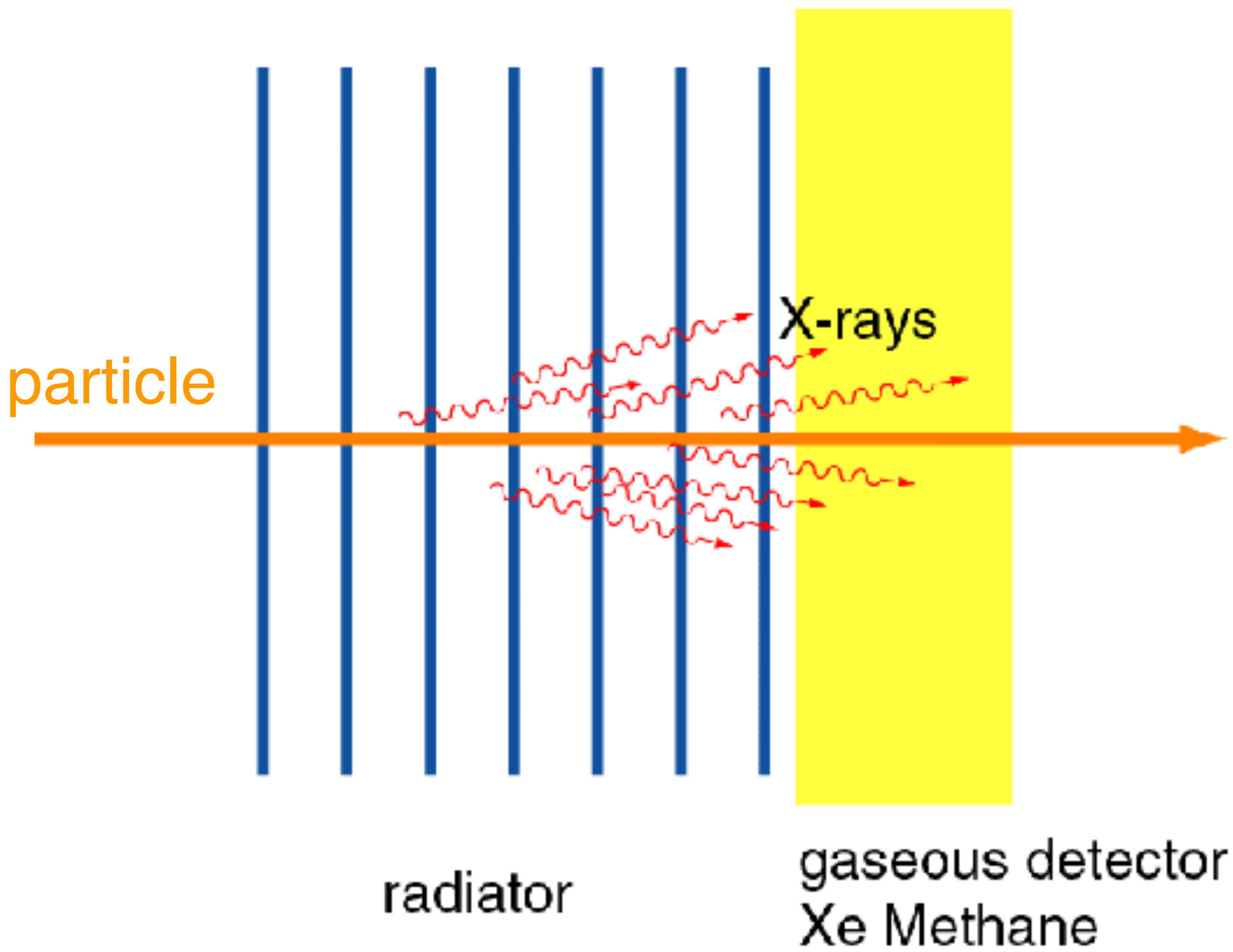

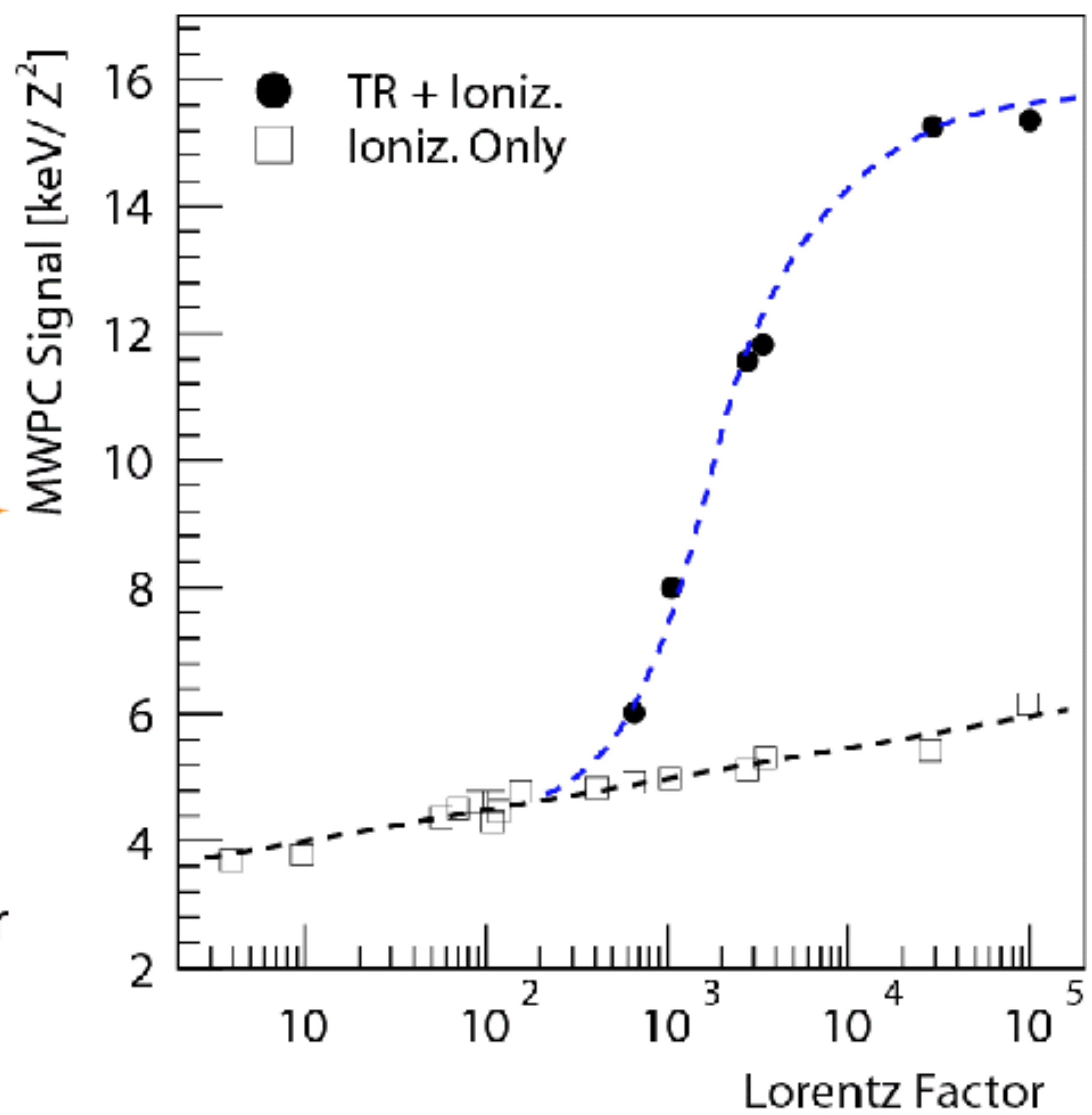

Transition radiation

particles traversing a boundary of media with different dielectric properties
--> emission of transition radiation (below Cherenkov threshold)

differential energy spectrum of emitted x-ray photons

$$\frac{\mathrm{d}^2 W_0}{\mathrm{d}\omega\,\mathrm{d}\theta} = \frac{2\alpha\hbar\theta^3 Z^2}{\pi} \left| \frac{1}{\gamma^{-2} + \theta^2 + \xi_1^2} - \frac{1}{\gamma^{-2} + \theta^2 + \xi_2^2} \right|^2$$

$$\xi_i \equiv \omega_i/\omega$$

ratio of material's plasma frequency to the emitted photon frequency

$$\epsilon_i \approx 1 - \xi_i^2$$

dielectric constant

emission of photons sharply peaked in forward direction $\theta \approx 1/\gamma$

total radiation yield (integrated over all angles and frequencies)

$$W_0 = \frac{\alpha\hbar Z^2}{3} \frac{(\omega_1 - \omega_2)^2}{\omega_1 + \omega_2} \gamma.$$

Transition radiation

interference effects between the emission amplitudes of all media boundaries of a radiator

for N-foil regular stack with constant spacing l_2 and foil thickness l_1

$$\frac{d^2 W_N}{d\omega\, d\theta} = \frac{d^2 W_0}{d\omega\, d\theta} 4 \sin^2\left(\frac{l_1}{z_1}\right) \frac{\sin^2[N(l_1/z_1 + l_2/z_2)]}{\sin^2(l_1/z_1 + l_2/z_2)}.$$

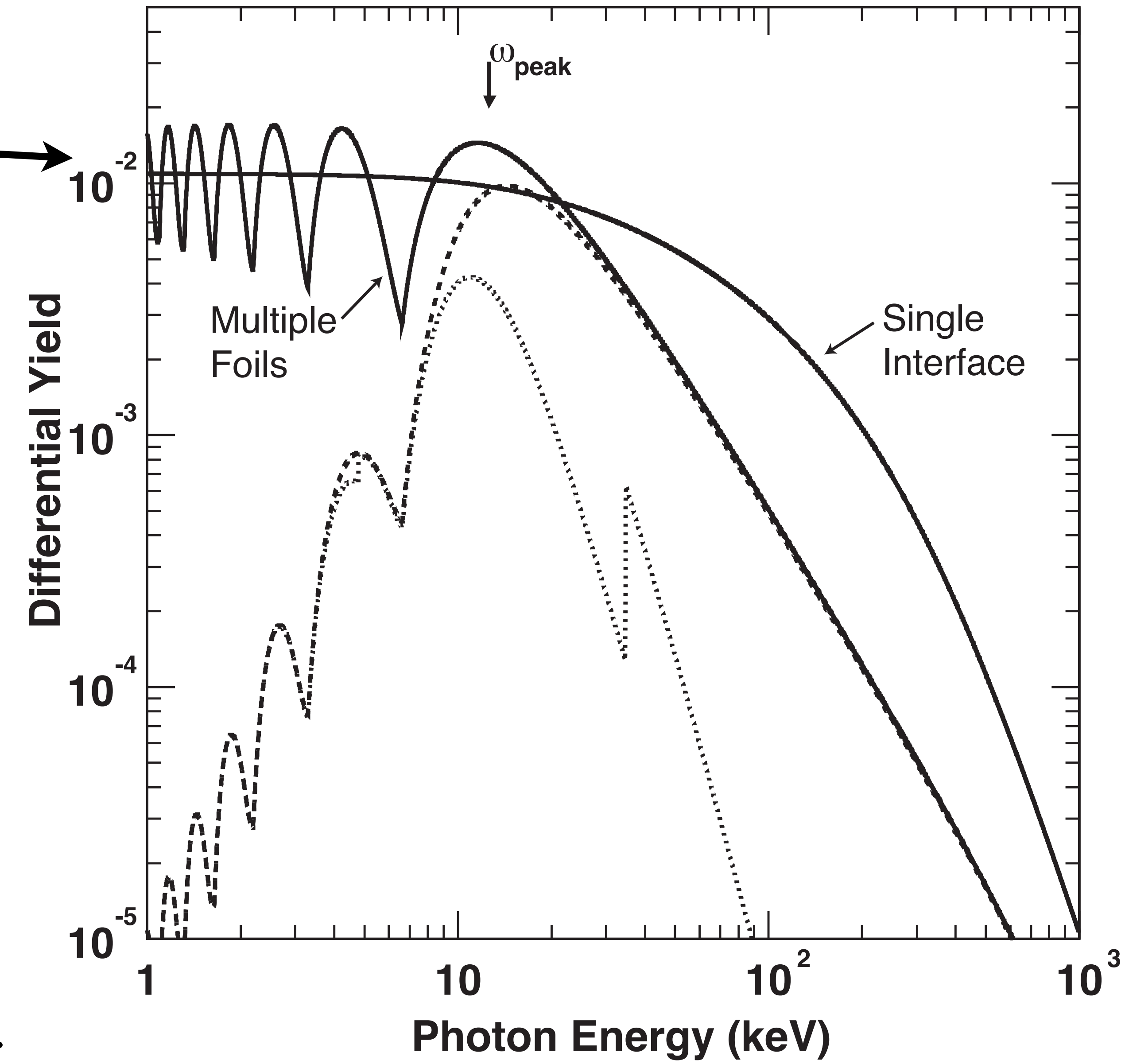

Fig. 1. Differential TR yield ($dW/d\omega$) versus Lorentz factor for several configurations. Shown are the single-interface (smooth line) and approximate multi-foil (oscillating line) energy spectra, as well as the multi-foil spectrum modified by self-absorption processes in the foil (dashed line). The dotted line shows the yield which would be captured in a single 1 cm thick layer of xenon. The characteristic peak emission energy ω_{peak} is also indicated. All spectra are normalized to a single-interface yield. The relevant parameters are $\gamma = 2 \times 10^4$, $l_1 =$ 35 μm, $l_2 = 1000$ μm, $\omega_1 = 21.2$ eV, and $\omega_2 = 0.75$ eV.

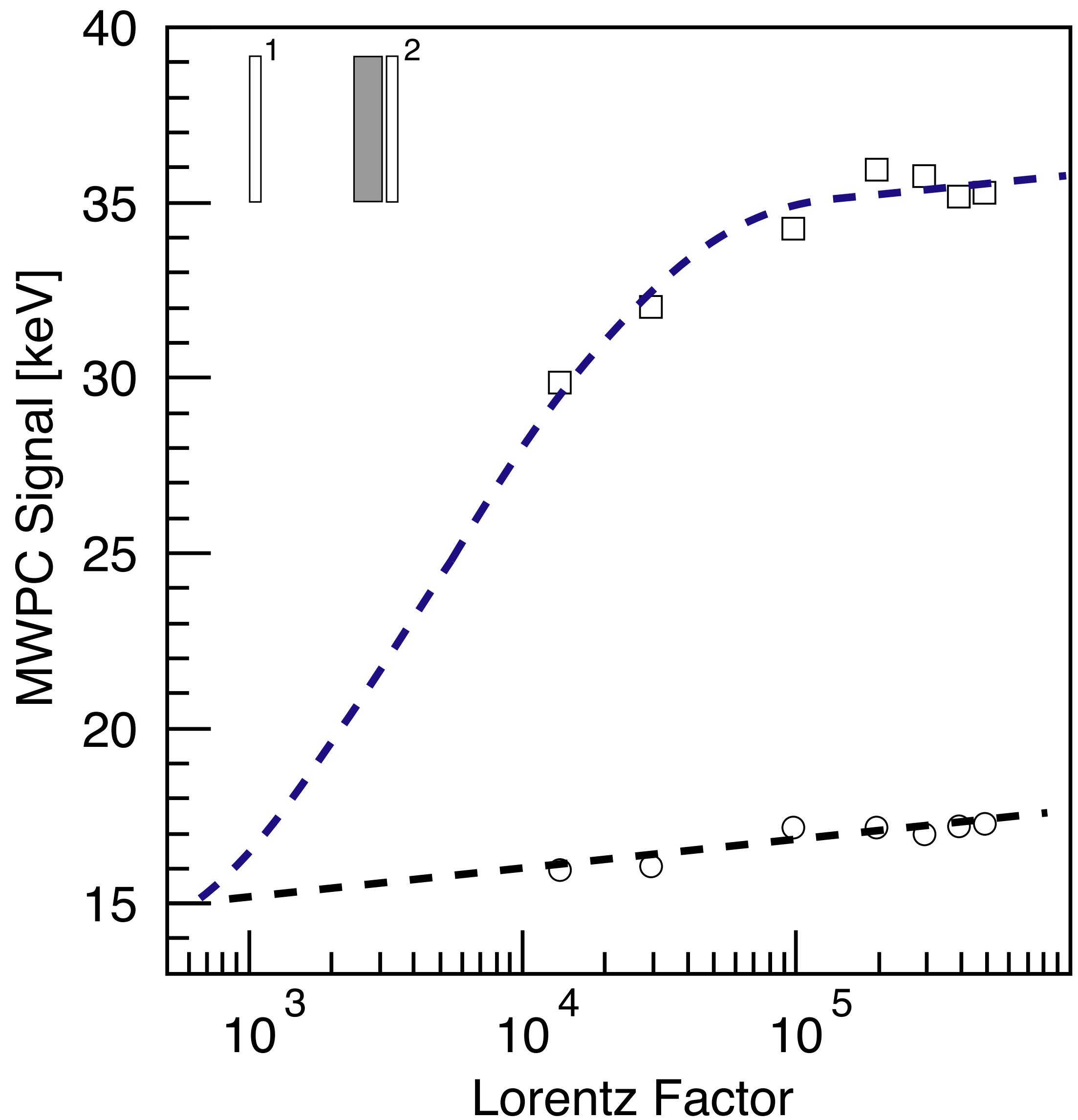

Fig. 8. Average detector signal versus Lorentz factor for a CRN-like radiator configuration. The open circles are data from MWPC 1, and the open squares are from MWPC 2, as shown in the inset schematic. The dashed lines serve to guide the eye.

Transition Radiation Detector

- particle identification (threshold detector)
- energy measurement (Lorentz factor)

TRD test at CERN

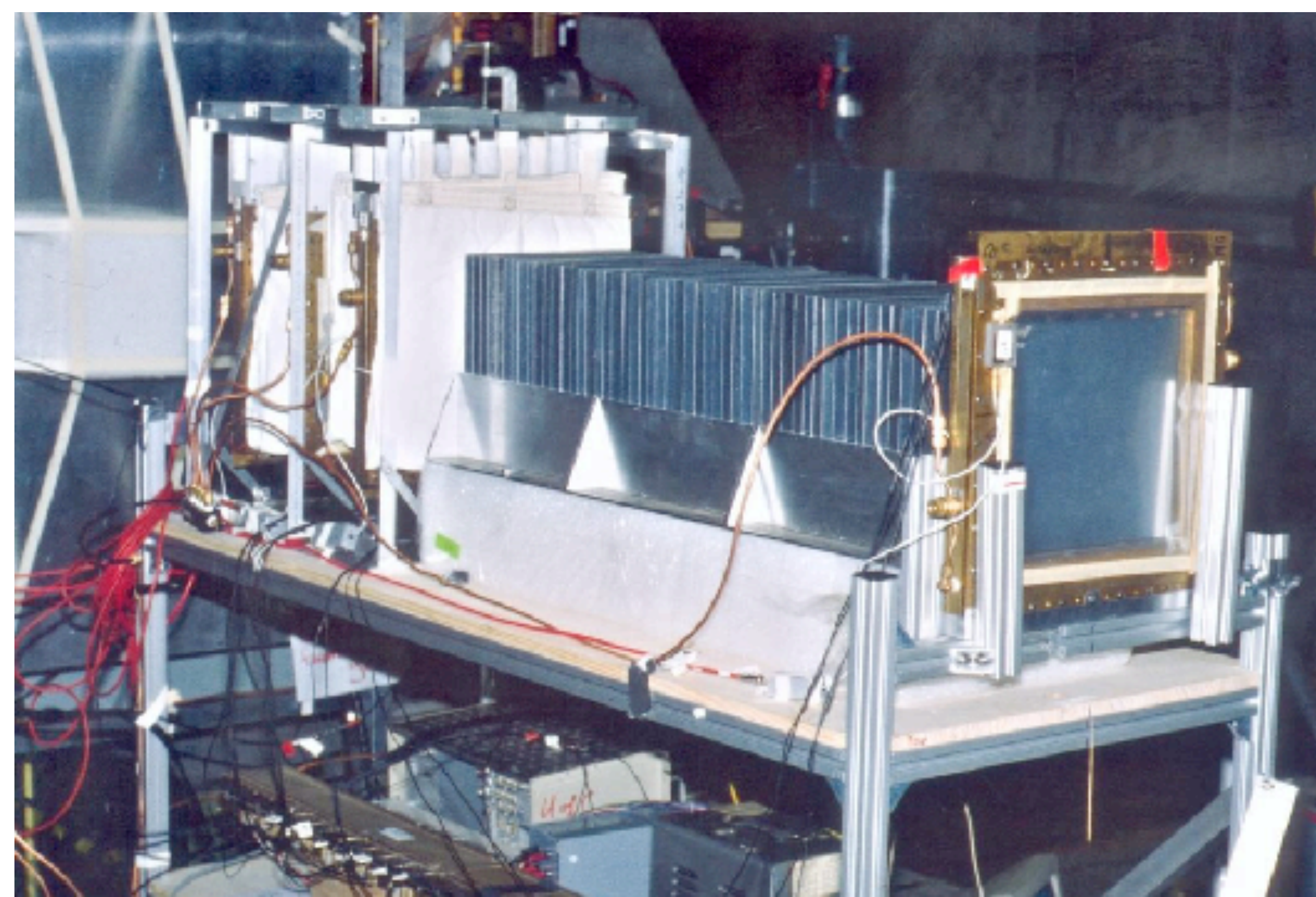

Cosmic Ray Nuclei detector

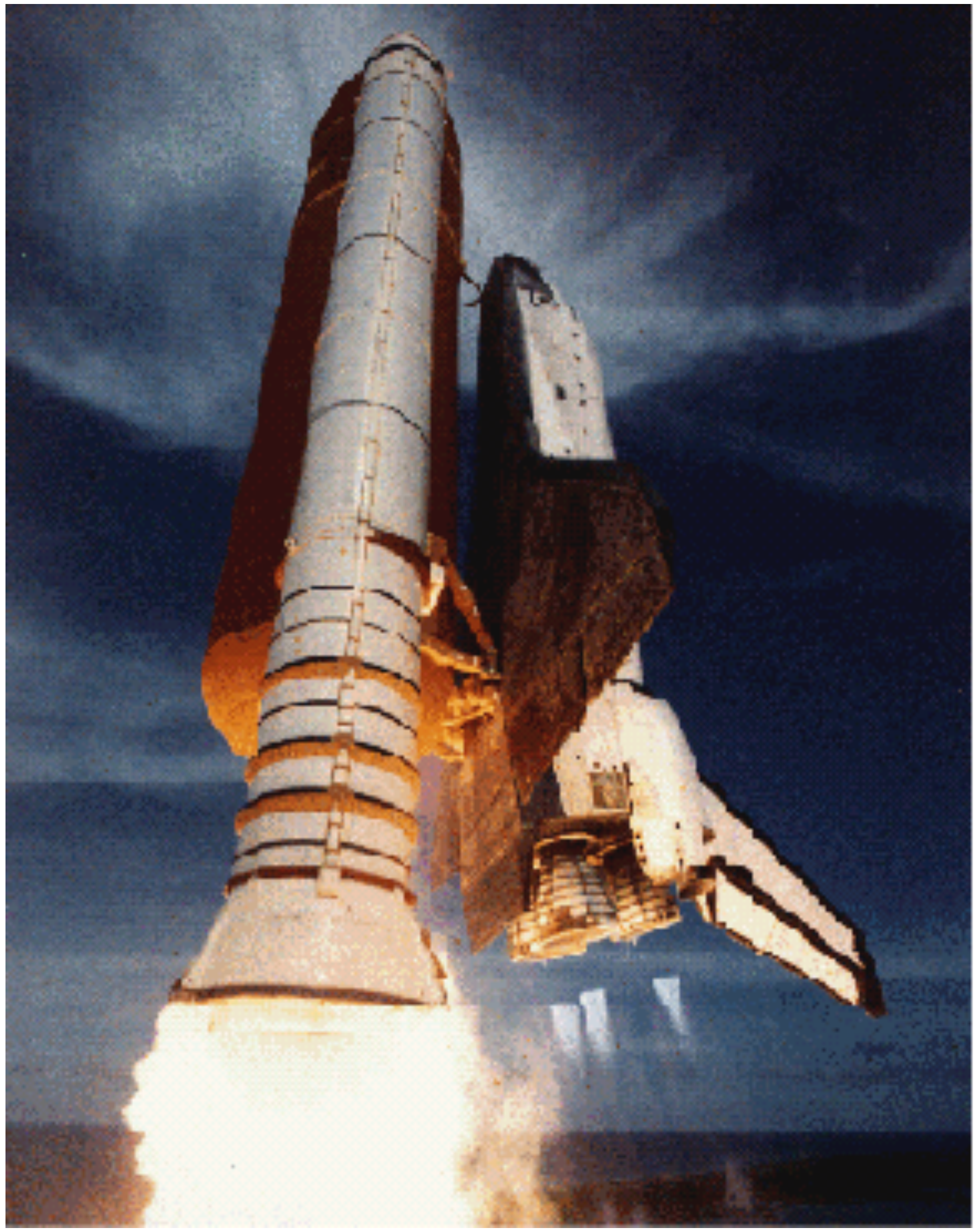

Spaceleb 2 July/August 1985
Spaceshuttle Challenger

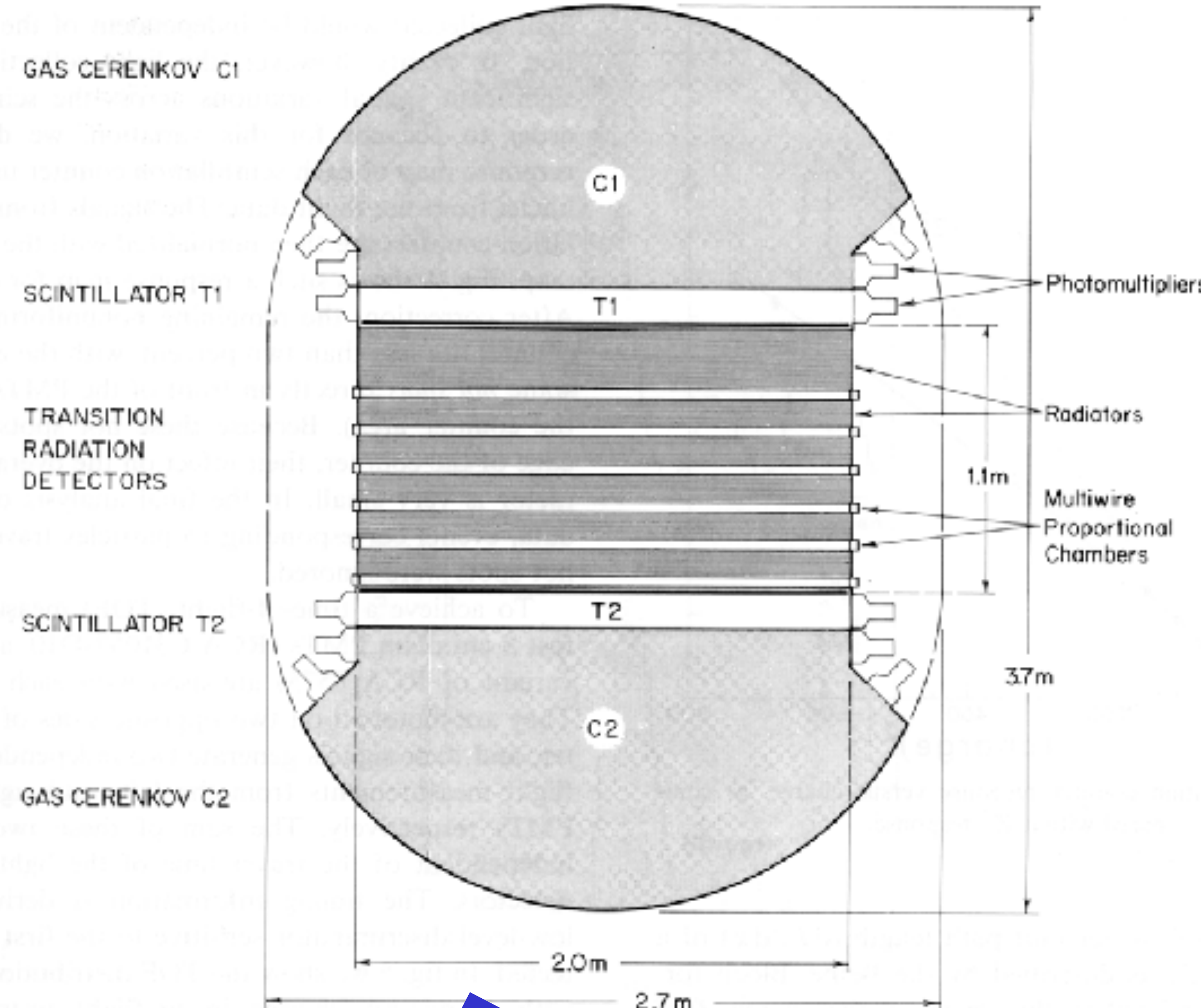

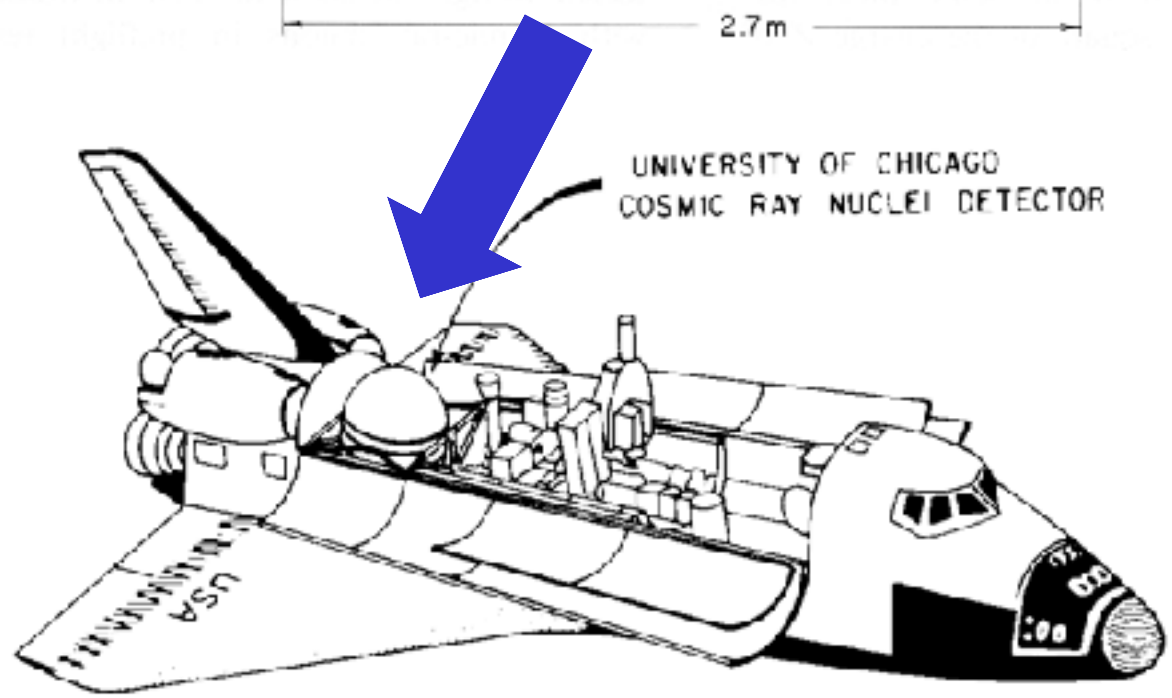

Fig. 14. Schematic view of the Spacelab-2 instruments mounted in the orbiter.

NIM A 295 (1990) 246

Transition Radiation Array for Cosmic Energetic Rays

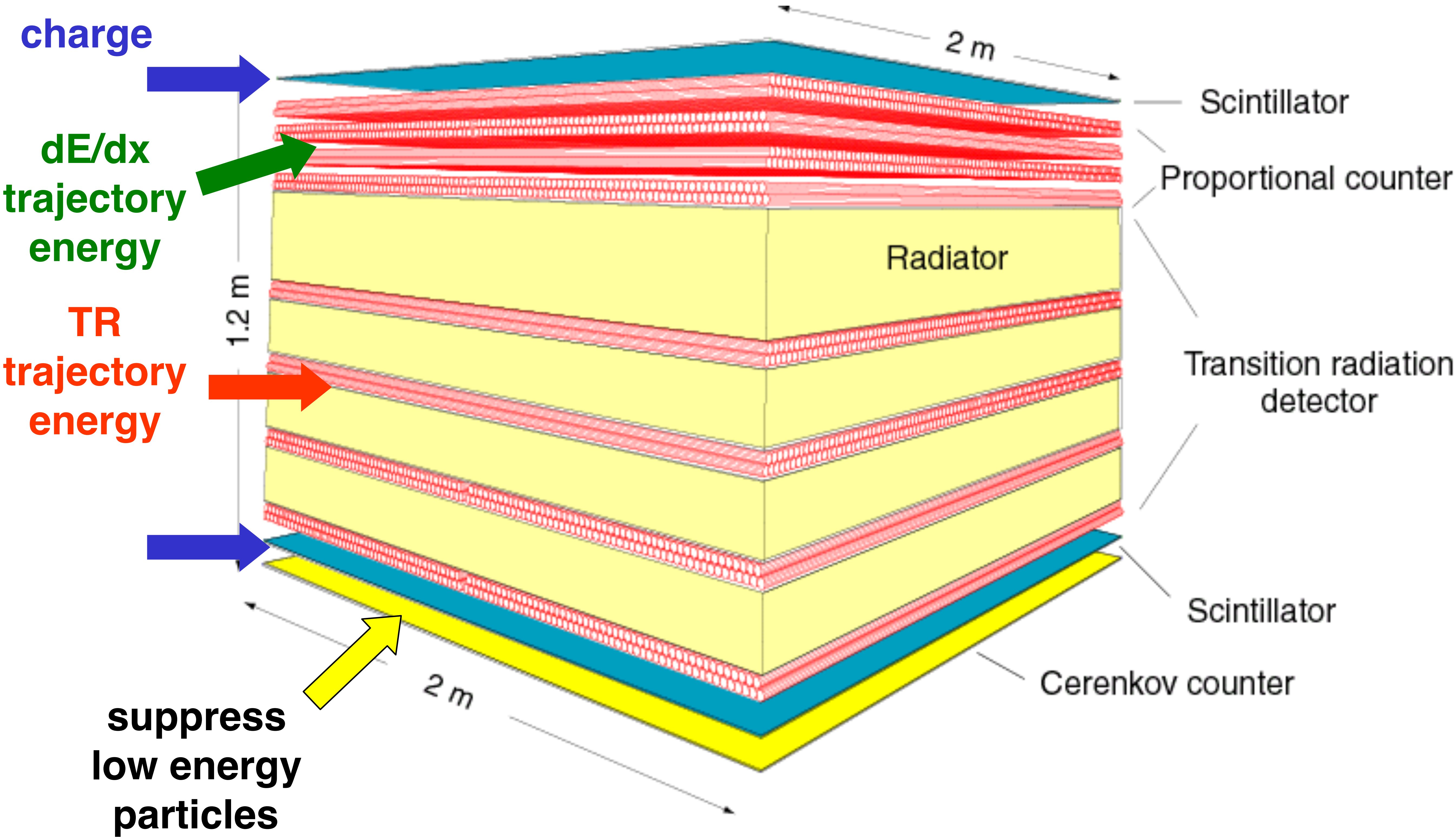

Geometric factor: 5 m² sr

1600 proportional tubes total

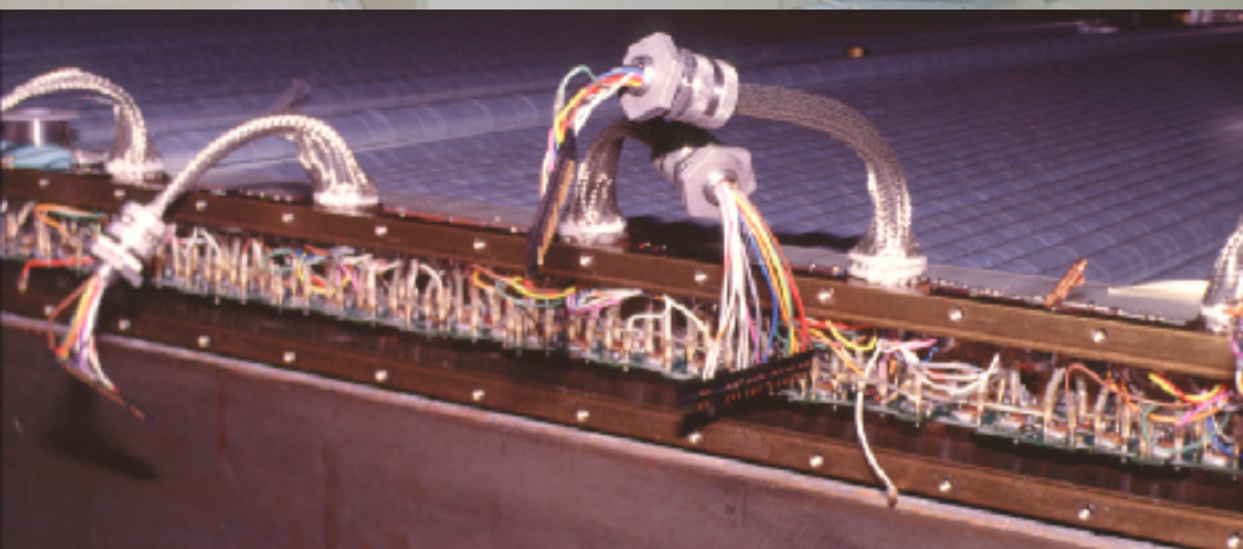

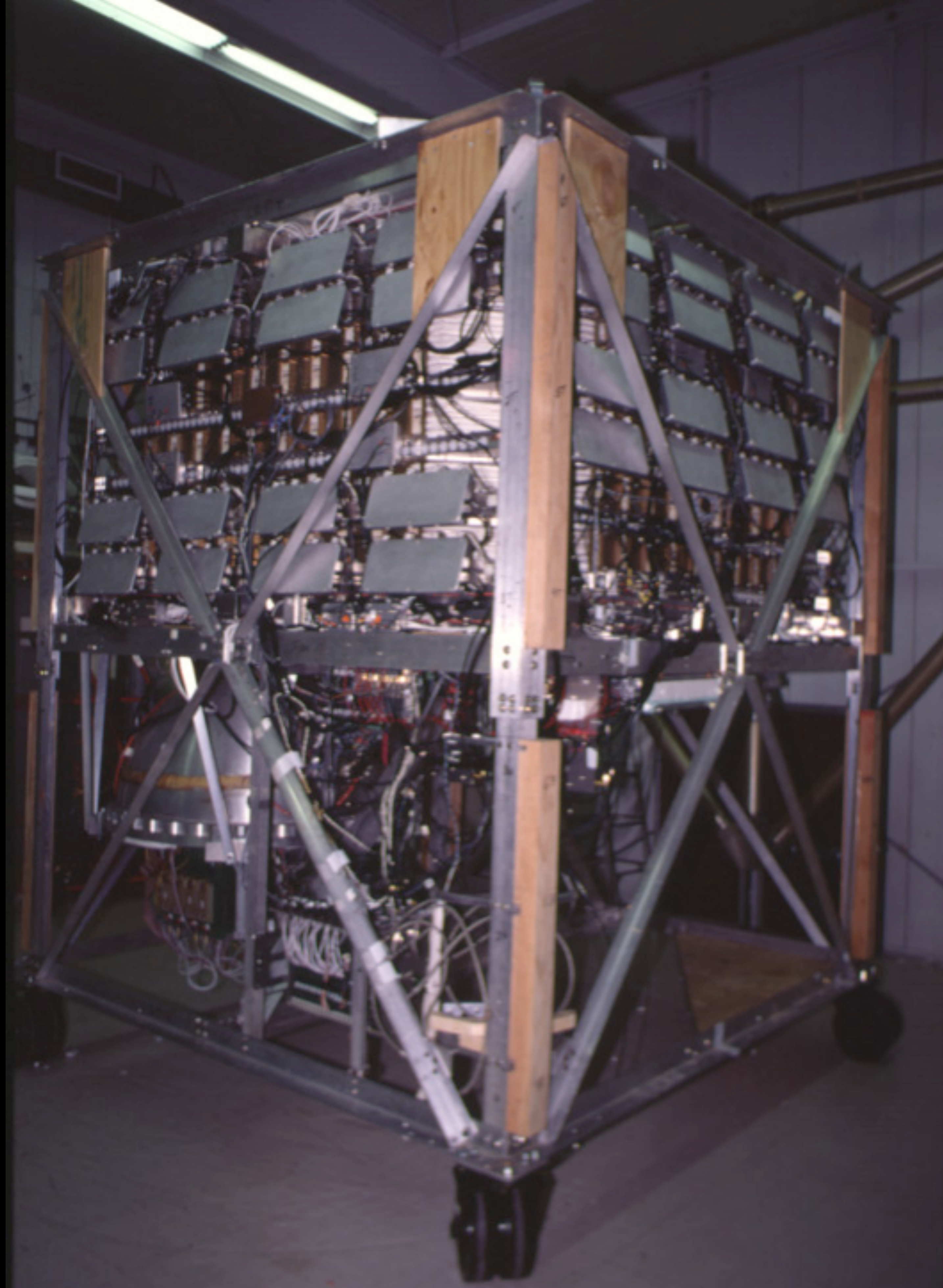

JRH 40220

Data Analysis Steps:

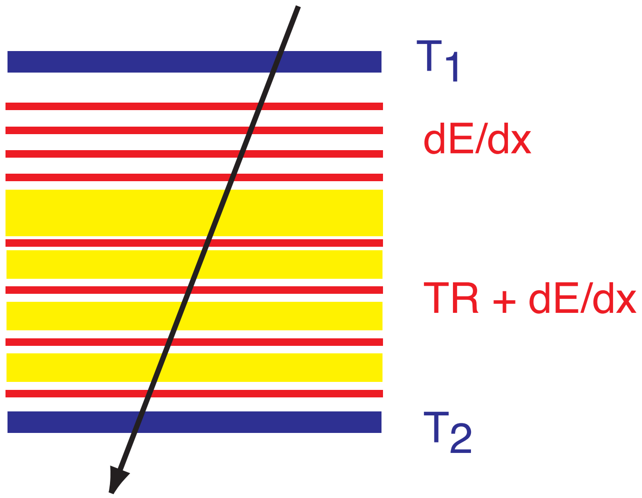

Charge assignment:

Events with clean tracks

Fine trajectory resolution (< 1 mm)
from signal distributions in proportional tubes

Correction of scintillator signals
for position and zenith angle

Rejection of interacting particles

Energy determination:

3 GeV/n to 1000 GeV/n:
use relativistic rise in specific ionization in
gas (Xe - CH_4 mixture)

above 1000 GeV/n:
strong energy dependence of transition radiation signal,
and dE/dx signal near saturation

Calibration of a transition radiation detector

Measured pulse height distribution in proportional tubes

35 GeV electrons

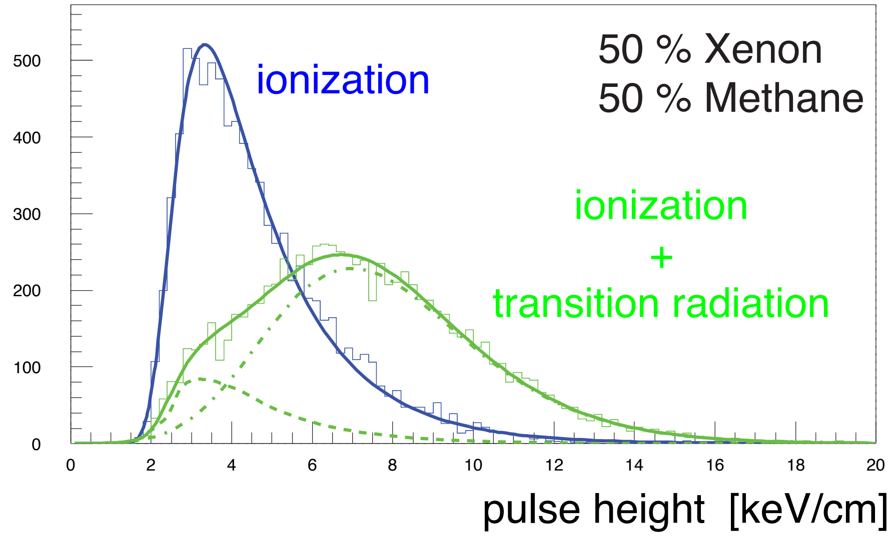

Measured detector response vs Lorentz factor

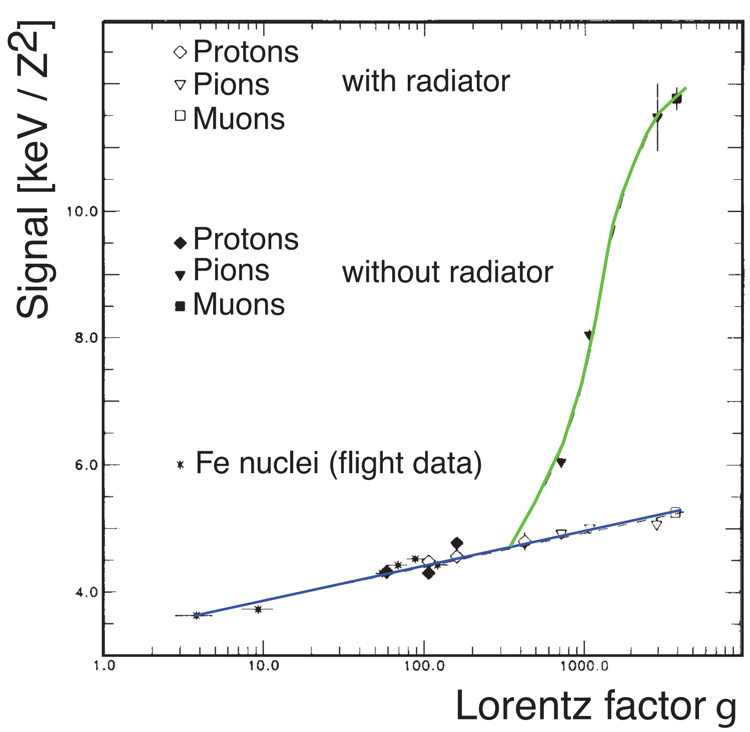

Detector Response TRD signal vs dE/dx signal

sample of flight data, oxygen nuclei

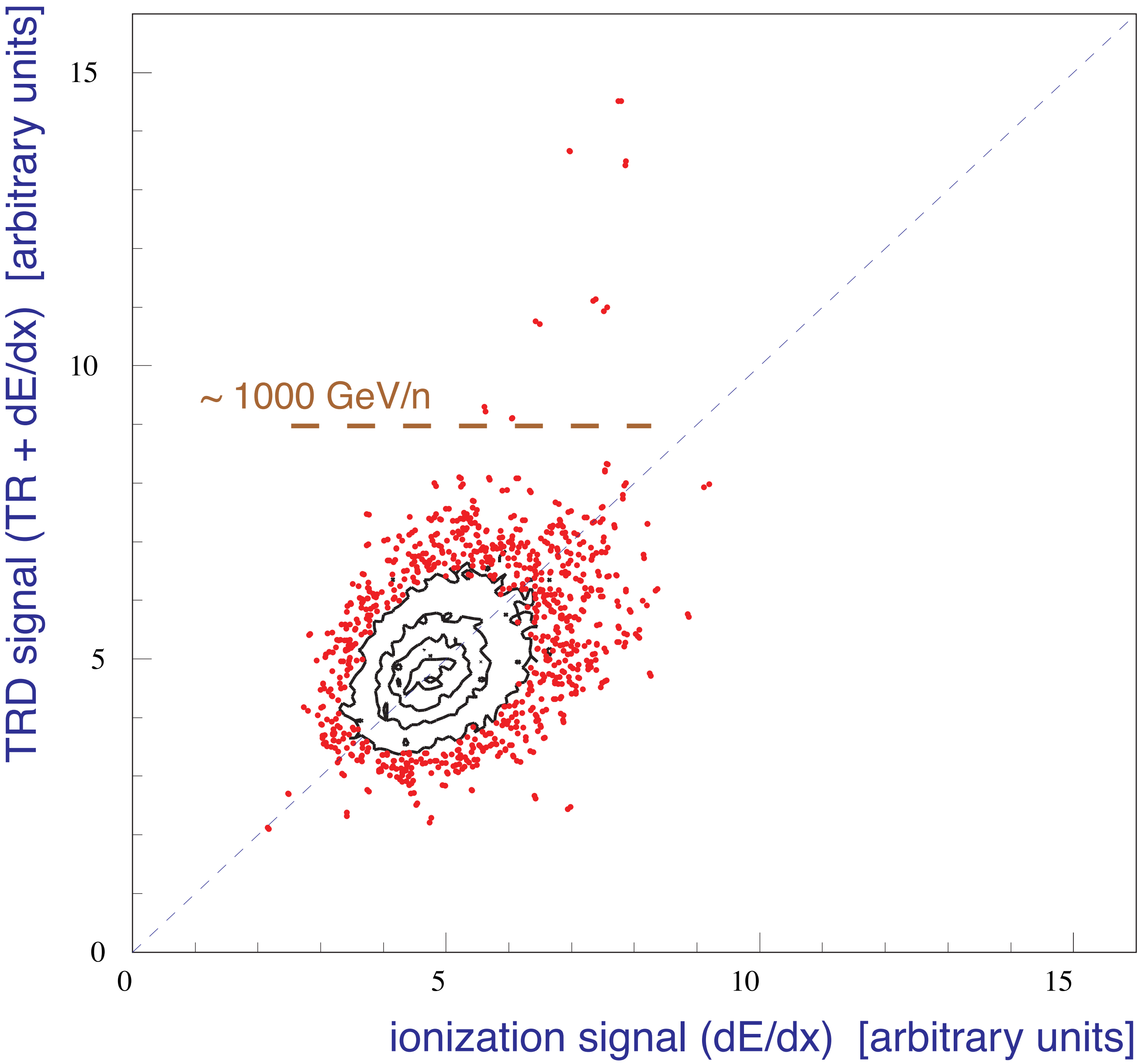

Measured relative width of the energy deposition

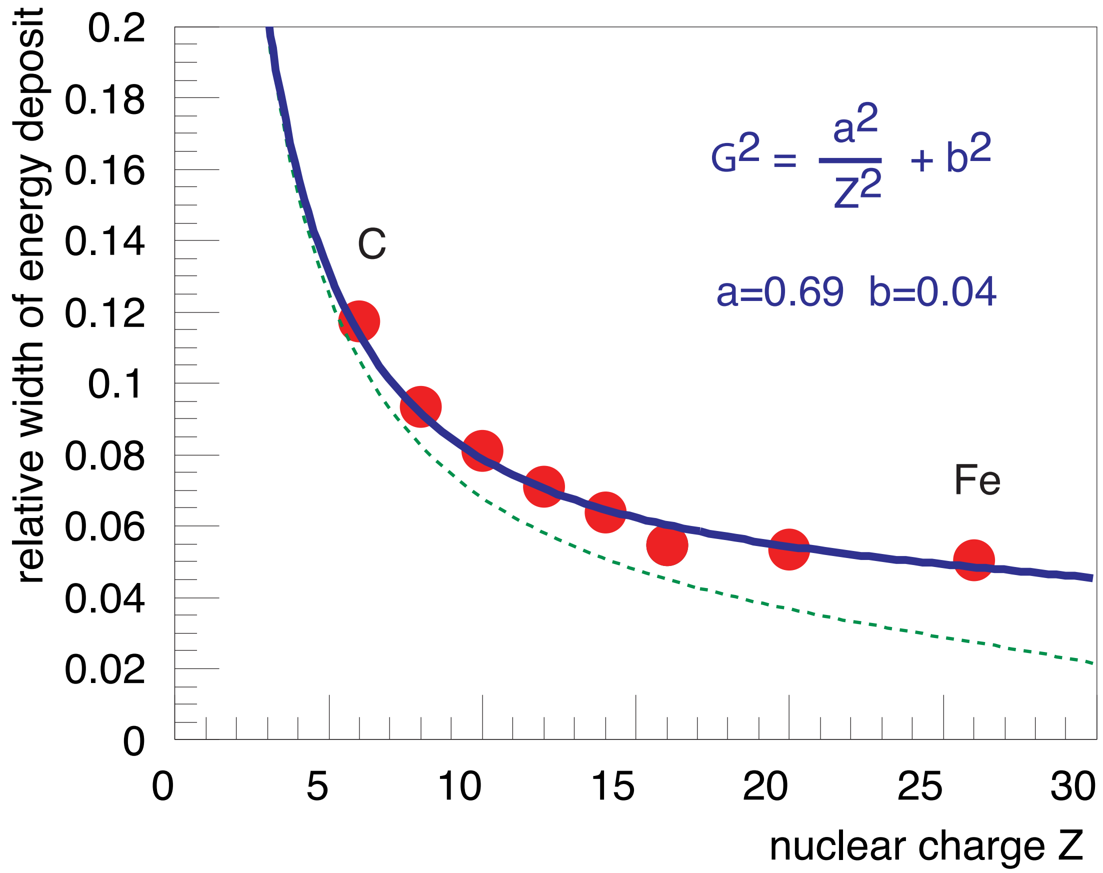

Spatial resolution of track reconstruction

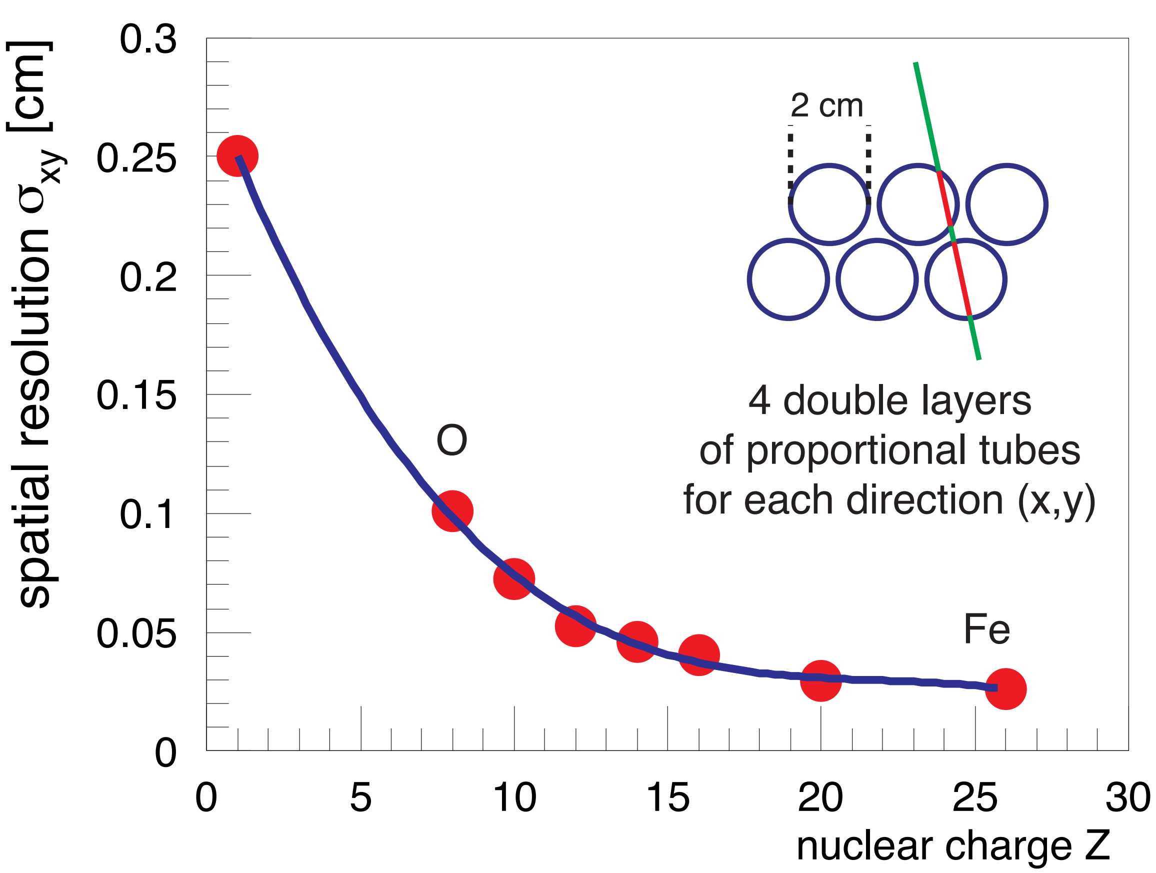

Spatial resolution dominated by (Landau-) fluctuations of energy deposit

Scintillator Response

Response map of scintillators for one of 12 PMT's

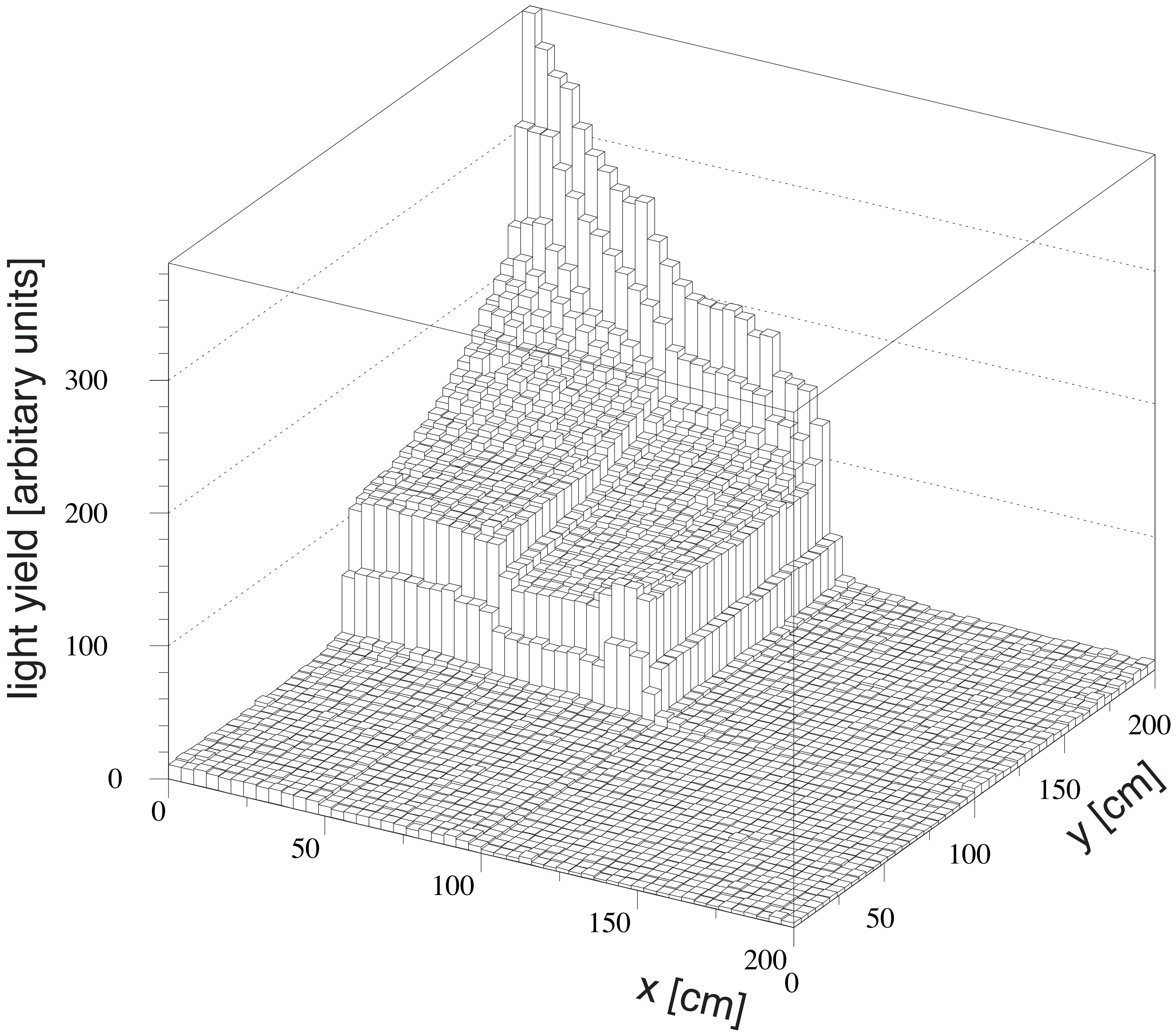

shematic view of scintillator plane

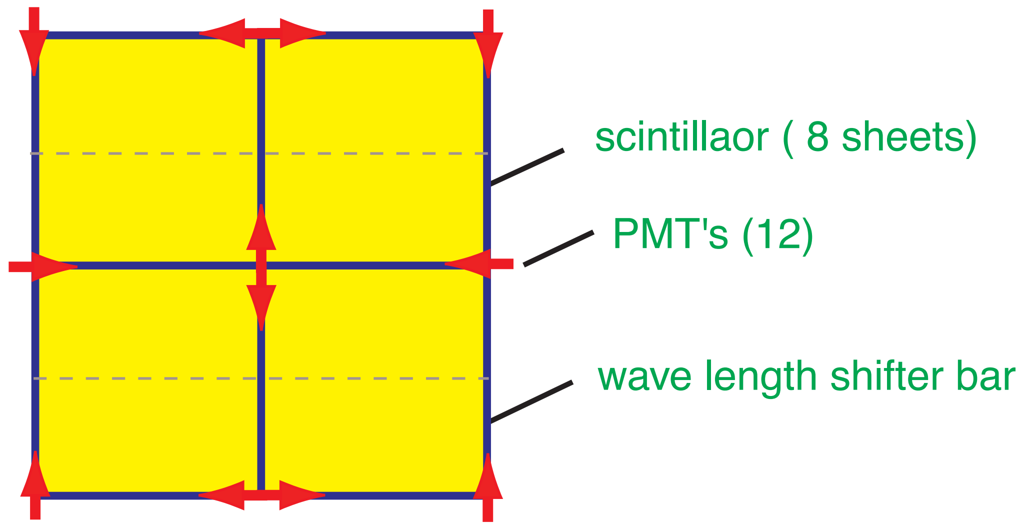

Cosmic-ray charge distrubution measured at instrument

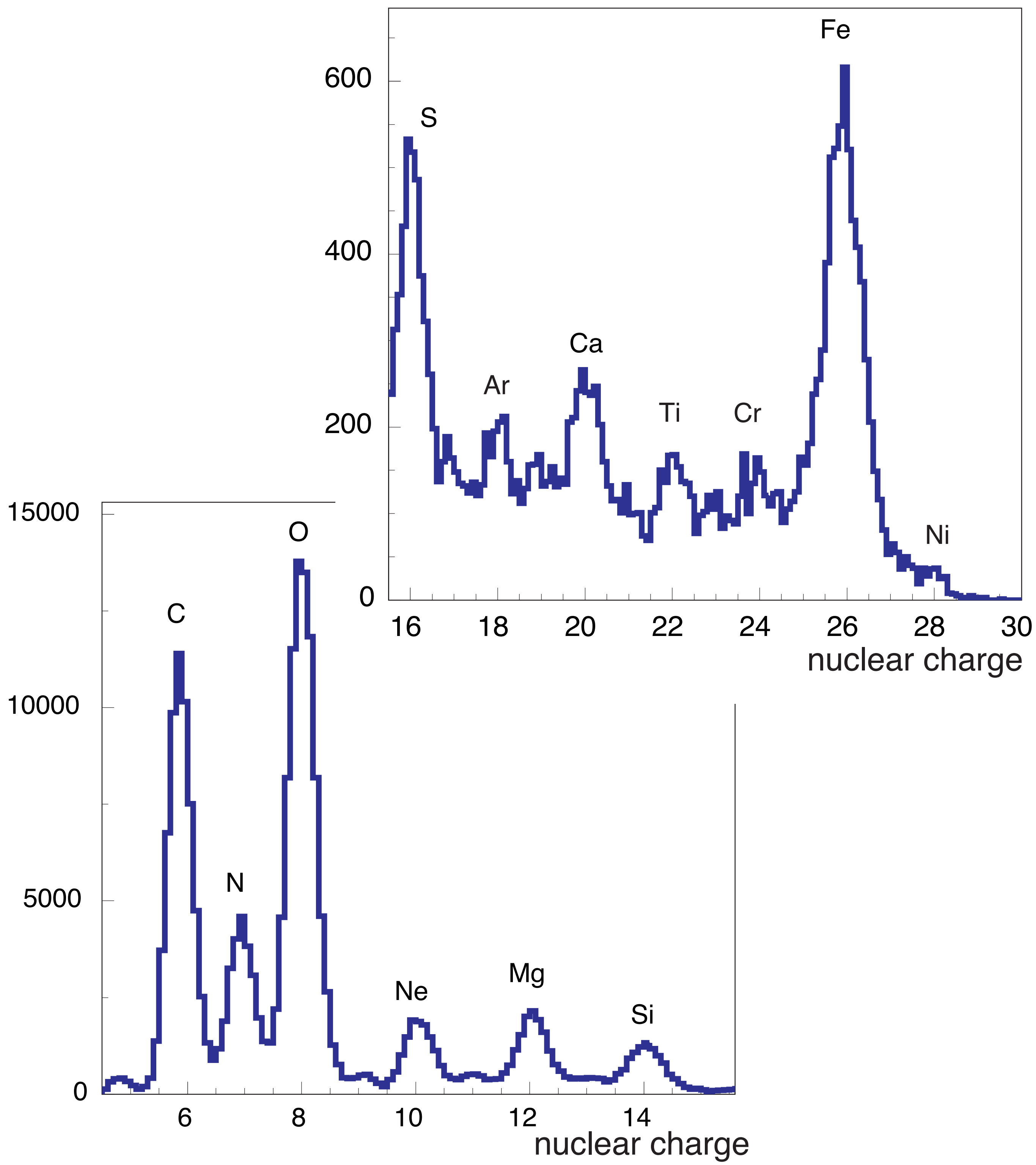

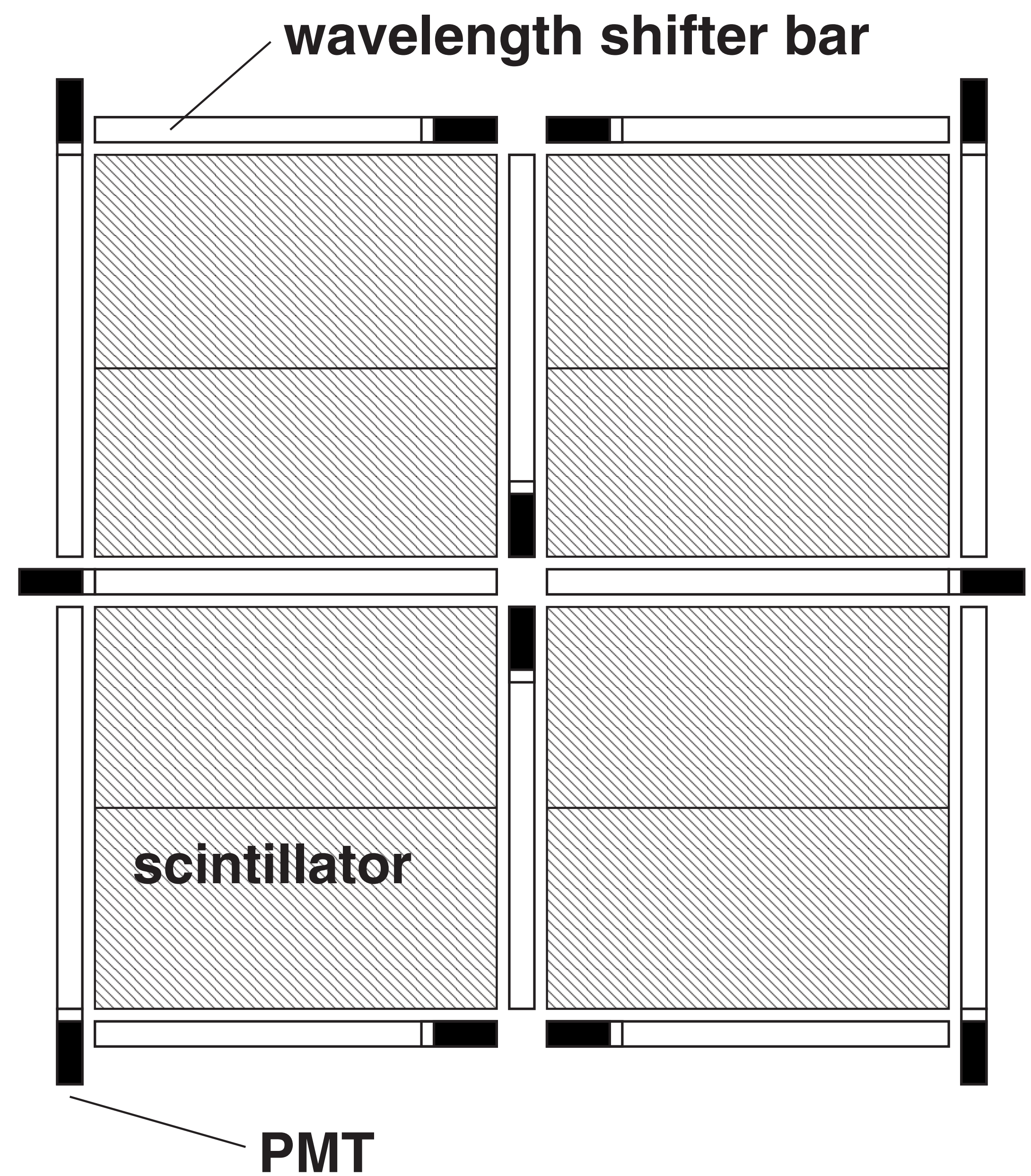

FIG. 3.—Schematic arrangement (not to scale) of scintillator sheets, wavelength shifter bars, and PMTs.

THE ASTROPHYSICAL JOURNAL, 607:333–341, 2004 May 20

A NEW MEASUREMENT OF THE INTENSITIES OF THE HEAVY PRIMARY COSMIC-RAY NUCLEI AROUND 1 TeV amu^{-1}

F. GAHBAUER,[1] G. HERMANN,[2] J. R. HÖRANDEL,[3] D. MÜLLER, AND A. A. RADU[4]
Enrico Fermi Institute, University of Chicago, 933 East 56th Street, Chicago, IL 60637
Received 2003 December 6; accepted 2004 February 3

obtained with two layers of scintillation counters (200 x 200 x 0.5 cm^3)

resolution dominated by spatial uniformity

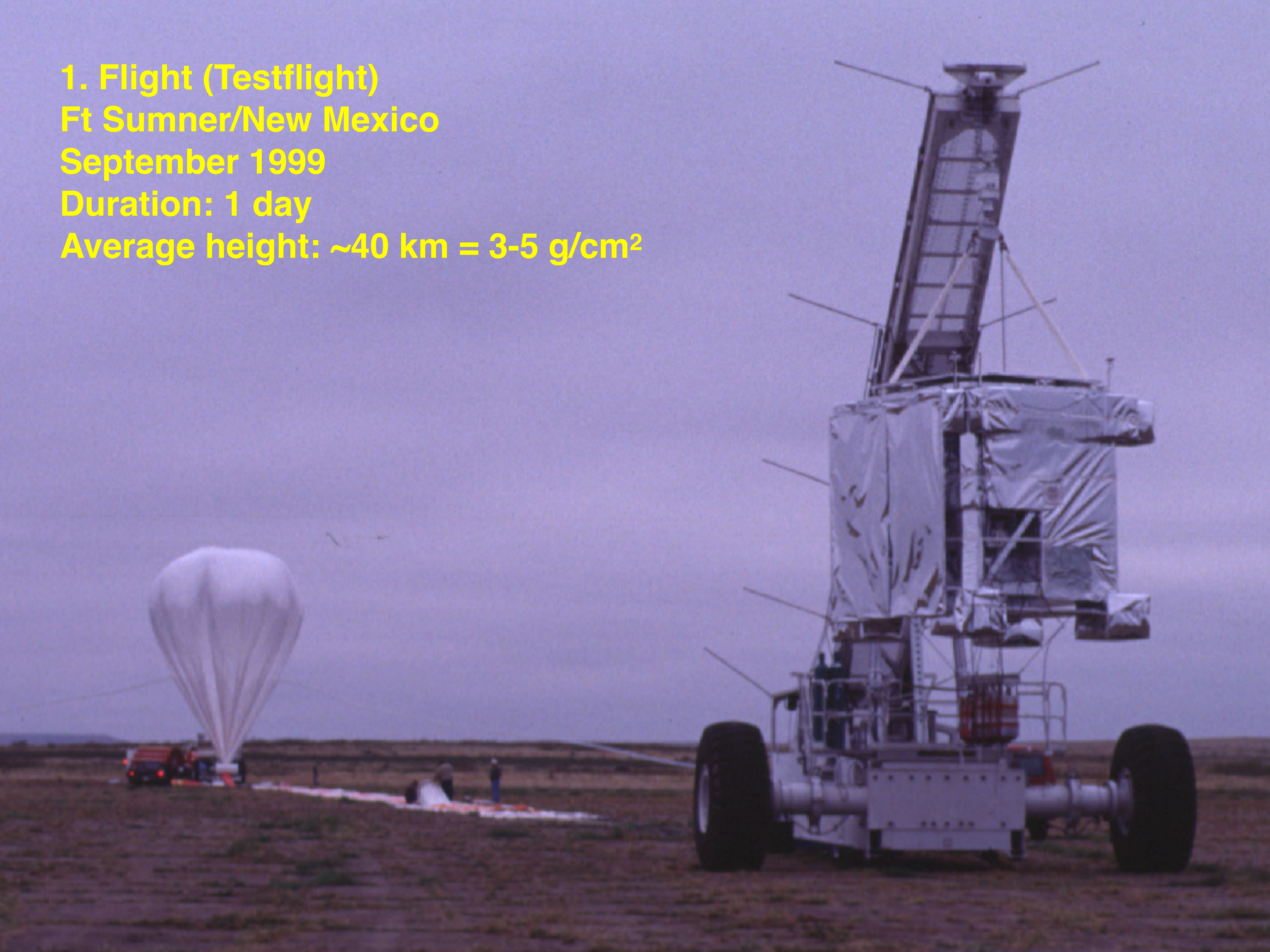
1. Flight (Testflight)
Ft Sumner/New Mexico
September 1999
Duration: 1 day
Average height: ~40 km = 3-5 g/cm²

TRACER Experiment - Mc Murdo, Antarctica

flight: 12. – 26. December 2003 ~ 40 km (3-5 g/cm^2)

TRACER Experiment

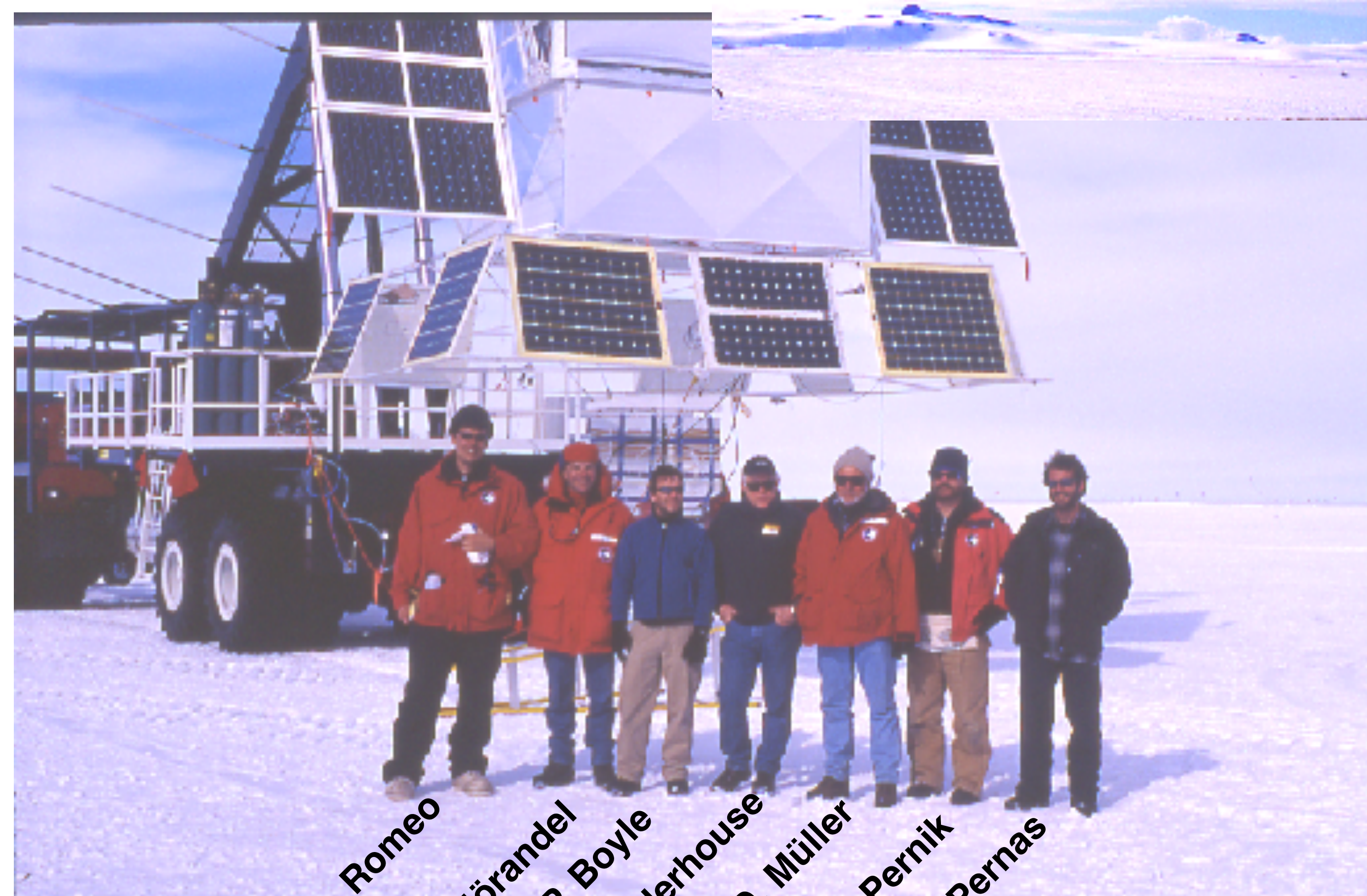

TRACER Experiment - Mc Murdo, Antarctica
flight: 12. – 26. December 2003 ~ 40 km (3-5 g/cm²)

Cherenkov Detectors

Cherenkov radiation

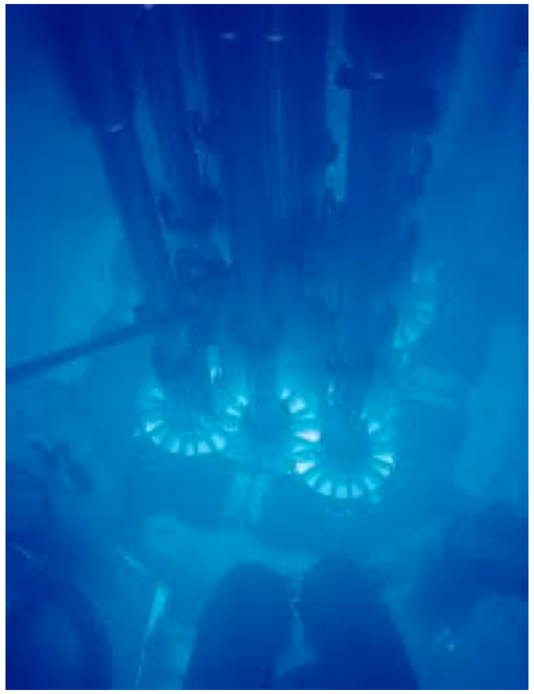

charged particles, moving in a medium with refractive index *n* with

$$v > \frac{c}{n}$$

emit electromagnetic radiation --> Cherenkov radiation

electrons passing through a dielectric at

$$v < \frac{c}{n}$$

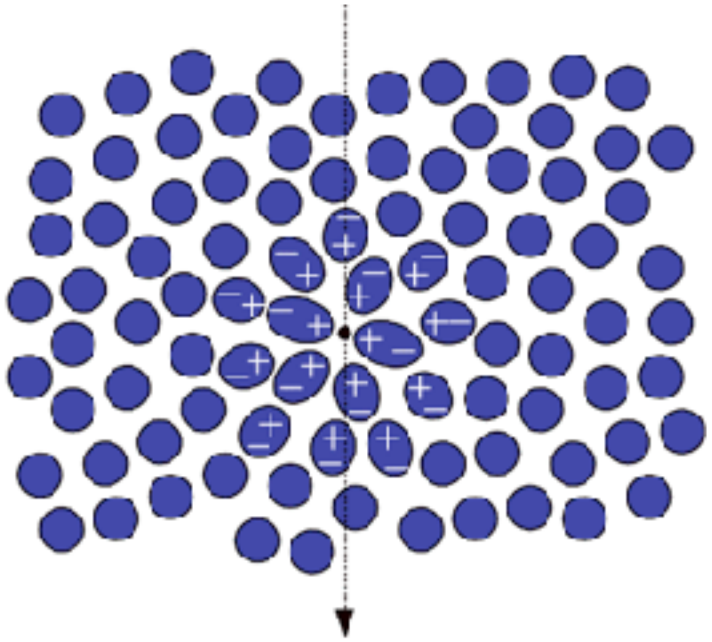

$$v > \frac{c}{n}$$

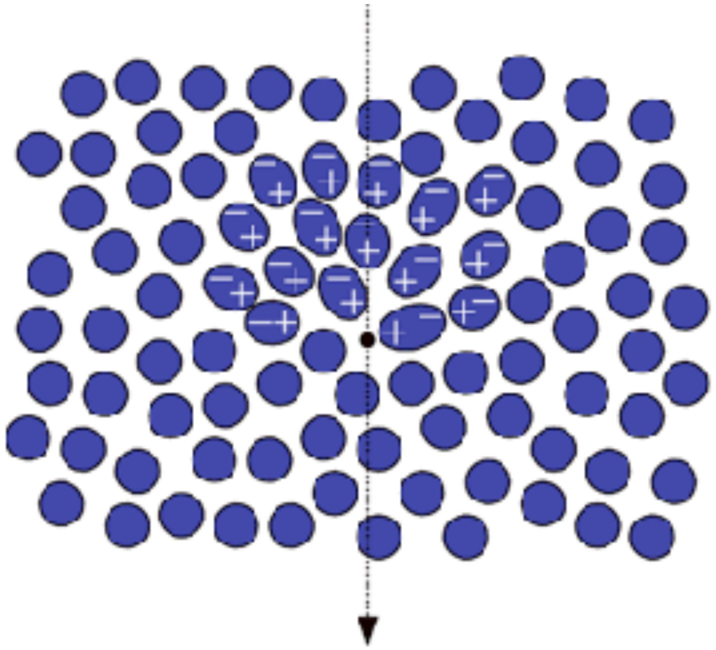

Charged particles, passing by the atoms in the dielectric, momentarily polarize them. Once the particle has passed, this polarized state collapses, causing each atom to emit Cerenkov radiation. For slow moving particles, the polarization is perfectly symmetrical, resulting in no electric field at long distances. When the particle is moving very quickly, however, the polarization is no longer perfectly symmetrical.

Cherenkov radiation

angle between the trajectory of the particle and the emitted photons

$$\cos\theta_c = \frac{c}{n\beta c} = \frac{1}{n\beta}$$

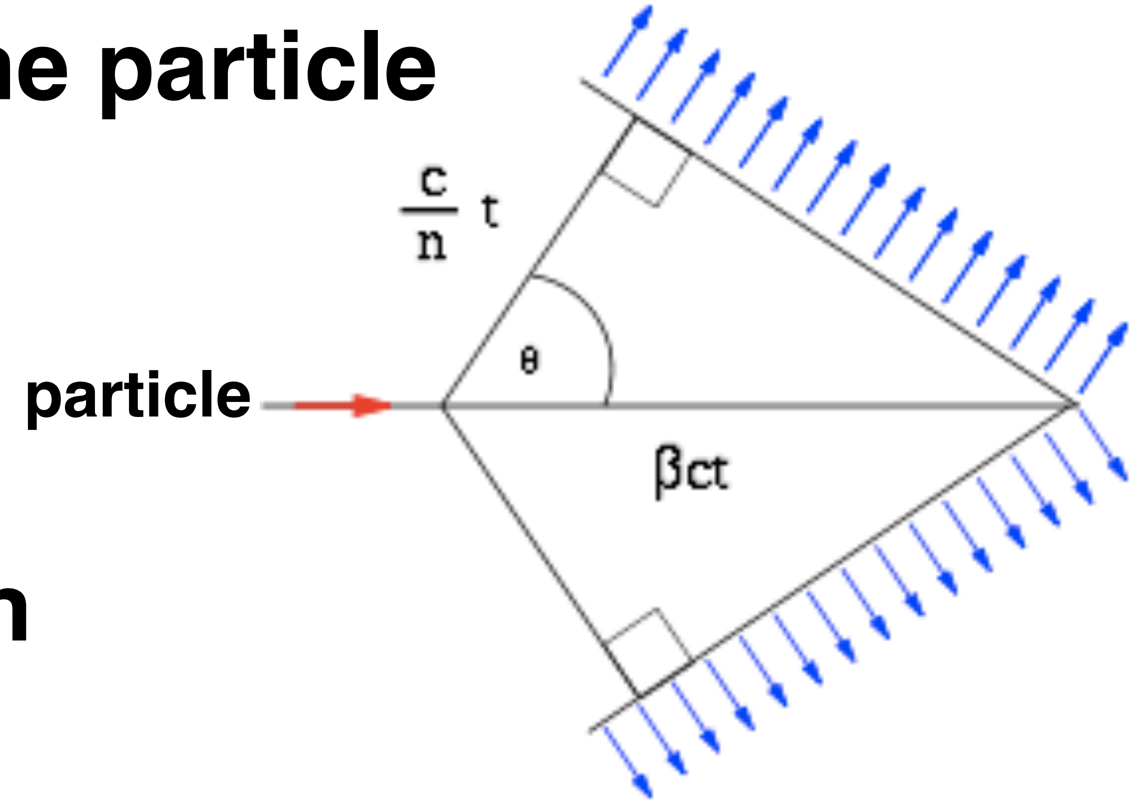

threshold for Cherenkov radiation

$$\beta > \frac{1}{n}$$

at threshold, the photons are emitted in forward direction

the Cherenkov angle increases to a maximum value for $\beta = 1$**:** $\theta_c = \arccos\frac{1}{n}$

threshold energy

$$\gamma_{th} = \frac{1}{\sqrt{1-\beta_{th}^2}} = \frac{1}{\sqrt{1-\frac{1}{n^2}}} \quad \text{with} \quad \gamma_{th} = \frac{E_{th}}{m_o c^2}$$

Cherenkov radiation

number of Cherenkov photons emitted per unit length

$$\frac{dN}{dx} = 2\pi\alpha z^2 \int_{\lambda_1}^{\lambda_2} \left(1 - \frac{1}{n^2\beta^2}\right) \frac{d\lambda}{\lambda^2}$$

z **charge of particle** α **Sommerfeld constant** **in the wavelength interval** $\lambda_1 \ldots \lambda_2$

neglecting dispersion yields

$$\frac{dN}{dx} = 2\pi\alpha z^2 \sin^2\theta_c \frac{\lambda_2 - \lambda_1}{\lambda_1\lambda_2}$$

which gives for a singly charged particle *(z=1)* in the wavelength range 400 to 700 nm

$$\frac{dN}{dx} = 490 \sin^2\theta_c \quad [\mathrm{cm}^{-1}]$$

Cherenkov detector

- **particle identification**
  threshold detector

$$\gamma_{th} = \frac{1}{\sqrt{1-\frac{1}{n^2}}} = \frac{E_{th}}{m_o c^2}$$

select material with appropriate *n*
--> light particles radiate

- **measurement of velocity**
  (kinetic energy)

$$\cos\theta_c = \frac{c}{n\beta c} = \frac{1}{n\beta}$$

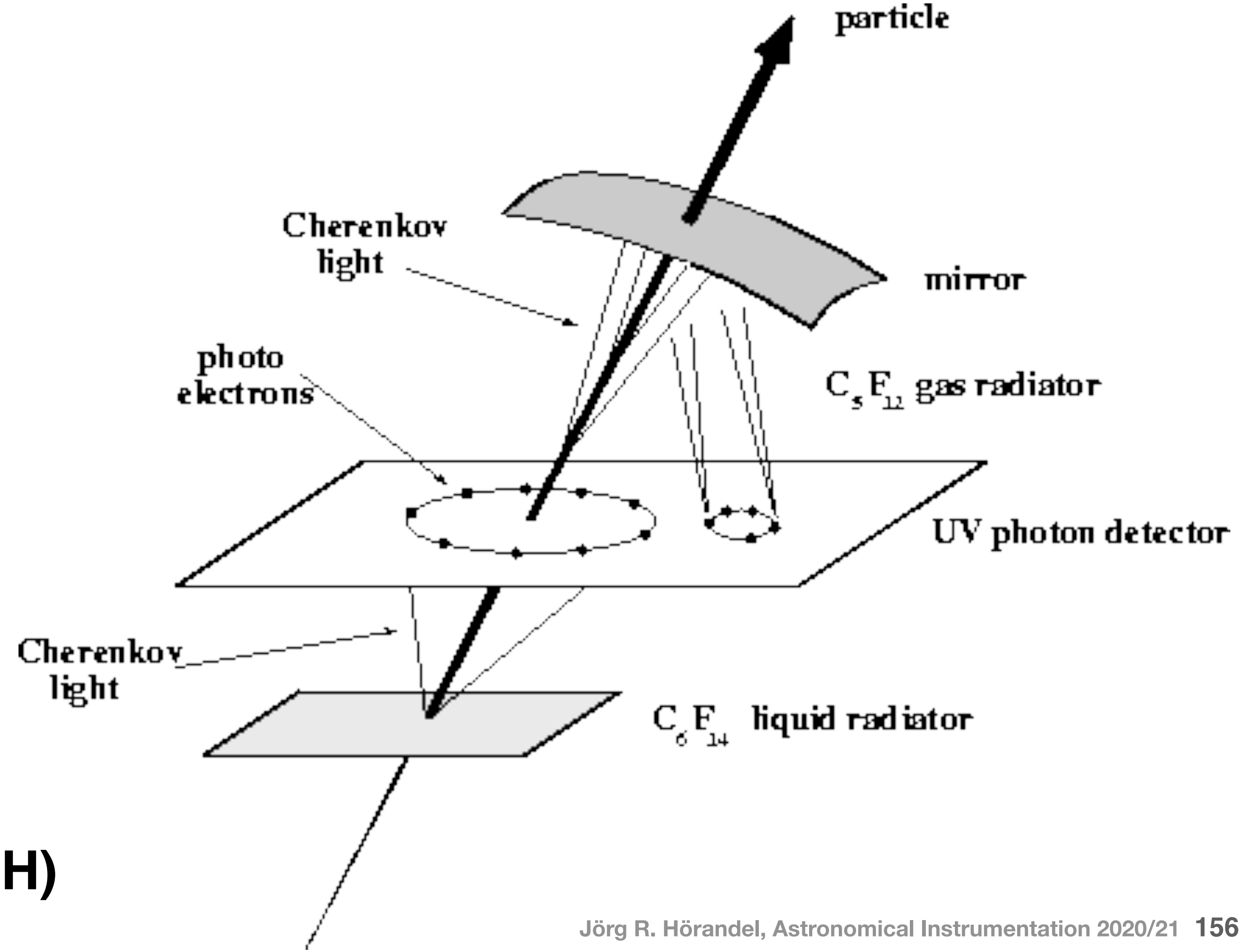

ring imaging Cherenkov detector (RICH)

Human Eye as Cherenkov detector - SilEye-2 experiment

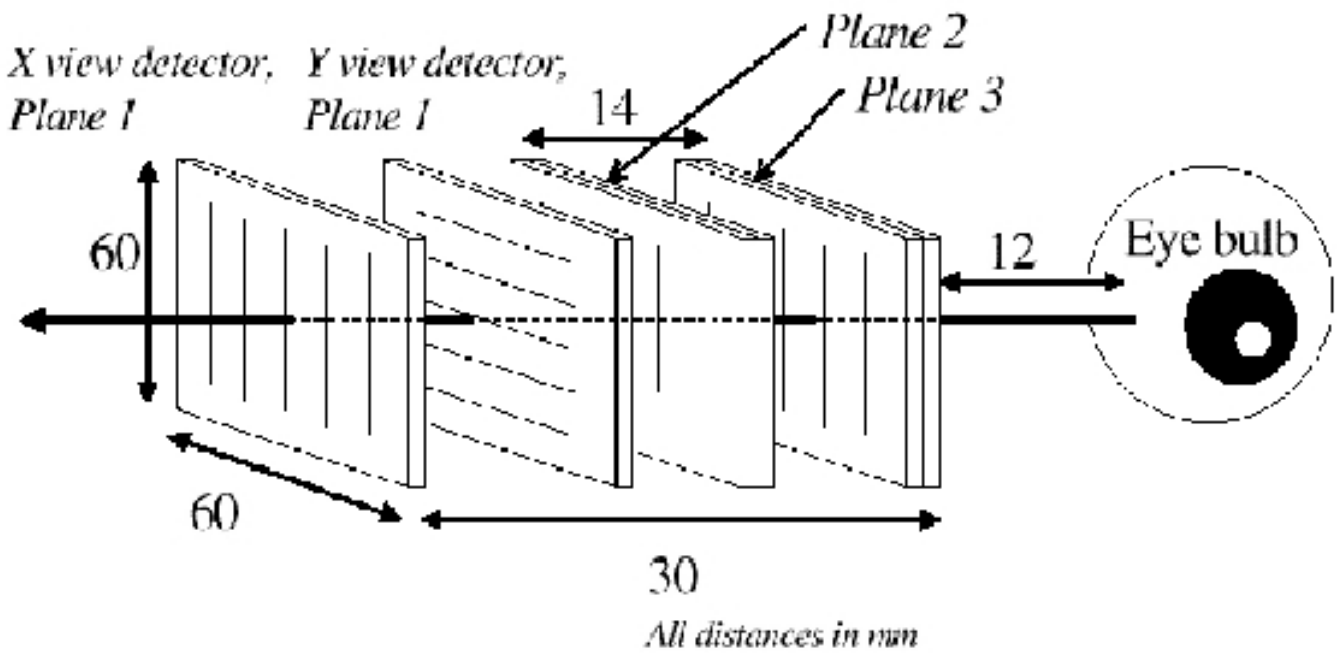

Figure 2. Scheme of the SilEye-2 silicon detector: six 16 strip silicon layers glued in pairs with strip orthogonally aligned form three planes (the two layers of the first plane are drawn separately). The position of the eye bulb is also shown.

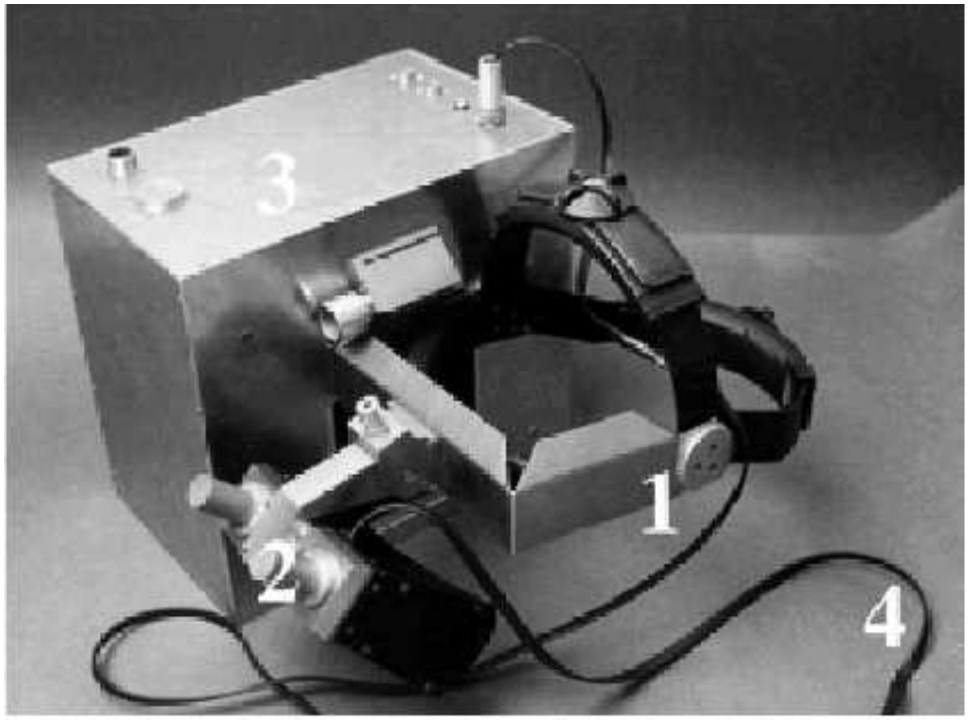

Figure 1. Photo of the SilEye-2 helmet and detector case: 1. Head Mounting. 2. Eye mask with internal LEDs. 3. Detector Box. 4. Connection cable for the LEDs used for dark adaptation tests .

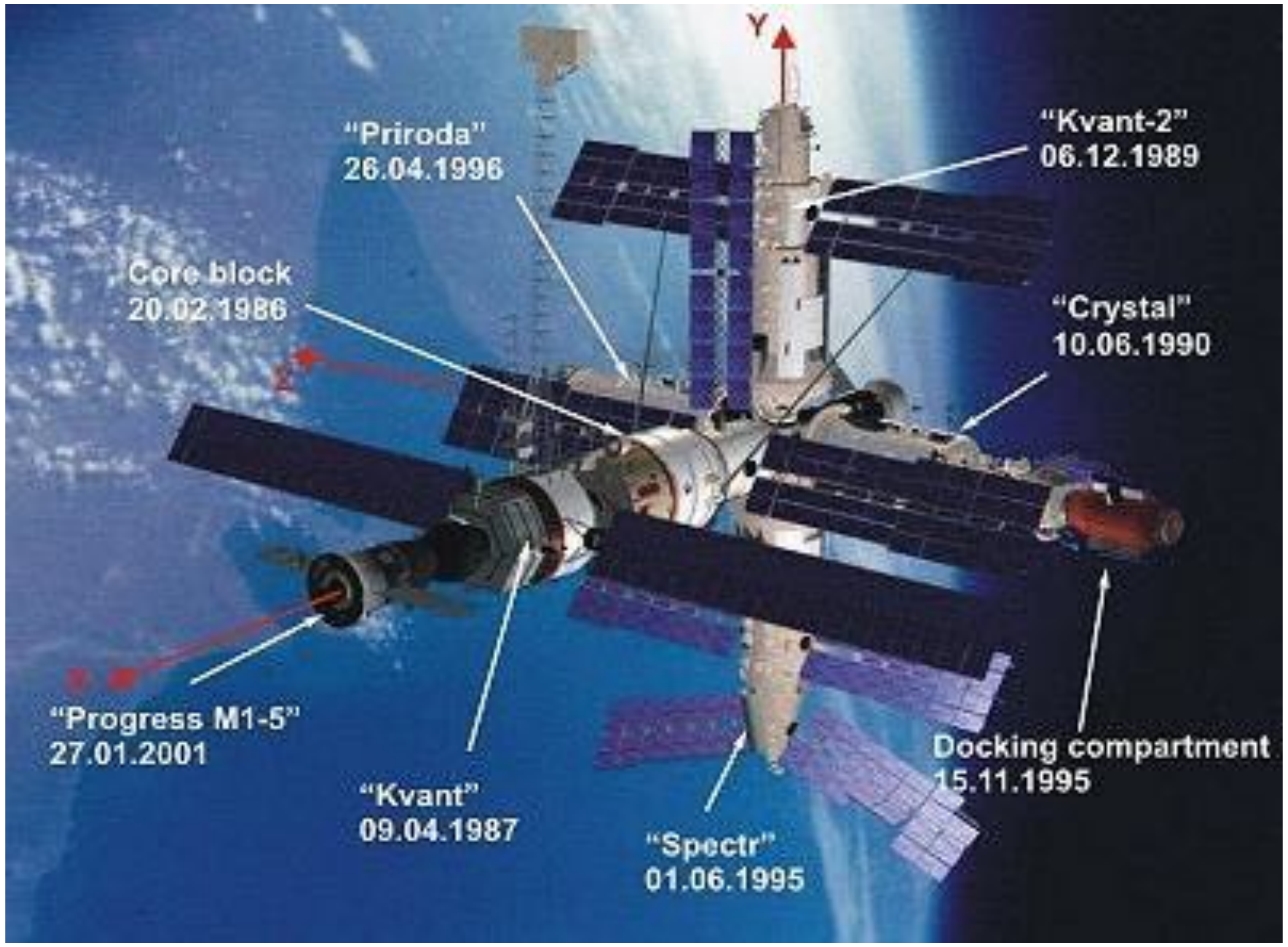

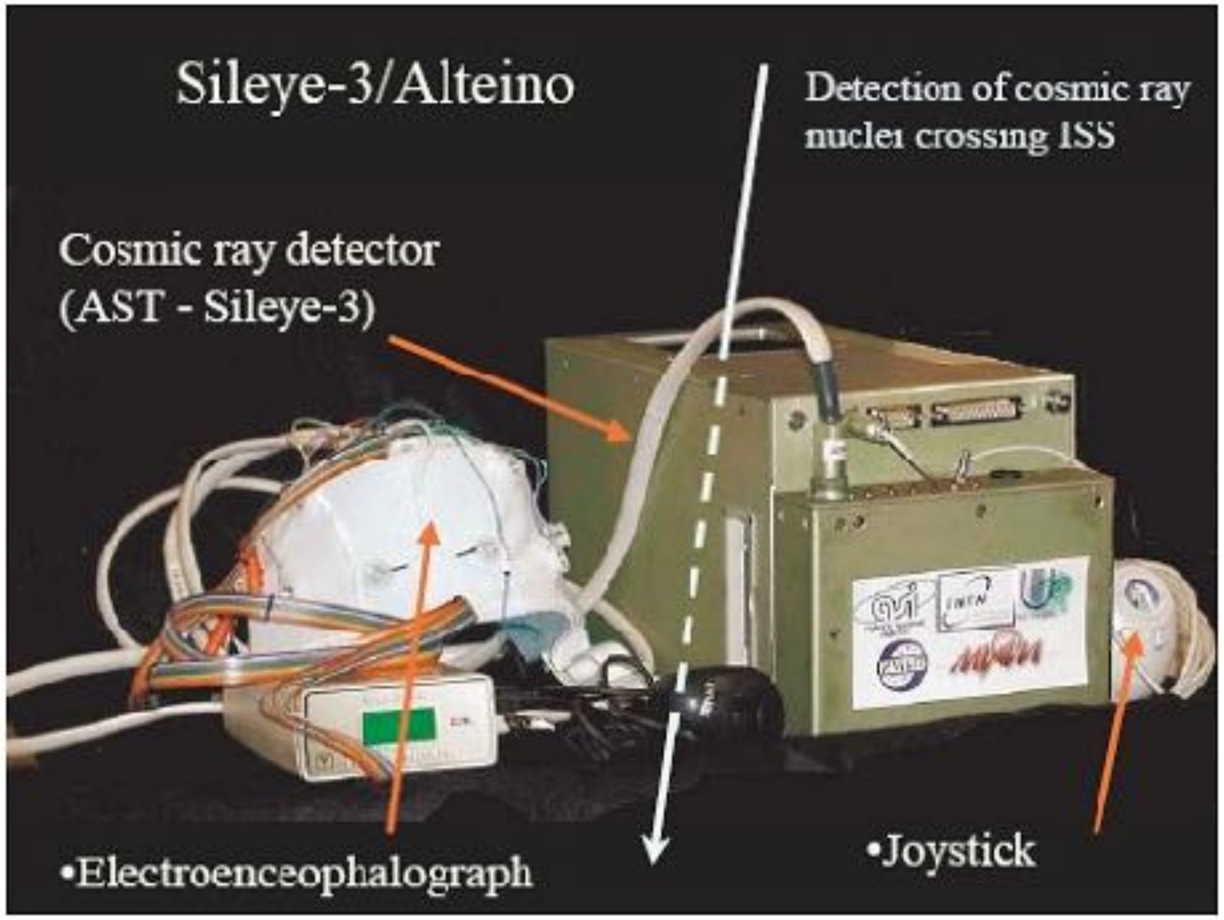

ELSEVIER

Astroparticle Physics 18 (2003) 487–500

Astroparticle Physics

www.elsevier.com/locate/astropart

The energy spectrum of cosmic-ray protons and helium near 100 GeV

E. Diehl [1], D. Ellithorpe, D. Müller, S.P. Swordy *

Department of Physics, Enrico Fermi Institute, University of Chicago, 5640 Ellis Avenue, Chicago, IL 60637-1433, USA

Received 15 February 2002; accepted 2 May 2002

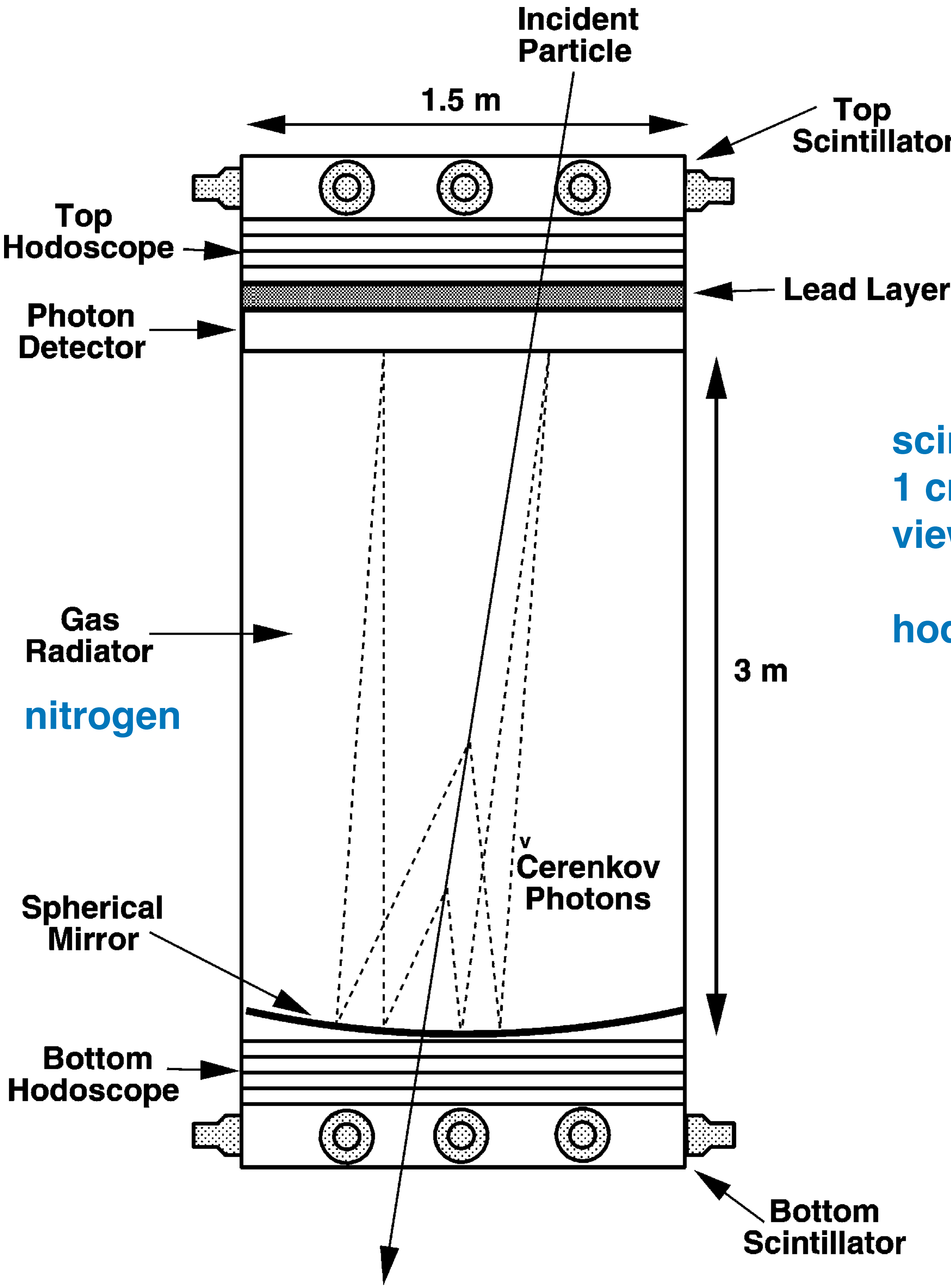

nitrogen

Fig. 1. Schematic cross-section of the instrument.

scintillator: 1.5 m x 1.5 m NE110 plastic scintillator, 1 cm thick
viewed by twelve 12.5 cm diameter PMTs

hodoscope filled with argon/methane 95:5

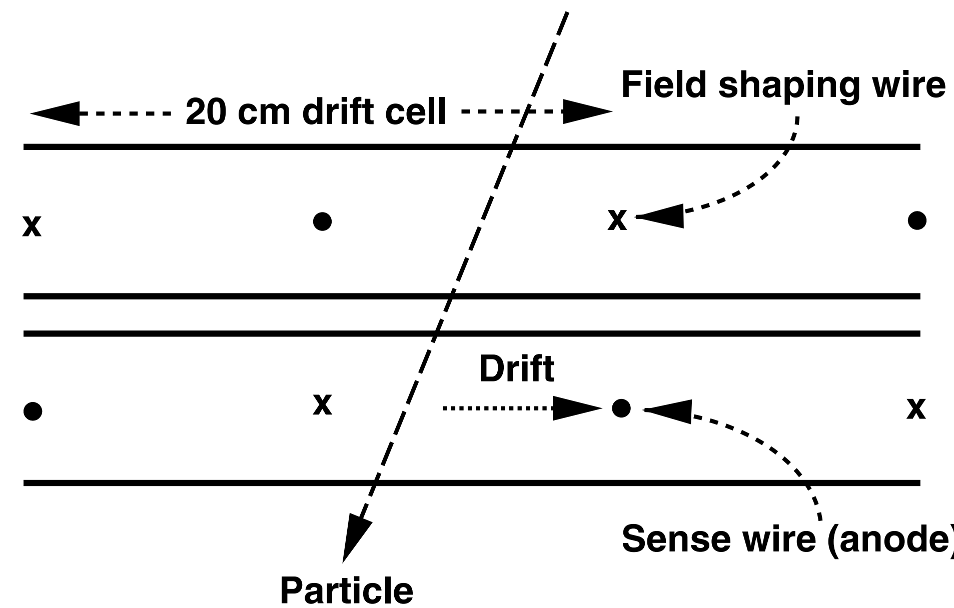

Fig. 2. Schematic cross-section view of hodoscope operation.

Multi-Wire Proportional Chamber

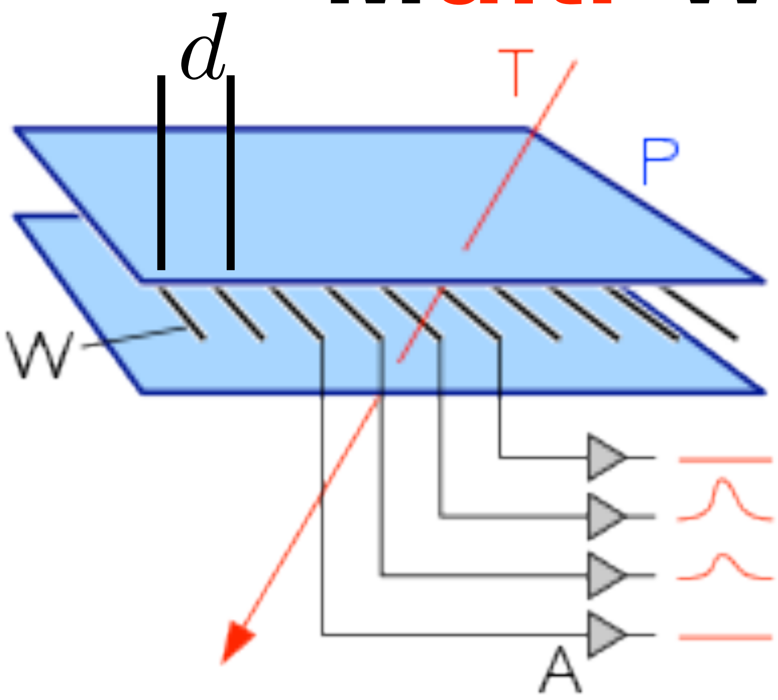

spatial resolution

$$\sigma(x) = \frac{d}{\sqrt{12}}$$

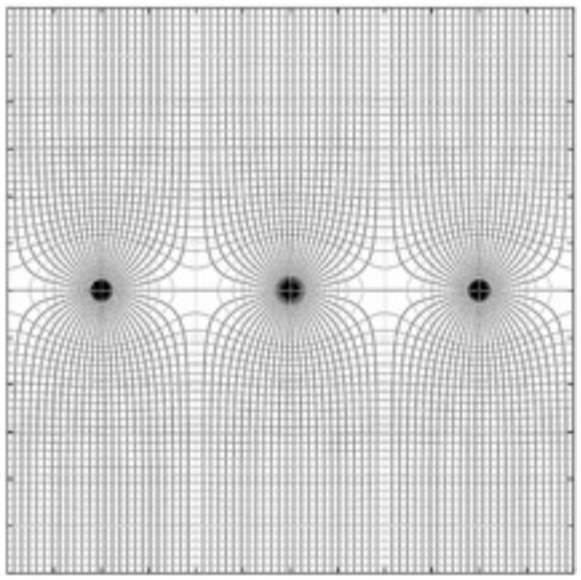

electric field

ionization liberates electrons
--> acceleration in electric field

energy gain between to electron collisions

$$\Delta E_{kin} = -e \int_{r_1}^{r_2} E(r) dr$$

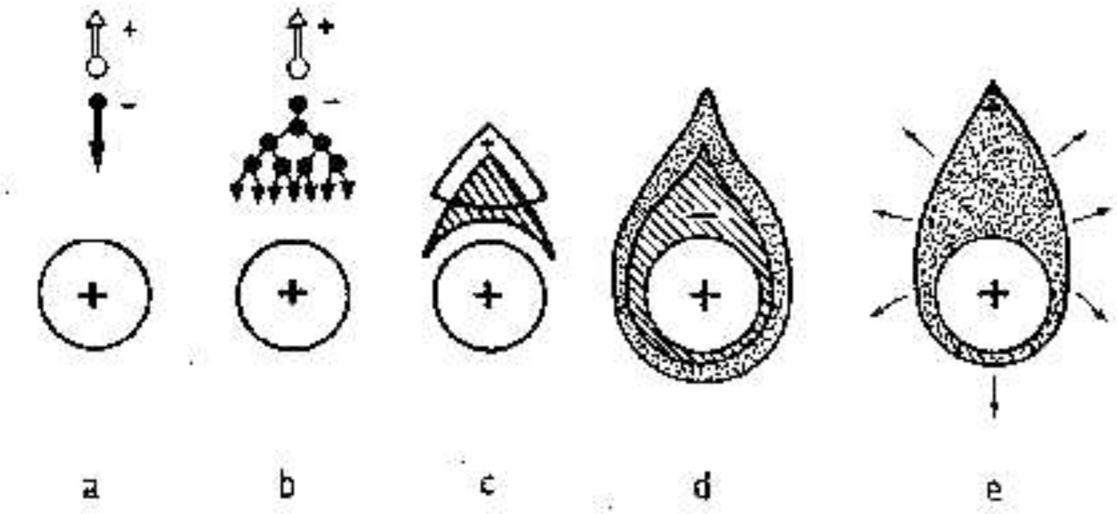

if energy gain is larger than ionization energy

--> development of electron avalanche

voltage signal $$\Delta U = -\frac{eN}{C} A$$

A gas amplification factor
N charge carrier pairs
C capacity

ELSEVIER

Astroparticle Physics 18 (2003) 487–500

Astroparticle Physics

www.elsevier.com/locate/astropart

The energy spectrum of cosmic-ray protons and helium near 100 GeV

E. Diehl [1], D. Ellithorpe, D. Müller, S.P. Swordy *

Department of Physics, Enrico Fermi Institute, University of Chicago, 5640 Ellis Avenue, Chicago, IL 60637-1433, USA

Received 15 February 2002; accepted 2 May 2002

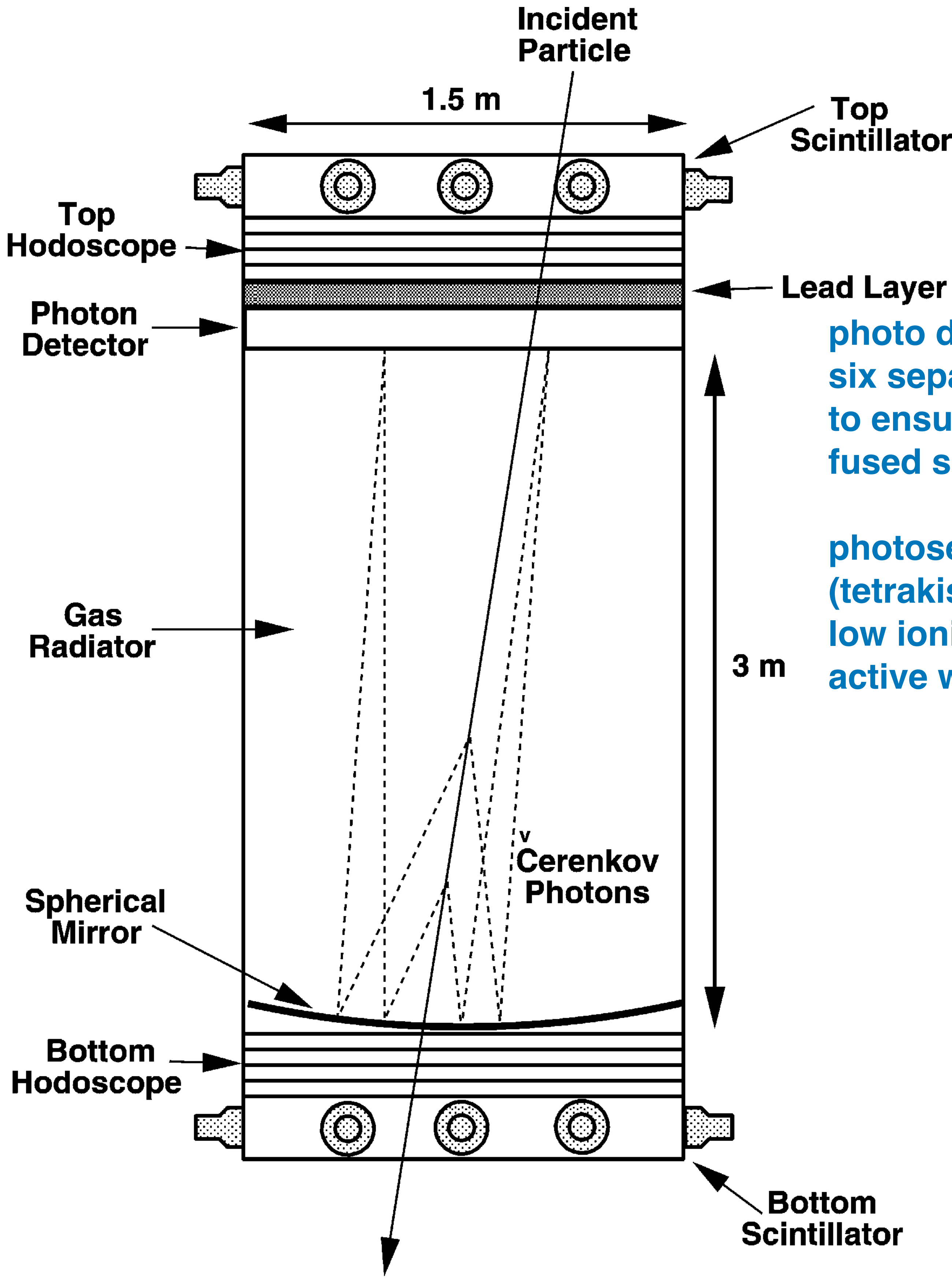

Fig. 1. Schematic cross-section of the instrument.

photo detector:
six separate MWPCs filled with ethane
to ensure the transmission of the UV Cherenkov light, fused silica is used for the entrance windows

photosensitivity is achieved with TMAE (tetrakis(dimethylamine)ethylene)
low ionization threshold 5.36 eV
active wavelength region 160 - 220 nm

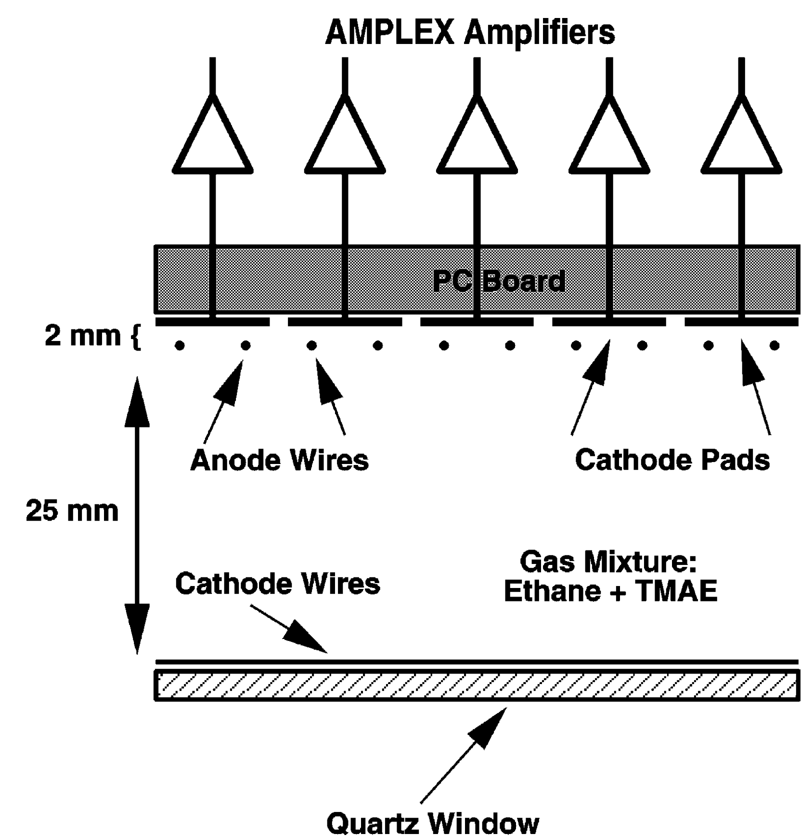

Fig. 3. Schematic cross-section of the photon detecting chamber.

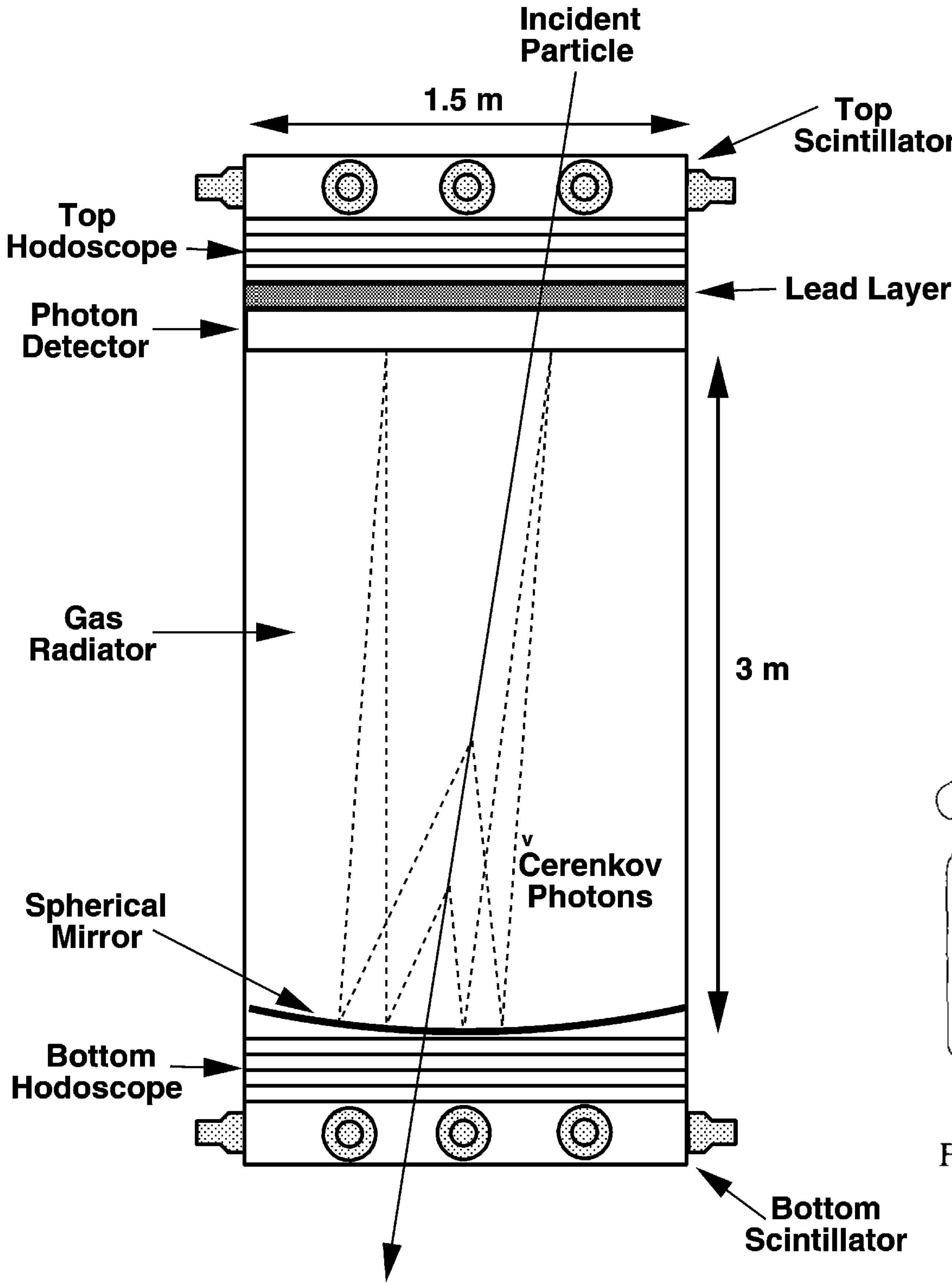

Fig. 1. Schematic cross-section of the instrument.

ELSEVIER
Astroparticle Physics 18 (2003) 487–500
Astroparticle Physics
www.elsevier.com/locate/astropart

The energy spectrum of cosmic-ray protons and helium near 100 GeV

E. Diehl [1], D. Ellithorpe, D. Müller, S.P. Swordy *

Department of Physics, Enrico Fermi Institute, University of Chicago, 5640 Ellis Avenue, Chicago, IL 60637-1433, USA

Received 15 February 2002; accepted 2 May 2002

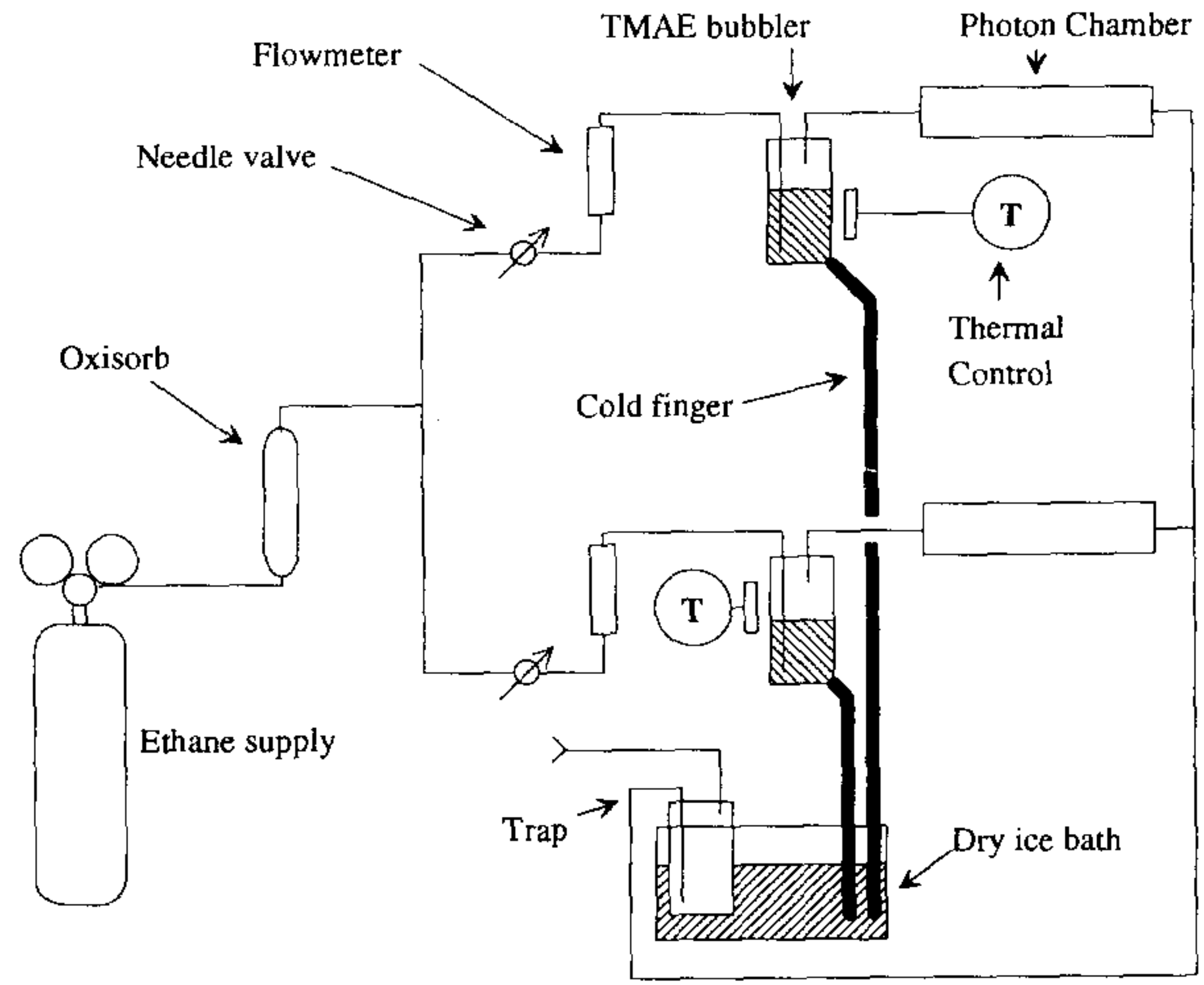

Fig. 4. Photon chamber TMAE/ethane gas system and control.

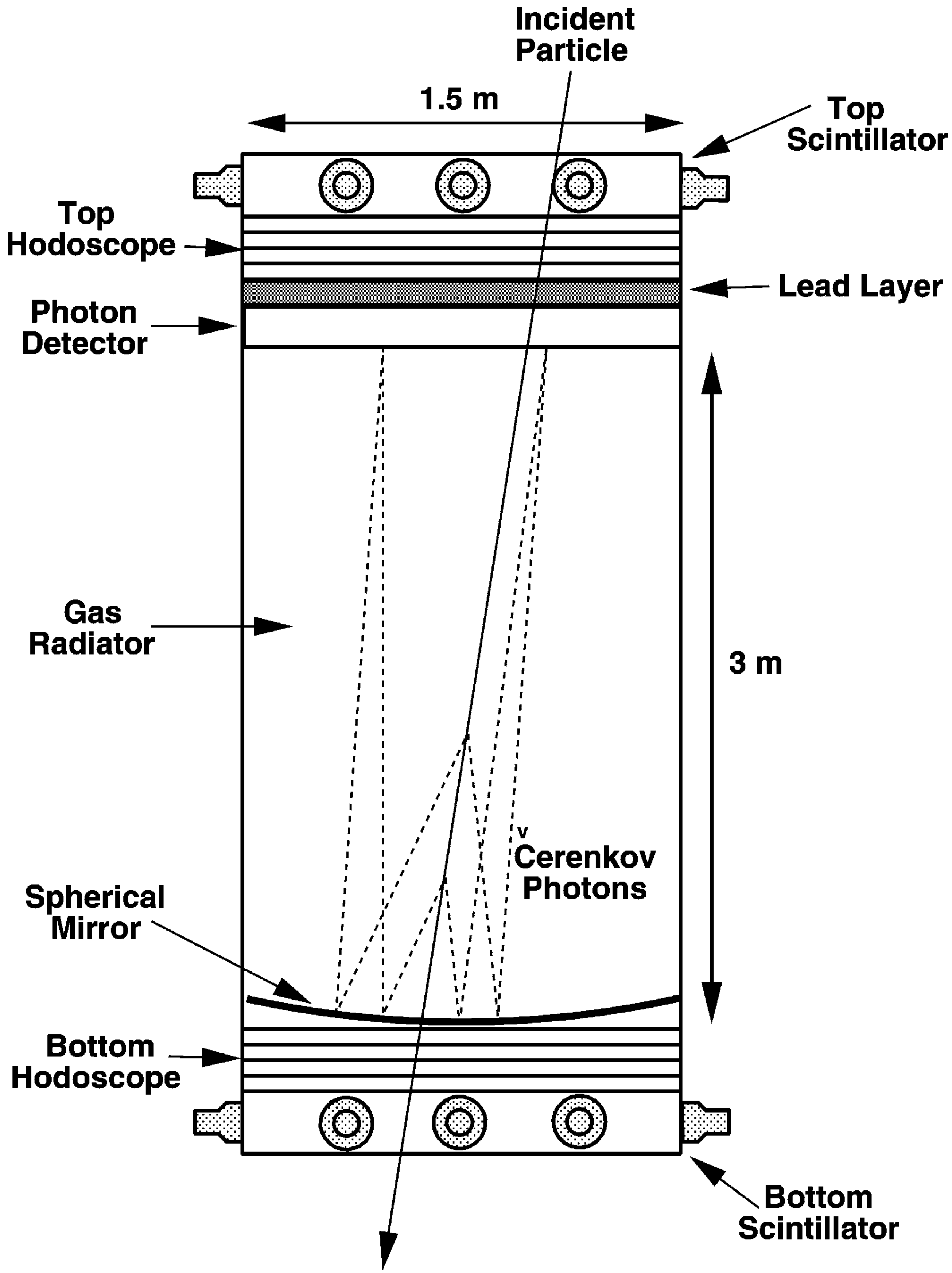

Fig. 1. Schematic cross-section of the instrument.

ELSEVIER
Astroparticle Physics 18 (2003) 487–500
Astroparticle Physics
www.elsevier.com/locate/astropart

The energy spectrum of cosmic-ray protons and helium near 100 GeV

E. Diehl [1], D. Ellithorpe, D. Müller, S.P. Swordy *

Department of Physics, Enrico Fermi Institute, University of Chicago, 5640 Ellis Avenue, Chicago, IL 60637-1433, USA

Received 15 February 2002; accepted 2 May 2002

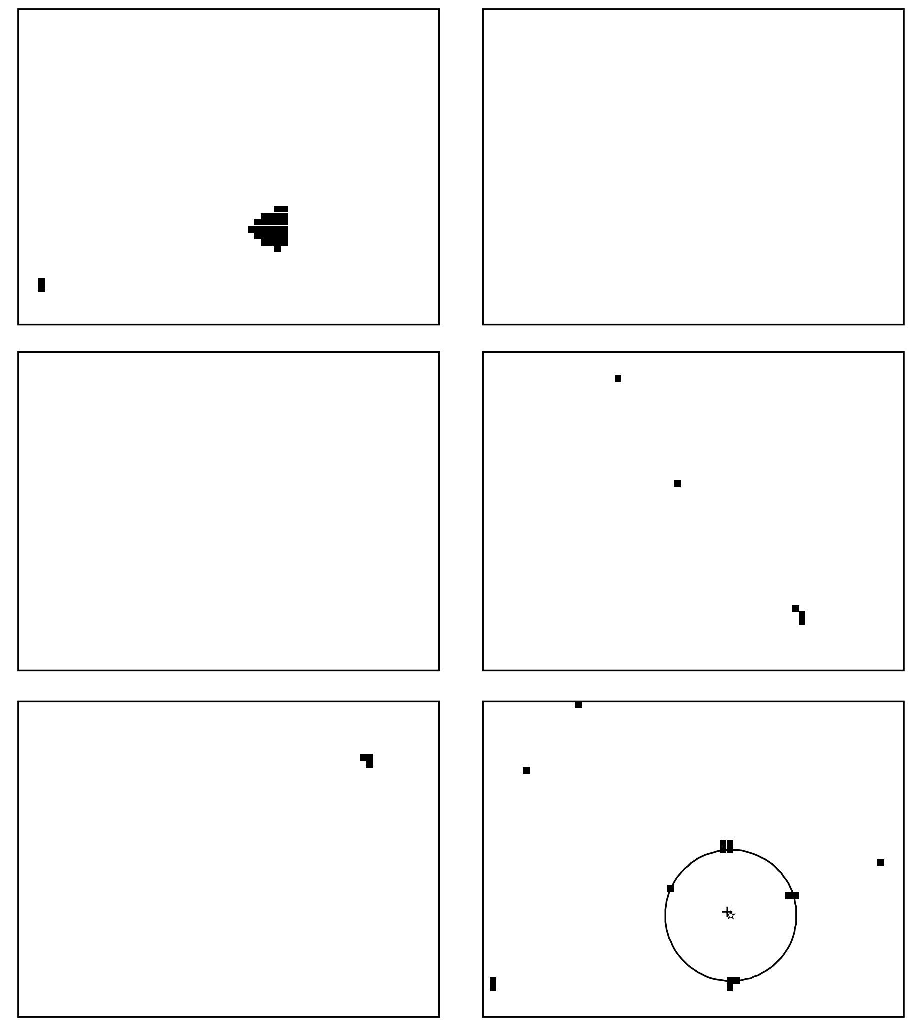

Fig. 6. A single event in the photon detecting chambers. The sensitive areas of the six chambers are shown as rectangles. Detector pads hit are shown as small black squares. The incoming particle produced a ring image of four clusters in the bottom right, the circle shows the fitted ring. The cross is the ring center predicted from the track fit, the star is the fitted center from the clusters detected. At the top left the incoming particle passed through the detector, leaving a cluster of hits. Other pads shown as hits are background.

Cherenkov Detectors
for
particle detection in air showers

Pierre Auger Observatory - Water Cherenkov Detector
to measure secondary particles in air showers

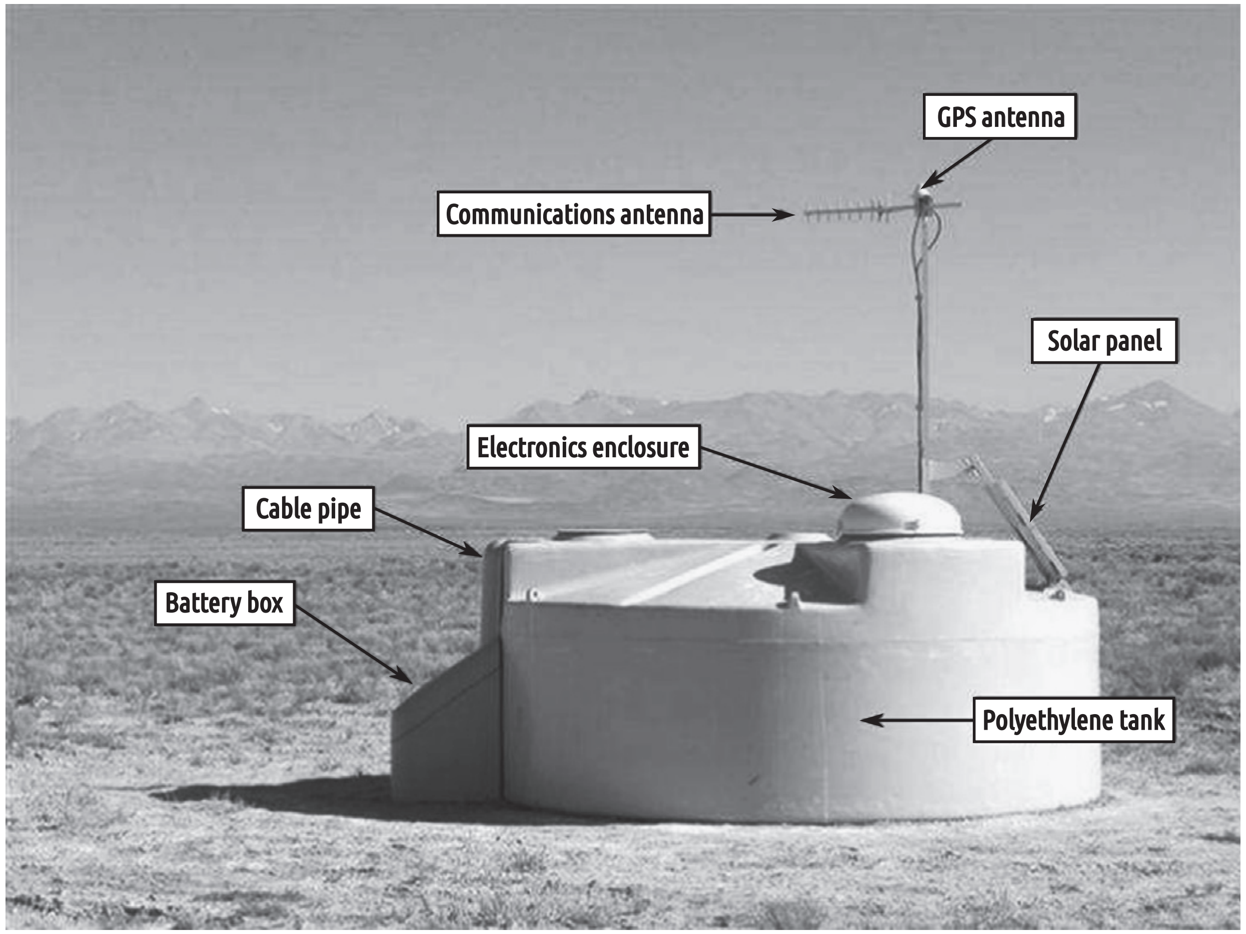

Fig. 3. A schematic view of a surface detector station in the field, showing its main components.

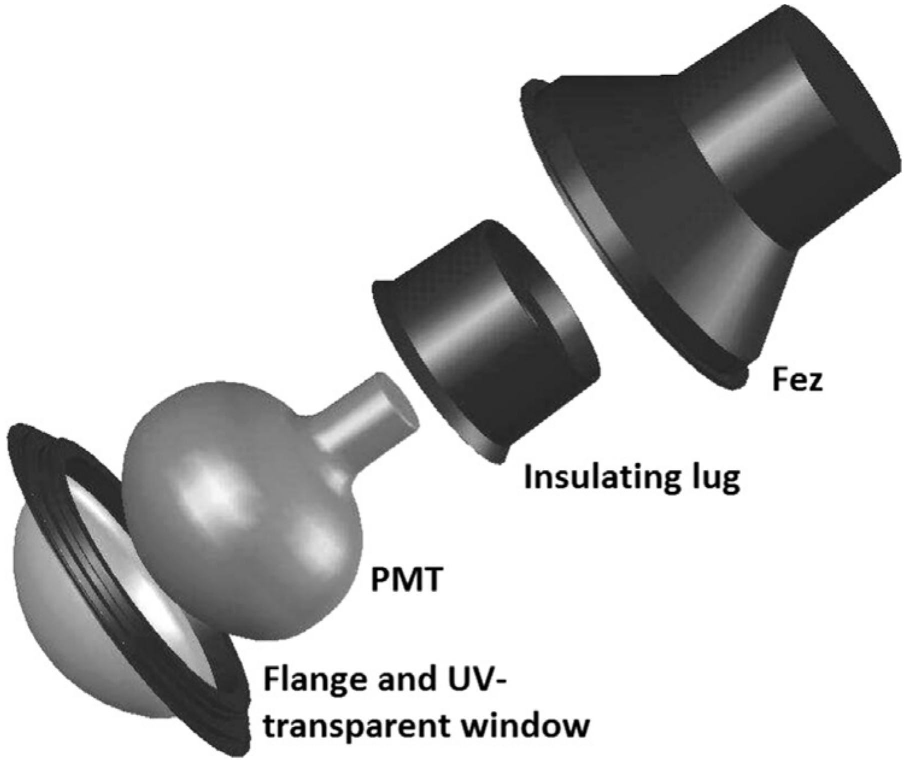

Fig. 4. Mechanical housing for the SD PMT. Top to bottom: outer plastic housing (fez), insulating lug, PMT, flange, and UV-transparent window.

expected to be available over 99% of the time. Batteries are charged through a commercial charge controller, which is epoxy encapsulated and has robust surge protection. The electronics

12000 l ultra pure water
three 9“ diameter PMTs - Photonis XP1805/D1

Pierre Auger Observatory - Water Cherenkov Detector
to measure secondary particles in air showers

wireless communication system

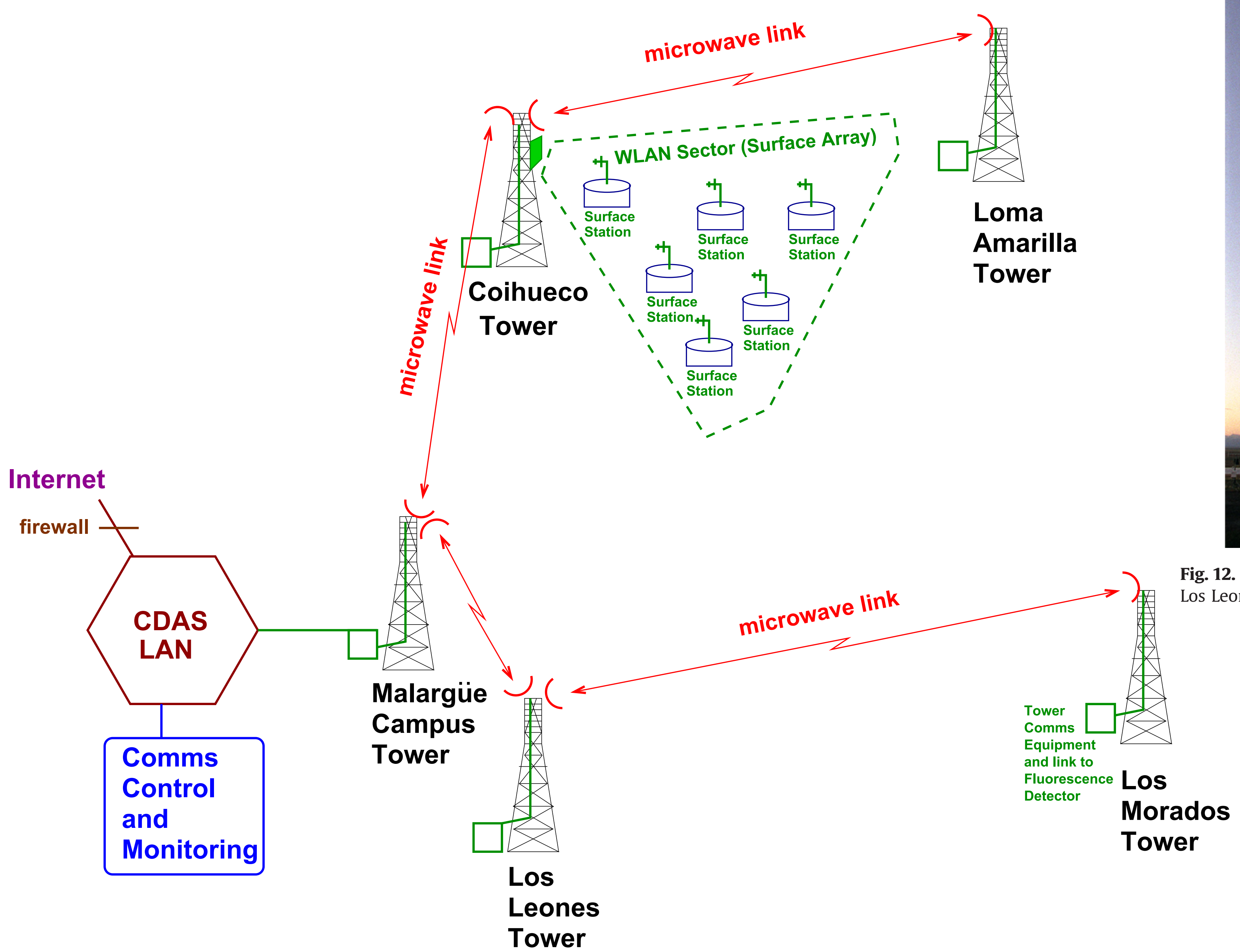

Fig. 11. Conceptual schematic of the overall radio telecommunications system for the Pierre Auger Observatory.

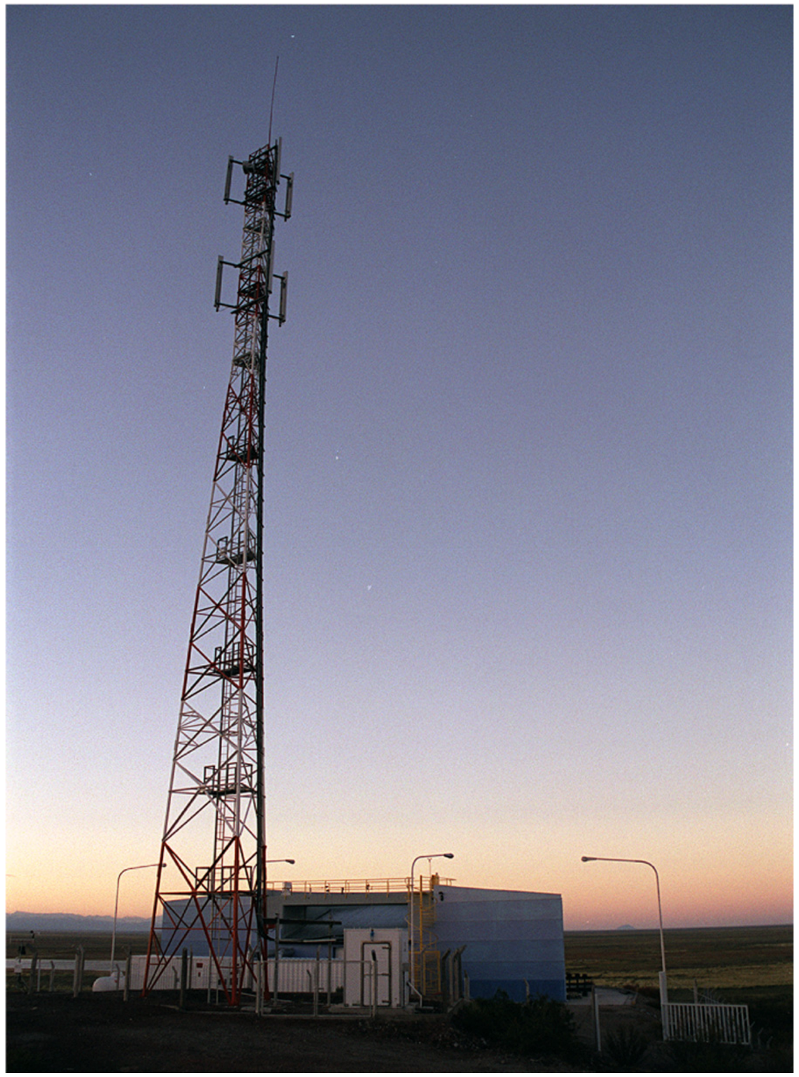

Fig. 12. One of the five communications towers: the one shown is deployed at the Los Leones site; see Fig. 11.

Pierre Auger Observatory - Water Cherenkov Detector
to measure secondary particles in air showers

trigger system to identify extensive air showers

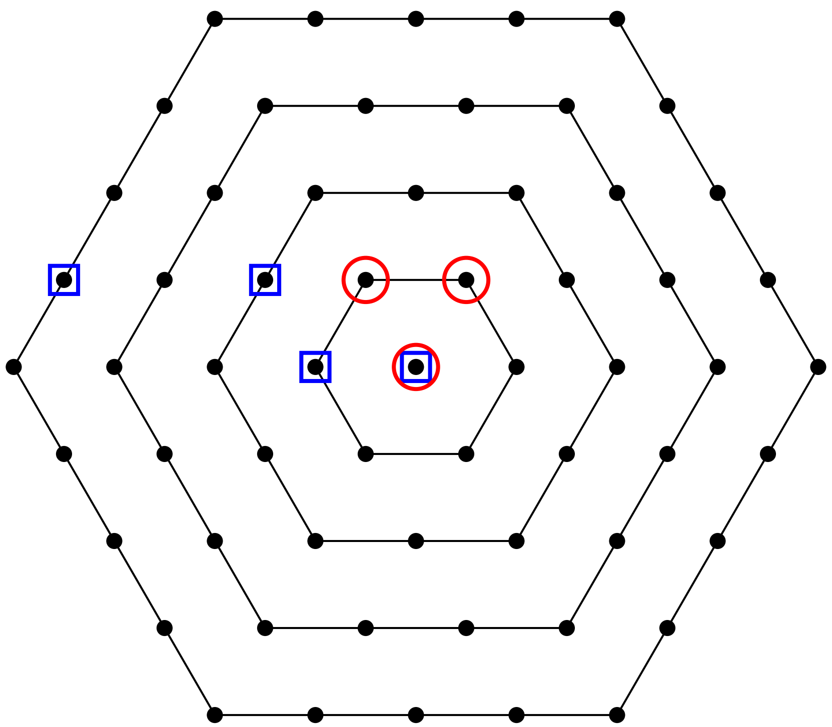

Fig. 16. Four hexagons, containing stations, are illustrated around a central surface station, for a portion of an ideal array. For a 3-fold coincidence, a T3 is issued if the 3 T2s are ToT, and if one of them is found in the first hexagon of the central station, and the other one no further than the second hexagon. A 4-fold coincidence applies to any kind of T2 and the additional station may be as distant as in the 4th hexagon. Two examples of the topology of triggers are shown: a 4-fold coincidence in which the triggered stations are identified by open blue squares, and a 3-fold coincidence identified by open red circles.

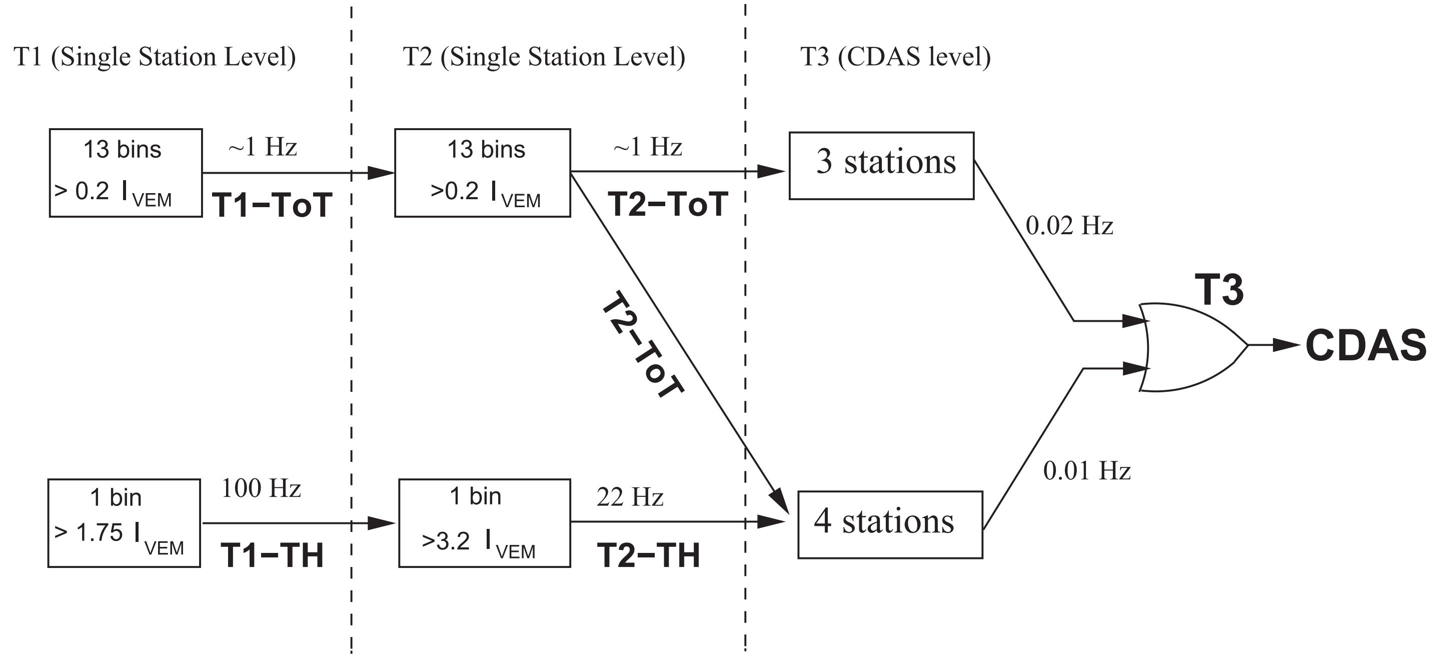

Fig. 15. Schematics of the hierarchy of the trigger system of the Auger surface detector.

Pierre Auger Observatory - Water Cherenkov Detector
to measure secondary particles in air showers

The Pierre Auger Collaboration / Nuclear Instruments and Methods in Physics Research A 798 (2015) 172–213 187

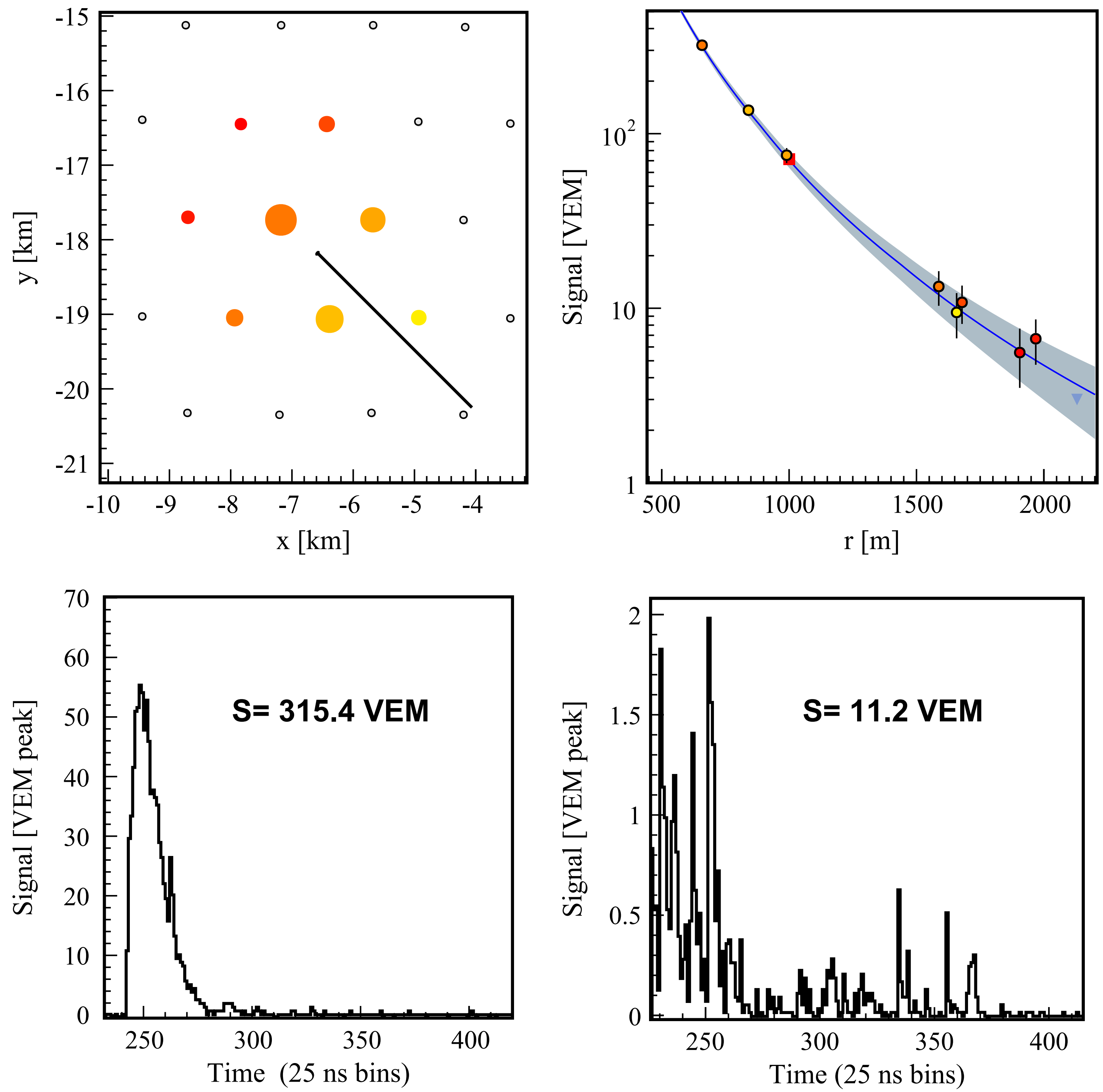

Fig. 17. Event 13357690: a typical vertical event of about 3×10^{19} eV. Top left: The array seen from above with the 8 triggered stations. Top right: The fit to the lateral distribution function (LDF) for this shower of zenith angle 28°. Bottom: The FADC traces from 2 detectors at distances of 650 and 1780 m from the shower core. The signal sizes are in units of VEM.